&EPA

Analysis of Ensemble Averaged Concentrations and Fluxes in a Tracer Puff

RESEARCH REPORTING SERIES

Research reports of the Office of Research and Development, U.S. Environmental Protection Agency, have been grouped into nine series. These nine broad categories were established to facilitate further development and application of environmental technology. Elimination of traditional grouping was consciously planned to foster technology transfer and a maximum interface in related fields. The nine series are:

1. Environmental Health Effects Research
2. Environmental Protection Technology
3. Ecological Research
4. Environmental Monitoring
5. Socioeconomic Environmental Studies
6. Scientific and Technical Assessment Reports (STAR)
7. Interagency Energy-Environment Research and Development
8. "Special" Reports
9. Miscellaneous Reports

This report has been assigned to the ENVIRONMENTAL MONITORING series. This series describes research conducted to develop new or improved methods and instrumentation for the identification and quantification of environmental pollutants at the lowest conceivably significant concentrations. It also includes studies to determine the ambient concentrations of pollutants in the environment and/or the variance of pollutants as a function of time or meteorological factors.

ANALYSIS OF ENSEMBLE AVERAGED CONCENTRATIONS
AND FLUXES IN A TRACER PUFF

by

Main R. Hutcheson
School of Meteorology
University of Oklahoma
Norman, Oklahoma   73019

Project Officer

Kenneth L. Demerjian
Meteorology and Assessment Division
Environmental Sciences Research Laboratory
Research Triangle Park, N.C.   27711

ENVIRONMENTAL SCIENCES RESEARCH LABORATORY
OFFICE OF RESEARCH AND DEVELOPMENT
U.S. ENVIRONMENTAL PROTECTION AGENCY
RESEARCH TRIANGLE PARK, N.C.   27711

DISCLAIMER

This report has been reviewed by the Environmental Sciences Research Laboratory, U.S. Environmental Protection Agency, and approved for publication. Approval does not signify that the contents necessarily reflect the views and policies of the U.S. Environmental Protection Agency, nor does mention of trade names or commercial products constitute endorsement or recommendation for use.

ABSTRACT

This research was initiated to analyze tracer concentrations and fluxes in a diffusing puff released from an instantaneous ground level point source. The concentration data used was made available by the Battelle Memorial Institute. Three basic steps are performed. First, an estimate of the ensemble averaged tracer fluxes is developed. Secondly, an estimate of the ensemble averaged tracer concentration is obtained. Then the estimates are used to determine concentrations and fluxes which satisfy the diffusion equation and are as close to the estimates as possible.

The tracer fluxes are estimated as the negative of the products of the appropriate diffusivities and concentration gradients. The diffusivities are derived using the fact that they are proportional to a characteristic length and velocity scale. This approach yields diffusivities which are the diffusion rates for a Gaussian puff. The flux estimates are shown to satisfy the diffusion equation for all puff diffusion rates when combined with a Gaussian concentration model.

Since the available observations are too sparse to use alone in obtaining a concentration analysis in space and time, a concentration model is developed to provide data at grid points where there are no observations. This model is a modification of the Gaussian one, taking into account surface scavenging and wind shear. A variational technique then incorporates the observations and model data into concentration analyses. A variable observational weight forces the analyses towards the observations, and time filtering in a Lagrangian coordinate system allows the effect of an observation to be felt over several analysis times. Spatial filtering spreads the effect of the observations and helps eliminate short waves. The resulting analyses conform to the observations and provide reasonable concentration distributions in both space and time.

A model to estimate the ensemble averaged concentration is developed based upon the above analyses. Due to the random nature of turbulence, concentrations averaged over many trials should be more nearly normally distributed in the horizontal than the analyses are. Therefore, the model estimates are normally distributed in the horizontal, but the centroid of the horizontal distribution at a given level is displaced downwind relative to the centroid at the adjacent lower level. This type

of distribution is in general agreement with the concentration analyses described above. The ensemble averaged concentration estimates are then made to conform to the analyses as closely as possible using a least squares technique. Concentration gradients are obtained from these estimates for use in computing the estimated fluxes.

The concentration and flux estimates are combined with the diffusion equation in a variational functional. The Euler equations resulting from taking the first variation of the functional may be solved so that concentrations and fluxes obtained satisfy the diffusion equation and are as close to the estimates as the observational weights allow. It is assumed that these quantities are the ensemble averaged concentrations and fluxes.

The ensemble averaged concentrations are close to the analyses obtained from the first variational technique in magnitude, but the ensemble averaged horizontal distributions are more Gaussian. Furthermore the ensemble averaged concentrations are in very close agreement with the observed concentrations. Since they also satisfy the diffusion equation, the ensemble averaged concentrations obtained are very reasonable.

The ensemble averaged concentrations and horizontal fluxes are very close to their estimates, but the vertical flux differs significantly from its estimate. Due to the manner in which the observational weights were chosen, this indicates that the concentration and horizontal fluxes may be modeled in the manner in which the estimates are obtained, but some modification must be made to correctly model the vertical flux. Since the horizontal fluxes are close to their estimates, they are nearly proportional to the concentration gradients. Therefore, in this case, the diffusivity concept has a physical significance. Since the diffusivities are the diffusion rates of the puff, they can be measured in the atmospheric surface layer.

CONTENTS

FIGURES

TABLES

ABBREVIATIONS AND SYMBOLS

A   scavenging factor

$\bar{A}$ amplitude of filtered analysis

$\tilde{A}$ amplitude of observations

a_1 constant of proportionality for downwind standard deviation relation

a_2 constant of proportionality for crosswind standard deviation relation

a_3 constant of proportionality for vertical standard deviation relation

B   the value of $\hat{\chi}$ on the ordinate

b_1 time power for downwind standard deviation relation

b_2 time power for crosswind standard deviation relation

b_3 time power for vertical standard deviation relation

$C(\tau)$ correlation between $u'(t_f - \tau)$ and $u'(t_f)$

$C(t)$ dimensionless time dependent parameter

C_1 time dependent proportionality parameter

C_2 correlation between ℓ_x and u'

C_3 ratio of C_1 to C_2

F   over relaxation factor

F_x flux in the x direction

F_y flux in the y direction

F_z flux in the z direction

$\hat{F}_x$ estimated flux in the x direction

$\hat{F}_y$ estimated flux in the y direction

$\hat{F}_z$ estimated flux in the z direction

G   constant determined by interval-halving

K_x diffusivity in the x direction

K_y diffusivity in the y direction

K_z diffusivity in the z direction

k   wave number

L_x wavelength, downwind direction

$L_{y \text{ or } z}$ transverse wavelength

ℓ_c characteristic length scale

ℓ_x distance that a tracer particle is displaced from the puff centroid in the x direction

Q   Actual source strength

Q'   virtual source strength

R   response function

R^ν residual of the Euler equation at the ν-th iteration

r   detector count rate

T   Lagrangian integral scale

T_o period of the wave

t   travel time from the source

t_i lower limit of the time integration

t_f observation time

Δt time interval

$\bar{u}$ mean wind velocity

u'   turbulent wind fluctuation in the x direction

u_o effective transport wind speed

v'	turbulent wind fluctuation in the y direction
VR	variance of the residual of the diffusion equation
w'	turbulent wind fluctuation in the z direction
x	distance of the puff centroid from the source
x'	distance that a tracer particle is carried in the x direction by turbulent wind fluctuations
y	crosswind distance from the puff centroid
y'	distance that a tracer particle is carried in the y direction by turbulent wind fluctuations
Δx	downwind grid interval
Δy	crosswind grid interval
z	vertical distance from the puff centroid
z'	distance that a tracer particle is carried in the z direction by turbulent wind fluctuations
Δz	vertical grid interval
z_o	height at which u_o is determined
α_1	observational weight
$\alpha_2, \alpha_3, \alpha_4, \alpha_5$	filtering weights
β	$-d\ln A/dt$
$\gamma_1, \gamma_2, \gamma_3, \gamma_4$	observational weights
λ_m	spectral scale of the vertical component of motion
ϵ	rate of dissipation of turbulent kinetic energy per unit mass of air
σ_x	concentration standard deviation in the x direction
σ_y	concentration standard deviation in the y direction
σ_z	concentration standard deviation in the z direction
τ	$t_f - t$

φ azimuthal angle to puff centroid

χ ensemble averaged puff concentration

$\hat{\chi}$ krypton-85 concentration

$\bar{\chi}$ analyzed concentration

$\tilde{\chi}$ model concentration or, if available, krypton-85 concentration

$\langle \chi \rangle$ ensemble averaged concentration estimates

ACKNOWLEDGEMENTS

SECTION 1

INTRODUCTION

This paper describes an analysis technique which has been developed to analyze ensemble averaged concentrations and fluxes for tracer puffs diffusing in the surface layer. It is not possible to achieve this goal using available observations directly, because it is impossible to measure the ensemble averaged properties of the puffs. The ensemble average is an average taken over a large number of individual events which occur under identical ambient conditions.

It is sometimes possible to estimate ensemble averages from time averages. As shown by Wyngaard (1973), the turbulent properties of a stationary flow may be derived from time averages, if the averaging period is sufficiently long. However, a tracer puff residing in stationary flow is continuously changing, due to the diffusion process. The puff, unlike a tracer plume, can never achieve a steady state. Therefore, long time averages are not representative of the ensemble averaged properties of the puff and other means of obtaining the concentrations and fluxes must be developed.

Fluxes are derived which satisfy the diffusion equation for a Gaussian puff spreading out at an arbitrary rate. These fluxes are then used as estimates of the ensemble averaged fluxes for a puff diffusing in the surface layer.

Concentration estimates may be based upon observed data; however, this information is usually too sparce to use alone in analyzing concentrations. Therefore, analyses are obtained by combining the data with a concentration model using a variational technique. The model is a modification of the Gaussian distribution which accounts for wind shear and surface scavenging. The ensemble averaged concentration is more nearly normally distributed than is the concentration in an individual puff, so the ensemble averaged concentration estimates are produced by the model such that they are normally distributed in the horizontal and as close to the analyses as possible.

In the next step the flux and concentration estimates are combined to produce ensemble averages which satisfy the diffusion equation. This is accomplished through the use of a variational formalism, which forces satisfaction of the diffusion equation

1

while keeping the analyzed fluxes and concentrations close to the estimates. These quantities are assumed to be the true ensemble averaged concentrations and fluxes.

The analysis technique has been tested on two data sets collected by the Battelle Memorial Institute. The data sets consist of radiation measurements obtained from Geiger Müller tubes when 85 Kr was released as instantaneous point sources. The Geiger Müller tubes were arranged on arcs at 200 and 800 m from the source. The radiation measurements are converted to concentrations and may be compared with the concentration analysis.

Horizontal and vertical cross sections of observed and analyzed concentrations are constructed. The analyzed concentrations agree closely with those observed.

Two research tools are developed which deserve special mention because of their applicability to other diffusion studies. In Section 3 a method of estimating diffusivities is explained. It is later shown that this method is valid for puffs which are reasonably Gaussian in shape. In Section 6 a variational formalism is developed which produces superior analyses of concentrations and fluxes, since the results are forced to satisfy the diffusion equation. While these techniques are developed for diffusing puffs, they can be adapted for use with plumes.

SECTION 2

REVIEW OF PERTINENT DIFFUSION THEORIES AND

ASSUMED PUFF DISTRIBUTION

In order to perform this research, it is necessary to obtain estimates of the ensemble averaged fluxes and concentrations in a diffusing tracer puff. To this end theories which attempt to explain the mechanism by which tracer fluxes diffuse the puff and describe the shape which the puff will subsequently assume will be examined below.

THE GAUSSIAN MODEL

The tracer puff concentration distribution upon which this research is based is the ubiquitous Gaussian diffusion model (Roberts, et al., 1970), which may be represented as

$$\chi = \frac{Q'}{(2\pi)^{3/2}\sigma_x\sigma_y\sigma_z} \exp\left\{-\left[\frac{(x-\bar{u}t)^2}{2\sigma_x^2} + \frac{y^2}{2\sigma_y^2} + \frac{z^2}{2\sigma_z^2}\right]\right\} . \tag{1}$$

The mean wind, $\bar{u}$, is in the x direction where x is the distance of the puff centroid from the source, and y and z are perpendicular horizontal and vertical, respectively, from the puff centroid. The σ_x, σ_y and σ_z are the time dependent standard deviations of the puff concentration, χ, in the respective coordinate directions and Q' is the virtual source strength. This is the source strength which, at a given travel time, t, would be required to produce the concentration observed at x, y, z (Van der Hoven, 1968). It is assumed, therefore, that the scavenging of the tracer is uniform throughout the puff, and Q' will decrease with increasing travel time, in the absence of sources other than the initial one. A scavenging factor A may be defined such that

$$Q' = AQ , \tag{2}$$

where Q is the actual source strength.

The Gaussian model is applicable only under homogeneous, stationary conditions in which the tracer concentration exhibits a normal distribution. While this model is not universally applicable, it will be used here to represent an ensemble averaged

3

puff concentration in the absence of external boundaries, because, due to the random nature of turbulence, the concentration averaged over many experiments within the same turbulent flow is more nearly normally distributed than is that of a single puff. The model will be modified to provide an estimate of the ensemble averaged concentration of a tracer puff diffusing in the atmospheric surface layer.

The concentration standard deviations are assumed to have a power dependence upon time which may be expressed as

$$\sigma_x \equiv a_1 t^{b_1}, \qquad \sigma_y \equiv a_2 t^{b_2}, \text{ and } \qquad \sigma_z \equiv a_3 t^{b_3}. \qquad (3)$$

Since the a's and b's are arbitrary and the standard deviations increase from zero at the source, little restriction is placed upon them or their derivatives by this assumption. Substitution of (3) into (1) yields

$$\chi = \frac{Q'}{(2\pi)^{3/2} a_1 a_2 a_3 t^{b_1+b_2+b_3}} \exp\left\{-\left[\frac{(x-\bar{u}t)^2}{2a_1^2 t^{2b_1}} + \frac{y^2}{2a_2^2 t^{2b_2}} + \frac{z^2}{2a_3^2 t^{2b_3}}\right]\right\}. \qquad (4)$$

DIFFUSIVITY AND THE DIFFUSION EQUATION

In order to develop reasonable extimates of tracer fluxes, the mechanism by which a puff diffuses must be examined. The diffusion equation and the diffusivity concept will be introduced in order to aid in this examination. It can be shown that, under the proper circumstances, (4) is a solution to the Fickian diffusion equation, modified to accomodate a sink term, $\beta\chi$. This will be done in order to examine the restrictions which must be placed on the concentration standard deviations and the sink term in order for (4) to satisfy the diffusion equation. This diffusion equation may be expressed as

$$\frac{\partial \chi}{\partial t} + \bar{u} \frac{\partial \chi}{\partial x} - K_x \frac{\partial^2 \chi}{\partial x^2} - K_y \frac{\partial^2 \chi}{\partial y^2} - K_z \frac{\partial^2 \chi}{\partial z^2} + \beta\chi = 0. \qquad (5)$$

The diffusivities, K_x, K_y and K_z, may be expressed in terms of the standard deviations (Pasquill, 1974) such that

$$K_x = \sigma_x^2/2t, \qquad K_y = \sigma_y^2/2t \text{ and } \qquad K_z = \sigma_z^2/2t. \qquad (6)$$

These relationships are obtained by equating the solution of the Fickian diffusion equation to Eq. (1). The analytical solution to the Fickian equation using the appropriate boundary conditions was first obtained by Roberts (1923).

The temporal and spatial derivatives in (5) are evaluated

4

using (2) and (4) as follows:

$$\frac{\partial \chi}{\partial t} + \bar{u}\frac{\partial \chi}{\partial x} = \frac{\chi}{t}\{b_1[\frac{(x-\bar{u}t)}{\sigma_x^2} - 1] + b_2[\frac{y^2}{\sigma_y^2} - 1]$$

$$+ b_3[\frac{z^2}{\sigma_z^2} - 1]\} + \chi\frac{\partial \ln A}{\partial t} , \tag{7}$$

$$\frac{\partial^2 \chi}{\partial x^2} = \frac{\chi}{\sigma_x^2}[\frac{(x-\bar{u}t)^2}{\sigma_x^2} - 1] , \tag{8}$$

$$\frac{\partial^2 \chi}{\partial y^2} = \frac{\chi}{\sigma_y^2}[\frac{y^2}{\sigma_y^2} - 1] , \tag{9}$$

and

$$\frac{\partial^2 \chi}{\partial z^2} = \frac{\chi}{\sigma_z^2}[\frac{z^2}{\sigma_z^2} - 1] . \tag{10}$$

Substitution of (6)-(10) into (5) yields

$$\frac{\chi}{t}\{(b_1 - \frac{1}{2})[\frac{(x-\bar{u}t)^2}{\sigma_x^2} - 1] + (b_2 - \frac{1}{2})[\frac{y^2}{\sigma_y^2} - 1]$$

$$+ (b_3 - \frac{1}{2})[\frac{z^2}{\sigma_z^2} - 1]\} + \chi(\frac{\partial \ln A}{\partial t} + \beta) = 0 . \tag{11}$$

Thus, the Gaussian model may be a solution to the Fickian diffusion equation when $b_1 = b_2 = b_3 = 1/2$. That this is the expected result may easily be demonstrated by combining (3) and (6) to obtain

$$K_x = \frac{a_1^2 t^{2b_1}}{2t} , \quad K_y = \frac{a_2^2 t^{2b_2}}{2t} , \quad \text{and} \quad K_z = \frac{a_3^2 t^{2b_3}}{2t} . \tag{12}$$

When $b_1 = b_2 = b_3 = 1/2$, K_x, K_y and K_z are constant. In addition to the diffusivities being constant, β must be equal to $- \partial \ln A/\partial t$ to satisfy (11).

THE GRADIENT TRANSFER HYPOTHESIS

The gradient transfer hypothesis assumes that turbulence causes a net movement of tracer down the gradient of material concentration at a rate proportional to the magnitude of the gradient (Pasquill, 1974). Therefore,

$$F_x \equiv -K_x \frac{\partial \chi}{\partial x} \; , \quad F_y \equiv -K_y \frac{\partial \chi}{\partial y} \quad \text{and} \quad F_z \equiv -K_z \frac{\partial \chi}{\partial z} \; . \qquad (13)$$

For $b_1 = b_2 = b_3 = 1/2$ the fluxes may be obtained since K_x, K_y, K_z and χ are known. However, when the puff is spreading such that $b_1 \neq b_2 \neq b_3 \neq 1/2$, the fluxes are not known since the diffusivities are no longer constant.

In general b_1, b_2 and b_3 are far from equal, and are usually not close to 1/2. In the data utilized in this study b_1 and b_2 are always much larger than 1/2. As Pasquill (1974) points out, the use of a constant diffusivity when dealing with atmospheric turbulence is obviously erroneous. Therefore, fluxes cannot be determined using (13) unless an expression for the diffusivities is found which is applicable to puff spreading out at an arbitrary rate. The diffusivities represented by (6) will therefore be a special case of this general formulation, valid when $b_1 = b_2 = b_3 = 1/2$. Since the diffusivities represented by (6) are not applicable to a puff diffusing in the surface layer, other formulations must be utilized.

Little is known about the nature of the diffusivity of an inert material. The gradient transfer hypothesis has proven useful, but there is no consistent means of accurately predicting eddy diffusivity variations under untested conditions (Lewellen, et al., 1972). Pasquill (1970) states that since no a priori specification of the eddy diffusivity is available, the K-theory approach is physically plausible and equivalent to other approaches only for the case of vertical spread from a source at ground level. The practical equivalence of the above approach and similarity theory may be demonstrated for short range vertical diffusion in neutral conditions. A form for K_z may be obtained (Pasquill, 1974) such that

$$K_z \approx \frac{1}{15} \epsilon^{1/3} \lambda_m^{4/3} \; , \qquad (14)$$

where ϵ is the rate of dissipation of turbulent kinetic energy per unit mass of air and λ_m is the spectral scale of the vertical component of motion. $\lambda_m \equiv \bar{u}/n_m$, where n_m is the frequency at which the normalized spectral density function is a maximum. Using (14) it is possible to specify a K profile over a considerable height range and in any stability, since turbulence data on ϵ and λ_m is becoming increasingly available. Profiles obtained using (14) for unstable, neutral and stable cases, respectively, are displayed in Fig. 1. Note that all profiles begin with a near-linear increase with height but then depart from this significantly.

THE STATISTICAL THEORY OF DISPERSION

In order to gain a better understanding of the diffusion

6
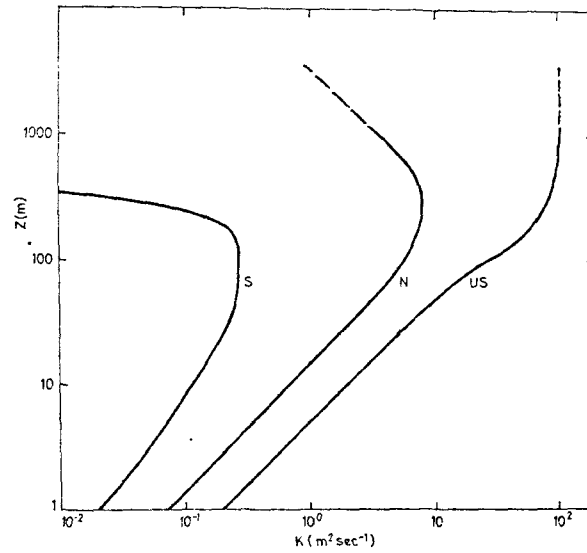
Fig. 1. Tentative profiles of
vertical diffusivity. (From
Pasquill, 1974)
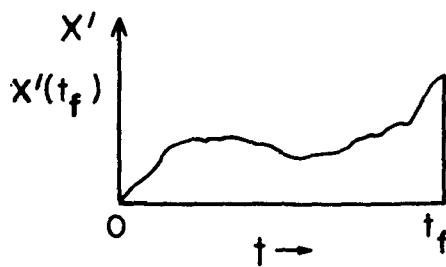
a. The path of a tracer
particle displaced a dis-
tance x' (t_f) at time t_f.
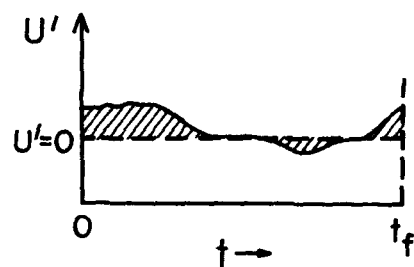
b. The distance x'(t_f)
is the shaded area under
the curve.

Fig. 2. Motion of a tracer particle in a turbulent flow.

mechanism, so that reasonable flux estimates may be obtained, the statistical theory of dispersion will be examined. Some of the concepts developed here will be used in the determination of diffusivities which yield reasonable flux estimates. Furthermore, it will be shown that at long travel times the diffusion rate obtained from the statistical theory is the diffusivity required to satisfy the diffusion equation. The above theory attempts to explain the mechanism by which tracer is spread in a puff. Taylor (1921) derived a fundamental diffusion theorem which applies to diffusion in one space dimension or to three-dimensional diffusion in a stationary, homogeneous turbulent flow. He postulated that the distance, x', that a tracer particle is carried away from an origin by turbulent wind fluctuations, u', at the observation time, t_f, is

$$x'(t_f) = \int_0^{t_f} u'(t) \, dt \ .$$ (15)

This relationship between distance and velocity perturbation is shown in Fig. 2. Since $u'(t_f)$ and the ensemble averaging process are independent of time,

$$\overline{x'(t_f)u'(t_f)} = \int_0^{t_f} \overline{u'(t)u'(t_f)} \, dt \ .$$ (16)

Taylor demonstrated that the usual laws of differentiation may be applied to the mean values of fluctuating variables and their products. Therefore,

$$\frac{d\overline{(x'^2)}}{dt} = 2\, \overline{x'u'} \ ,$$ (17)

where

$$\frac{dx'}{dt} = u' \ .$$

Substitution into (16) yields

$$\frac{1}{2} \frac{d\overline{(x'^2)}}{dt} = \int_0^{t_f} \overline{u'(t)u'(t_f)} \, dt \ .$$ (18)

In the stationary flow that is considered here, the origin of time is irrelevant, so that the correlation between $u'(t)$ and $u'(t_f)$ will depend only upon the time difference $\tau = t_f - t$. Since $\overline{u'(t_f - \tau)u'(t_f)}$ is the covariance of u', a correlation coefficient, $C(\tau)$ may be defined:

$$C(\tau) \equiv \frac{\overline{u'(t_f - \tau)u'(t_f)}}{\overline{u'^2}} \ ,$$ (19)

where $\overline{u'^2}$ is the variance of the downwind component of the wind

8

velocity perturbation. The correlation coefficient decreases as the time interval τ increases, and at large values of τ the velocities are uncorrelated. Substitution of (19) into (18) and use of the definition of τ yields

$$\frac{1}{2} \frac{d(\overline{x'^2})}{dt} = \overline{u'^2} \int_0^{t_f} C(\tau) \, d\tau \; . \tag{20}$$

A Lagrangian integral scale, T, may be defined (Tennekes and Lumley, 1972) such that

$$T \equiv \int_0^{\infty} C(\tau) \, dt \; . \tag{21}$$

It is assumed that $C(\tau)$ decreases rapidly enough that at large τ the Lagrangian integral scale is finite.

Therefore, far from the source (where t_f is sufficiently large)

$$\frac{1}{2} \frac{d\overline{x'^2}}{dt} = \overline{u'^2} \, T \; , \tag{22}$$

so that the diffusion rate of the puff is constant in this region. There are several ways to demonstrate that the puff should in fact diffuse at a constant rate far from the source (Gifford, 1968). It will be shown in the next section that at long travel times the diffusivity required for satisfaction of the diffusion equation at all diffusion rates is $\overline{u'^2} T$. Using (13), the desired fluxes may therefore be obtained far from the source using the statistical theory of turbulence.

A basis for the required ensemble averaged flux and concentration estimates has been developed using established theories. The Gaussian model will be modified to provide reasonable concentration estimates in the atmospheric surface layer. Fluxes will be estimated with the air of the diffusivity concept. The validity of the diffusivities derived in the next section will be tested to show that the resulting fluxes satisfy the diffusion equation. Furthermore, it will be shown that far from the source the diffusivities are the diffusion rates obtained using the statistical theory of turbulence.

9

SECTION 3

DETERMINATION OF THE TURBULENT FLUX ESTIMATES

In the preceding section it was shown that fluxes obtained from the gradient transfer hypothesis, using the conventional expressions for diffusivity, do not satisfy the diffusion equation for a Gaussian puff except when the diffusion rate is constant. Since the diffusion rate observed for puffs in the atmospheric surface layer is not constant except far from the source, it is desirable to use other expressions for the diffusivities. In this section it will be shown that, if the diffusivity is expressed as the diffusion rate, the diffusion equation for a Gaussian puff is satisfied for all diffusion rates. Fluxes obtained using these diffusivities will be employed later as estimates of the fluxes in a puff diffusing in the surface layer.

DIFFUSIVITY AND THE DIFFUSION RATE

Pasquill (1974) expressed the diffusivity as the diffusion rate at large travel times. His formulation, which may be written as

$$K_x = \frac{1}{2} \frac{\overline{dx'^2}}{dt} ,$$ (23)

employs the diffusion rate derived from Taylor's fundamental diffusion theorem. It was shown in Section 2 that the diffusion rate in (23) is valid for a diffusing puff only at distances far from the source. Therefore, a limiting value, which the diffusivity must approach at long travel times, may be obtained by combining (23) and (22) to obtain

$$K_x = \overline{u'^2} \, T .$$ (24)

Hildebrand (1977) defined an apparent eddy diffusivity as

$$K_x = \frac{1}{2} \frac{d\sigma_x^2}{dt} .$$ (25)

Similar expressions may be defined for the y and z directions. In order to illustrate the nature of this diffusivity a derivation is shown in Appendix A.

10

SATISFACTION OF THE DIFFUSION EQUATION

Using the procedure employed in Section 2, it may be shown that the diffusivities defined by (25) satisfy the diffusion equation for all puff diffusion rates. Since the diffusivities are functions of time only, the diffusion equation may be expressed as

$$\frac{\partial \chi}{\partial t} + \bar{u}\frac{\partial \chi}{\partial x} - K_x \frac{\partial^2 \chi}{\partial x^2} - K_y \frac{\partial^2 \chi}{\partial y^2} - K_z \frac{\partial^2 \chi}{\partial z^2} - \frac{d(\ln A)}{dt}\chi = 0 \ , \qquad (26)$$

if the sink term used in Section 2 is included. Substituting (7)-(10) and (25) into (26) one may obtain

$$\frac{\chi}{t}\{ (b_1 - b_1)[\frac{(x - \bar{u}t)^2}{\sigma_x^2} - 1] + (b_2 - b_2)[\frac{y^2}{\sigma_y^2} - 1]$$

$$+ (b_3 - b_3)[\frac{z^2}{\sigma_z^2} - 1]\} + \chi \ (\frac{d(\ln A)}{dt} - \frac{d(\ln A)}{dt}) = 0 \ . \qquad (27)$$

This equation, as opposed to (11), is identically zero. Therefore, (4) is a solution to the diffusion equation for the values of the a's and b's one expects to find in the atmospheric surface layer.

BOUNDARY CONDITIONS

A restriction is placed upon these quantities by the boundary conditions. The conditions specifying a point source are (Sutton, 1953):

$$\chi \to 0 \text{ as } t \to \infty \qquad (28)$$

$$\chi \to 0 \text{ as } t \to 0 \quad \text{(except at the source)} \qquad (29)$$

and

$$\int_{-\infty}^{\infty} \chi dV = Q' \ . \qquad (30)$$

In order for (4) to satisfy the first boundary condition, b_1, b_2 and b_3 must be positive. For the second boundary condition to hold, a_1, a_2 and a_3 must be positive. Remembering the definition of the density function of a normal distribution and its special properties (Mood and Graybill, 1963), it is easy to show that under these circumstances the third boundary condition is also satisfied by the Gaussian model. Using (1) Eq. (30) becomes

$$Q' \int_{-\infty}^{\infty} \int_{-\infty}^{\infty} \int_{-\infty}^{\infty} \frac{1}{(2\pi)^{3/2}\sigma_x\sigma_y\sigma_z} \exp\{-[\frac{(x-\bar{u}t)^2}{2\sigma_x^2} + \frac{y^2}{2\sigma_y^2} + \frac{z^2}{2\sigma_z^2}]dxdydz = Q' \ . \qquad (31)$$

Since the concentration distribution is jointly as well as separately normal, (31) may be written as

$$Q' \int_{-\infty}^{\infty} \int_{-\infty}^{\infty} \int_{-\infty}^{\infty} n(x)\ n(y)\ n(z)\ dx dy dz = Q' , \qquad (32)$$

where n(x), n(y) and n(z) represent the density functions of the normal distributions in the respective coordinate directions. Since

$$\int_{-\infty}^{\infty} n(x)\ dx \equiv \int_{-\infty}^{\infty} n(y)\ dy \equiv \int_{-\infty}^{\infty} n(z)\ dz \equiv 1 , \qquad (33)$$

the third boundary condition is indeed satisfied.

Even though the three boundary conditions discussed above are adequate for Fickian diffusion, a more stringent boundary condition is needed when the diffusivity is time dependent. It can be shown that an inverse relationship between diffusivity and travel time is unreasonable for a Gaussian puff. As seen in Appendix A, the diffusivity is proportional to the product of a characteristic eddy velocity scale, which must be constant in a stationary flow, and a characteristic length scale. Therefore, the length scale must decrease with travel time if K_x does. This cannot occur under the conditions necessary for the tracer concentration to obtain a normal distribution. Under these conditions the eddy size most effective in transporting tracer particles, hence the characteristic length scale, will increase as the puff grows, until the largest eddies are dominant.

Since the diffusivity, hence diffusion rate, must increase with travel time or remain constant for a Gaussian puff, a new boundary condition may be formulated. Using (3),

$$\frac{1}{2}\frac{d\sigma_x^2}{dt} = a_1^2 b_1 t^{2b_1-1} \quad , \quad \frac{1}{2}\frac{d\sigma_y^2}{dt} = a_2^2 b_2 t^{2b_2-1} \quad \text{and}$$

$$\frac{1}{2}\frac{d\sigma_z^2}{dt} = a_3^2 b_3 t^{2b_3-1} \ . \qquad (34)$$

In order for the diffusion rates to increase or remain constant with travel time, b_1, b_2 and b_3 must be equal to or greater than 1/2. This is a more stringent requirement than (28), which required that the b's be positive.

A RELATIONSHIP WITH THE STATISTICAL THEORY OF TURBULENCE

It is important to understand the relationship between the diffusion rates used in this section and those derived from the statistical theory of turbulence. Then it will be possible to

12
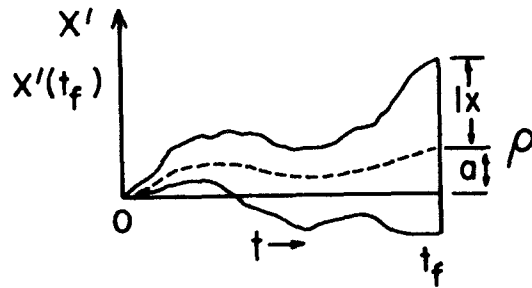
Fig. 3. Motion of two particles in a puff. The puff centroid is at ρ at time t_f.
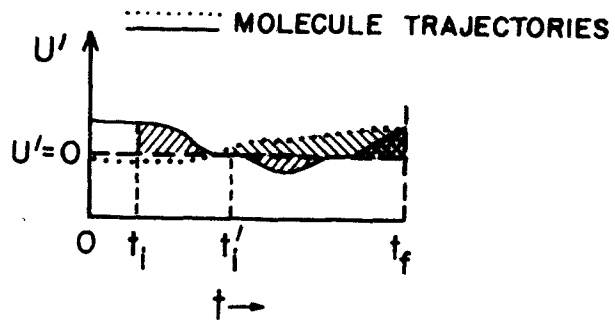
Fig. 4. Relationships between ℓ_x and u'. The shaded areas equal ℓ_x, and t_i^x and t_i are the lower integration limits required.

13

compare these diffusivities with those obtained by Pasquill. Proceeding in a manner similar to that used in Section 2, (A.9) may be integrated to obtain

$$\ell_x = \int_{t_i}^{t_f} u' \, dt \, , \tag{35}$$

where ℓ_x is the distance that a tracer particle is displaced from the puff centroid in the downwind direction. The above expression is similar to Taylor's diffusion theorem, Eq. (14), except that the integration is from a time t_i rather than the initial time, as seen in a comparison of Figs. 2, 3 and 4. The $t_i \neq 0$ unless $x'(t_f) = \ell_x$. Multiplying both sides of (35) by $u'(t_f)$ and taking an ensemble average, we obtain

$$\overline{\ell_x u'(t_f)} = \int_{t_i}^{t_f} \overline{u'u'(t_f)} \, dt \, . \tag{36}$$

Changing the viewpoint from which Taylor observed the diffusion process, a series of puffs released from a point source under identical conditions are considered here. The particle which arrives at $x'(t_f)$ after each release is studied. As depicted in Fig. 3, the position of the puff centroid with respect to the abscissa is variable. Therefore, the position at travel time t_f will change for each release. The length ℓ_x, for particles which arrive at $x'(t_f)$ will be different, due to the change in centroid position. Furthermore, the path which the particles took to arrive at $x'(t_f)$ changes due to the randomness of the turbulence. While the total area under the curve in Fig. 4 is always $x'(t_f)$, the area under any segment of the curve varies. For these reasons the time t_i must be different for each release.

Since t_i is variable, in general

$$\overline{\int_{t_i}^{t_f} u'u'(t_f) \, dt} \neq \int_{t_i}^{t_f} \overline{u'u'(t_f)} \, dt \, . \tag{37}$$

However, under the proper circumstances, the variation of t_i is not important. For stationary turbulence Eq. (36) may be written as

$$\overline{\ell_x u'(t_f)} = \overline{\int_{o}^{\delta t} u'(t_f - \tau) \, u'(t_f) \, d\tau} \, , \tag{38}$$

where $\delta t = t_f - t_i$ and τ was defined in the preceding section. Where t_f is very large in comparison with t_i, δt is essentially constant and the ensemble average may now be taken inside the integral. In this case (38) may be written as

14

$$\overline{\ell_x u'(t_f)} = \overline{u'^2} \int_o^{\delta t} C(\tau) \, d\tau \,, \tag{39}$$

where $C(\tau)$ was defined in (19). The consequence of a large δt is the same as described for a large t_f in Section 2. When $t_f - t_i$ is large the integral becomes constant, regardless of δt. In this case (39) may be written as

$$\frac{1}{2} \frac{d\sigma_x^2}{dt} = \overline{u'^2} \, T \,, \tag{40}$$

using (A.10) and the definition of the Lagrangian integral scale. Since δt can only be large at long travel times, (40) is valid far from the source.

A comparison of (40) and (22) shows that the diffusion rate employed in this section is identical to that obtained using Taylor's classical diffusion theorem at distances far from the source. Therefore, the diffusivities reach the limiting value obtained by Pasquill (1974) at large distances.

EXPRESSIONS FOR THE FLUXES

Since the diffusivities in (25) satisfy the diffusion equation under the specified restrictions, exact expressions for the fluxes under these conditions may be obtained. Using (25) and (13),

$$F_x = -\frac{1}{2} \frac{d\sigma_x^2}{dt} \frac{\partial \chi}{\partial x} \,, \qquad F_y = -\frac{1}{2} \frac{d\sigma_y^2}{dt} \frac{\partial \chi}{\partial y} \quad \text{and}$$

$$F_z = -\frac{1}{2} \frac{d\sigma_z^2}{dt} \frac{\partial \chi}{\partial z} \,, \tag{41}$$

where F_x, F_y and F_z are the fluxes in the respective coordinate directions. Therefore, the fluxes are known as a function of space and time for a puff diffusing in a stationary, homogeneous non-isotropic flow in which the scavenging of the tracer is uniform. It has not been shown how well the true fluxes are represented by (41) for a puff diffusing in the atmospheric surface layer. In this case the flow is neither stationary nor homogeneous. Furthermore the contact of the puff with the surface ensures that the scavenging is not uniform throughout the puff.

Because the fluxes represented by (41) have been shown to be valid for a Gaussian puff diffusing at an arbitrary rate, they will be used as estimates of the ensemble averaged fluxes in the puffs selected for analysis. The validity of the estimates will be examined further in a later section.

15

SECTION 4

DATA UTILIZED IN THIS RESEARCH

In order to develop an estimate of the ensemble averaged puff concentrations as a function of space and time, analyses of puffs of tracer material released from an instantaneous point source must be obtained. Details for the ensemble averaged concentration estimates are then deduced from these analyses.

KRYPTON-85 AS AN ATMOSPHERIC TRACER

Since the small puffs rapidly pass the concentration measuring devices, instruments with fast response times must be used. The best concentration measurements available for analysis were obtained from the release of the radioactive gas krypton-85 as an atmospheric tracer. Since the gas is radioactive, measuring devices with very high response times may be used to sample it. Krypton-85 is inert, so the tracer has minimum interaction with structures or vegetation, and it does not react with other atmospheric constituents (Nickola et al., 1970a).

Nickola et al. (1970b) published the concentration measurements as a volume of atmospheric diffusion data, due to their high quality. Measurements were made simultaneously at 64 field locations. The sampling array, on arcs at distances of 200 and 800 m from the source, consisted of 40 Geiger-Müller tubes at $2°$ intervals and an elevation of 1.5 m above the surface with 24 more tubes on 6 towers (see Fig. 5). The 200 m arc towers were instrumented at .8, 1.5, 3.0, 6.1 and 10.7 m. The 800 m arc towers were instrumented at .8, 1.5, 4.6, 10.7 and 21.3 m.

The dispersing krypton-85 gas emitted .69 MeV (max) beta particles which were detected by the halogen-quenched Gerger-Müller tubes. Information from these detectors was relayed to a 4096 address memory, programed to accept data simultaneously from the 64 detectors for 64 time increments. Time intervals permitted were 1.2, 2.4, 4.8 and 38.4 sec.

Ambient wind and stability data are available from two meteorological towers located near the source. The wind speed sensors were three-cup anemometers, and the wind direction transducers were Beckman and Whitley Model 1565 vanes. Since the wind vanes were poorly oriented, no mean wind directions were published.

16
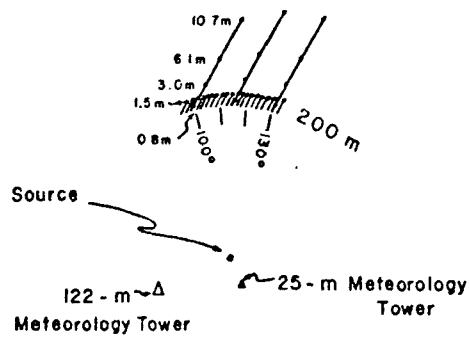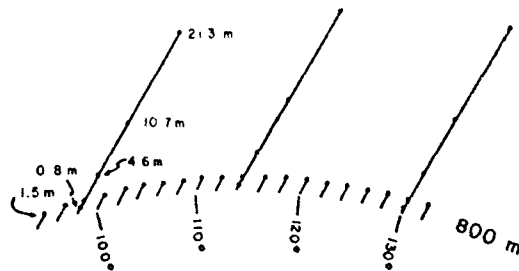
Fig. 5. Schematic representation of the field grid.
(From Nickola et al., 1970a)

17

Table 1. Meteorological data for the two tests. (From Nickola et al. (1970b))

a. Test P5 - Generation 1052:40 PST 10 Curies - October 23, 1967

Time, PST	Mean Wind Speed in MPS			Speed Standard Deviation, MPS			Dir Standard Deviation, DEG			Temperature in Degrees F		
	1.5m	6.1m	24.4m	1.5m	6.1m	24.4m	1.5m	6.1m	24.4m	0.9m	15m	30m
1052*	8.1	11.6	13.5	0.62	0.65	0.82	3.5	5.4	1.9			
1053	7.4	9.9	12.8	1.70	1.67	1.03	7.4	4.8	1.8			
1054	8.4	10.7	12.4	1.06	1.02	1.21	4.9	4.6	3.3			
1055	7.4	9.9	11.9	1.42	1.54	1.35	3.4	4.0	2.9			
1056	6.9	8.7	12.1	2.02	2.33	2.15	5.6	7.1	5.4			
1057	8.6	11.7	13.5	1.43	1.44	1.36	4.5	3.4	4.7			
1052:40 to 1056	7.6	9.9	12.4	1.58	1.80	1.48	6.4	6.1	4.9	60.0	57.5	56.6

*Data for 1052:40 to 1053:00 only.

b. Test P7 - Generation 1052:30 PST 10 Curies - October 24, 1967

Time, PST	Mean Wind Speed in MPS			Speed Standard Deviation, MPS			Dir Standard Deviation, DEG			Temperature in Degrees F		
	1.5m	6.1m	24.4m	1.5m	6.1m	24.4m	1.5m	6.1m	24.4m	0.9m	15m	30m
1052*	4.7	5.1	6.2	0.57	0.55	0.43	4.3	1.8	3.5			
1053	5.4	6.3	6.9	0.59	0.76	0.33	5.5	3.1	2.3			
1054	4.3	5.1	6.1	0.83	0.74	0.29	4.1	3.3	4.2			
1055	4.3	5.4	6.3	1.05	1.18	0.61	6.6	7.9	6.8			
1056	4.0	4.9	6.0	0.42	0.53	0.59	8.6	7.7	10.7			
1057	3.9	5.1	6.3	0.96	0.83	0.82	9.8	7.9	7.1			
1052:30 to 1056	4.5	5.4	6.3	0.87	0.94	0.57	9.1	8.8	8.9	54.4	51.9	50.8

*Data for 1052:30 to 1053:00 PST only.

18

There were thirteen releases of the noble gas tracer. Eight of these were in the form of instantaneous puffs, while the remaining five took the form of plume releases of 10 to 20 minutes duration. The puffs were generated by crushing quartz ampules containing the tracer in a guillotine-like device at ground level. The gas in each ampule was sealed at mean atmospheric pressure to minimize the initial volume of the instantaneous point source.

The data from two of the eight puff releases are available for analysis here. In experiments P5 and P7 the puff centroids passed close enough to one of the instrumented towers so that a reliable vertical profile of the puff is available for the 200 m arc. Puff P5 was released during a period of high wind speeds. It was therefore considered practical to start the automatic data storage increments well before tracer arrival and concentration measurements taken every 2.4 sec sampled the entire puff within the 64 time increment limit. The meteorological data for test P5 is given in Table 1. While the highest wind speed was observed in this experiment, the speed and direction standard deviations are not larger than in some other cases. The Richardson number computed by Nickola (1971) for this case is -.02, indicating an essentially neutral atmosphere.

Puff P7 was released on the day following the release of P5 when the wind speeds were lower. In this case some tracer arrived at the 200 m measuring arc prior to switching the monitoring system from accumulate to automatic. Therefore, the concentrations were not observed at specified times until the puff was well into the monitoring system. As is the case with test P5, the tracer is completely embraced within the horizontal extent of the grid, and tracer concentration at all detectors returned to the background level prior to the completion of the data storage period. Due to the slower wind speed, which kept the puff in the field grid for a longer period of time than in the previous experiment, a time increment of 4.8 seconds was used. The meteorological data for test P7 is given in Table 1. The Richardson number for this test was -.16, indicating an unstable situation.

The concentrations used in this study were deduced from the detector count rates. A total of 1.9 counts/sec was subtracted by Nickola et al. (1970a). This subtracted value consists of a background mean of about 1.2 counts/sec plus approximately three standard deviations from that mean. The relative concentrations listed in the volume of atmospheric diffusion data are in counts per 10 sec. Meaningful atmospheric concentrations may be obtained from these count rates by using the relationship

$$\hat{\chi} = .103r \, , \tag{42}$$

where $\hat{\chi}$ is the krypton-85 concentration in $\mu C_i/m^3$ and r is

19

detector count rate in counts/sec.

PUFF DIMENSIONS

Nickola (1971) computed the puff dimensions at the 200 and 800 m arcs. The array of samplers is relatively dense in terms of atmospheric sampling grids, but is inadequate for completely defining concentration distribution in a small puff. Spacing between sampling arcs is 600 m, and between towers is 56 m and 224 m, on the 200 and 800 m arcs, respectively. Since none of the puffs intersect more than two towers at a given distance from the source, we have little knowledge of the distribution of concentration with time on a horizontal plane other than $z = 1.5$ m. The puffs generally extended above the top of the sampling array, so the puff distribution could not be completely determined on any vertical plane.

Since the distribution of concentration with time is well defined for the 1.5 m height, Nickola computed the crosswind and downwind standard deviations of the distribution at this height. He assumed that the mean transport wind is applicable during an entire puff passage at a given distance and at the 1.5 m elevation, so the observed distribution with respect to time may be converted to a distribution with respect to downwind distance. The standard deviation of the crosswind summed concentration distribution of ^{85}Kr, σ_{yI}, may therefore be computed.

The downwind integration of concentration with time may be performed using $\Delta x = \bar{u} \Delta t$, where Δx is the downwind grid interval and Δt is the time increment over which the χ's were successively measured. The exposure, $\Sigma \chi \Delta t / Q$, was computed by Nickola, and the standard deviation of the downwind summed concentration distribution, σ_{xI}, obtained from the exposure distribution.

The vertical concentration profiles obtained did not, in general, resemble those obtained from the Gaussian model, which predicts that, for perfect surface reflection of the tracer, a half-bell shape is obtained from a surface release. Because of this, Nickola computed the σ_{zI} values by two different methods. Where possible, the data was used directly and total perfect reflection was assumed. This technique was used only in cases where the vertical profile approached the half-bell shape, such as for puff P7 on the 200 m arc. In an attempt to eliminate the interferring effects of the surface, σ_{zI} values were usually generated using a second technique. The observed exposures were redistributed into a virtual distribution extending below ground level, assuming that the tracer was partially rather than totally reflected. The exposures were then subtracted from a given level above the surface and added to a level below the surface on a trial and error basis until a curve with a reasonably smooth, bell like shape was obtained. Computation of σ_{zI} was then

20

Table 2. Measurements of puff dimensions. (From Nickola (1971))

Test	Ri	Data plane	200 m from source					800 m from source				
			σ_x^I (m)	σ_y^I (m)	σ_z^I (m)	σ_y^I/σ_x^I	σ_z^I/σ_x^I	σ_x^I (m)	σ_y^I (m)	σ_z^I (m)	σ_y^I/σ_x^I	σ_z^I/σ_x^I
P7	-0.16	z=1.5m θ=114°	32 30	9.9 -	(6.7) 5.4-7.2	0.30 -	- 0.18-0.24	75 84	54 (60)	- 9.8	0.72 -	- 0.12
P6	-0.04	z=1.5m θ=114° θ=130°	39 38 20	11.0 - -	(6.4) 5.0-7.4 3.1	0.26 - -	- 0.13-0.20 0.16	83 60 -	44 - -	(11) 7.6 -	0.53 - -	- 0.13 -
P3	-0.03	z=1.5m θ=114°	33 37	12.6 (14.1)	- 4.9-6.1	0.38 -	- 0.13-0.16	112 64	28 -	(16) 9.2	0.25 -	- 0.14
P5	-0.02	z=1.5m θ=114°	40 41	9.0 (9.2)	- 4.5-5.9	0.23 -	- 0.11-0.14	95 -	50 -	- -	0.53 -	- -
P8	0.07	z=1.5m θ=114° θ=130°	48 33 -	12.1 - -	(6.3) 4.3 -	0.25 - -	- 0.13 -	151 - 67	37 - -	(16) - 6.9	0.24 - -	- - 0.10
P2	0.13	z=1.5m	60	13.8	-	0.23	-	236	50	-	0.21	-

Figures in parentheses are estimates from measurements made outside the indicated data plane.

21

performed. Because the puffs were not, in general, normally distributed in the vertical, σ_{zI} does not define the puff as uniquely as σ_{xI} or σ_{yI} do.

The values that Nickola obtained for the puff dimensions are displayed in Table 2. Note that for puff P5 no σ_{zI} value was given at the 800 m arc. Examination of the data shows that the vertical concentration profiles bears no resemblance to a normal distribution at the observation tower. However, a value for σ_{zI} is needed in order to determine the rate at which the puff is spreading in the vicinity of the 200 m arc. Since the puff diffuses very slowly in the vertical under all conditions, an average σ_{zI} was computed from the σ_{zI}'s determined for the other puffs. This value was used for puff P5 on the 800 m arc.

Since it takes a finite time for a puff to pass an arc, the instantaneous width of the puff will be less than the width of arc intercepted by the puff, due to the effect of meander of the wind. However, Nickola (1971) points out that, for a puff released under the unstable or neutral conditions considered here, there is essentially no difference in these two widths, due to the relatively high wind speeds and resulting short period of puff passage at an arc. Therefore, it is assumed that the instantaneous and integrated standard deviations are identical.

Since most of the data was collected at the 1.5 m level, it is at this level that σ_x and σ_y are valid. However, useful standard deviations are in the plane passing through the puff centroid, which may be at a different level. Since the puffs were released at the surface, it is assumed that their centroids remain at this level, but that the standard deviations are those measured at the 1.5 m level.

The a's and b's used to define the standard deviations in (3) may now be determined using the σ_{xI}, σ_{yI} and σ_{zI} computed by Nickola at 200 and 800 m from the source. A system of two equations in two unknowns may be set up for each coordinate direction. In the downwind direction,

$$\ln \sigma_{x_{200}} = \ln a_1 + b_1 \ln t_{200}$$

$$\ln \sigma_{x_{800}} = \ln a_1 + b_1 \ln t_{800} . \tag{43}$$

Similar equations may be derived in the other directions.

The a_1, etc., obtained yield the measured standard deviations at 200 and 800 m from the source, but σ_x, σ_y and σ_z determined when the puff centroid is not on a measuring arc are valid only if the time rate of change of puff size is correct.

The puff's diffusion rates are determined using (34). The

Table 3. Puff diffusion rates.

time	experiment	$\frac{1}{2}\frac{d\sigma_x^2}{dt}$	$\frac{1}{2}\frac{d\sigma_y^2}{dt}$	$\frac{1}{2}\frac{d\sigma_z^2}{dt}$
37.6	P5	32.6	3.09	.547
40.0	P5	33.9	3.54	.568
66.4	P7	11.7	2.21	.232
71.2	P7	12.2	2.55	.227

experiment	a_1	a_2	a_3	b_1	b_2	b_3
P5	2.034	.02452	.2704	.8131	1.612	.8070
P7	1.247	.01544	1.573	.7718	1.537	.3446

results are displayed in Table 3 for the travel times on either side of the time the puff centroid crossed the 200 m arc. The diffusion rates all increase with time except for vertical diffusion in experiment P7. In this case the diffusion rate decreases, since b_3 is less than 1/2. This cannot occur under the assumptions stated in Section 2. It is shown in Section 3 that the diffusion rate for a Gaussian puff increases with travel time until the puff is far from the source. However, the assumptions used in the previous sections are not applicable in the atmospheric surface layer.

It was shown in Section 2 that the nature of the functional dependence of the puff growth rate upon time changed as the travel time increased. It must be assumed that this is true for the growth rate of the analyzed puffs also. Since the puff's dimensions were measured on only two arcs, only one set of a's and b's are obtained for each experiment. Therefore, only one functional dependence is computed using (43), so the puff diffusion rates obtained cannot be valid over the entire travel time of the puff. The diffusion rates obtained are therefore a reasonable estimate of the true diffusion rates for some time interval within the time required for the puff centroid to reach the 800 m arc. It is assumed that this time interval includes those observation times when the puff centroid is near the 200 m arc.

SECTION 5

DETERMINATION OF THE ENSEMBLE AVERAGED

CONCENTRATION ESTIMATE

Since the array of samplers is inadequate to completely define the concentration distribution in a tracer puff, conventional analysis techniques cannot be used here. The data used at the six times closest to the time the puff passed the 200 m arc are given in Tables 4 and 5. The analyses are most likely to be correct at times when the puff centroid is near the measuring arc. However, analyses are produced at fourteen times in test P5, and ten times in test P7, so that the temporal boundaries will be far from the analyses of interest.

A modified analysis, based upon Sasaki's (1970a, b and c) variational method is performed. First, a concentration model is fitted as closely as possible to the available data. The model values are replaced by Nickola's observations at the appropriate grid points. The results are then filtered in space and time using the variational technique. The concentration model is modified and refitted to the resulting analysis in order to obtain an estimate of the ensemble averaged concentration.

THE INITIAL CONCENTRATION MODEL

The basic concentration model utilized is defined by (4). However, the Gaussian model does not account for two processes which occur in the atmospheric surface layer. Wind speed shear is present in any boundary layer. Also, since the ^{85}Kr tracer is inert, scavenging occurs only at the surface. These processes tend to deform the puff from a normal distribution.

In order to account for these processes, the Gaussian model is modified by making $\bar{u}$ a function of height such that

$$\bar{u} = u_o + G(z - z_o) \, , \tag{44}$$

where u_o is the effective transport wind speed, computed by Nickola (1971) at the observation level $z_o = 1.5$ m. A linear wind profile is assumed because both surface scavenging and wind shear are accounted for by this method. This produces a distinctly different concentration distribution than would be

Table 4. Available data for test P5 when the puff centroid is near the 200 m measuring arc. (From Nickola et al. (1970b))

a. Concentrations ($\mu Ci/m^3$) at the 1.5 m level

					Azimuth (degrees)						
Time	104	106	108	110	112	114	116	118	120	122	124
32.8	1.5	4.7	63.8	120.0	167.9	203.4	64.6	9.2	4.5	2.5	.2
35.2	.9	5.6	62.3	162.1	210.9	132.5	48.7	5.7	3.4	2.1	.3
37.6	.7	2.7	37.2	191.5	176.7	127.4	26.8	4.1	1.0	1.1	.1
40.0	1.	12.5	55.0	166.7	157.4	117.2	14.6	2.0	.3	1.5	0.
42.4	.4	2.0	11.5	93.3	100.1	87.3	24.6	1.1	.7	.4	0.
44.8	.3	1.8	9.7	77.7	114.4	58.8	50.7	6.2	1.3	.6	.1

b. Concentrations ($\mu Ci/m^3$) at the 114° azimuth

	Level (m)		
Time	.8	3.	6.1
32.8	214.4	208.5	191.7
35.2	161.6	96.1	54.5
37.6	130.0	71.8	29.3
40.0	121.4	84.8	26.5
42.4	110.0	76.1	34.3
44.8	78.0	34.4	16.9

Table 5. Available data for test P7 when the puff centroid is near the 200 m measuring arc. (From Nickola et al. (1970b))

a. Concentrations (μCi/m^3) at the 1.5 m level

Azimuth (degrees)

Time	104	106	108	110	112	114	116	118	120	122	124
56.8	.2	0.	2.2	34.1	134.7	212.5	126.9	24.8	15.	6.	.3
61.6	.2	.1	4.	15.	85.4	213.6	100.6	58.7	27.6	10.4	.9
66.4	.3	12.3	22.2	49.9	90.7	160.9	68.7	50.9	20.2	5.2	.2
71.2	2.1	12.7	25.9	53.4	111.6	107.5	32.2	36.7	21.2	3.2	.3
76.0	1.2	5.8	25.2	63.2	70.2	71.5	32.5	22.1	4.8	.8	.1
80.8	0.	1.1	6.7	32.3	30.5	44.9	19.3	10.6	5.1	1.5	.8

b. Concentrations (μCi/m^3) at the 114° azimuth

	Level		
Time	.8	3	6.1
56.8	237.3	221.2	234.0
61.6	240.4	214.0	78.2
66.4	181.2	158.4	61.0
71.2	132.6	75.9	24.3
76.0	90.2	43.1	17.8
80.8	46.8	37.3	6.8

27

obtained using a traditional power law vertical profile, such
as the one employed by Yeh and Huang (1975). Since the centroids
of the horizontal concentration distributions are displaced down-
wind with height, the maximum concentration in the forward part
of the puff is aloft, while the maximum concentration in the
rearward portion is on the surface. This is in agreement with
the observations. The G is then chosen such that the model con-
centrations are as close to those observed as possible. It is
implicitly assumed here that while tracer is scavenged only at
the surface, small turbulent eddies with time scales smaller
than the incremental averaging time tend to smooth our discon-
tinuities produced by the surface scavenging and the effect of
wind shear. The concentration model therefore has a normal dis-
tribution in the horizontal, but the vertical concentration dis-
tribution is not Gaussian.

The variables which must be determined such that the model
fits the observed data as closely as possible are: $A(t)$, a_1, a_2,
a_3, b_1, b_2, b_3, $\bar{u}(z)$, $x(t)$ and $y(t)$. The a_1, a_2, a_3, b_1, b_2 and
b_3 are obtained by the method described in the previous section
and $A(t)$ is defined in (2).

The $x(t)$ and $y(t)$ may be computed when the azimuth, $\varphi(t)$,
of the puff centroid is known. The azimuth must be determined
at each observation time to ensure optimal fit to the data, so
an interval-halving technique is utilized for this purpose. An
azimuth interval is chosen which contains the optimal azimuth.
The interval is then halved until the quantity $\Sigma(\chi - \hat{\chi})^2$ is mini-
mized, where $\hat{\chi}$ is the measured concentration and χ is obtained
from (4). When the quantity is a minimum the optimal azimuth is
obtained.

Since data useful in determining the optimal azimuth is
contained only in the measuring arc at 1.5 m elevation, other
data may be ignored in this interval-halving technique. Nichola
computed the transport wind speed at the arc level, so $\bar{u}(1.5\ m)$
is known. Since the interval-halving technique minimizes the
difference between the model value and the data, it is not nec-
essary to optimize $A(t)$ at this point. Therefore, $A(t)$ is taken
to be 1 without loss of accuracy in determining the optimal azi-
muthal angle.

The optimal azimuth displays some variability, as seen in
Table 6, for two reasons. As the puffs move with the flow, wind
fluctuations cause the puff centroids to meander. Furthermore,
the actual puffs are somewhat non-Gaussian, as seen in Fig. 6
to 9. As the model adjusts to the tracer observations on the
200 m arc, shifts in the optimal azimuth will occur. Therefore,
the variability of the azimuth is not due solely to changes in
the centroid's azimuthal position, it is partly due to irregu-
larities in the puff's concentration distribution. This intro-
duces an error in the estimate of the puff's azimuth.

28

Table 6. Parameters optimized to fit the model to observations

Travel time	B(t)	A(t)	ω(t)
a. Test P5			
23.2	.7708	1.207	115.8
25.6	.4261	1.008	112.6
28.0	2.260	.8978	112.6
30.4	6.854	.7309	113.3
32.8	4.271	.6701	112.8
35.2	1.639	.5632	111.8
37.6	−2.151	.5420	111.6
40.0	−1.922	.5794	111.4
42.4	− .4363	.4675	112.1
44.8	−1.142	.5036	112.3
47.2	.04	.4494	111.5
49.6	− .2584	.5275	110.9
52.0	− .4419	.4654	112.2
54.4	− .577	.4514	113.6
b. Test P7			
52.0	5.586	.9881	113.7
56.8	2.669	.8061	113.9
61.6	−1.827	.5983	114.3
66.4	.5847	.5047	113.8
71.2	.0433	.4790	112.8
76.0	− .5869	.5051	112.4
80.8	− .4587	.4292	113.0
85.6	− .7582	.4267	113.5
90.4	− .2361	.3247	113.7
95.2	.01481	.1775	113.4

ω(t) = optimal azimuthal angle
A(t) = coefficient obtained from least squares fit
B(t) = constant obtained from least squares fit
Optimal G for release P5 = .1875
Optimal G for release P7 = .1016
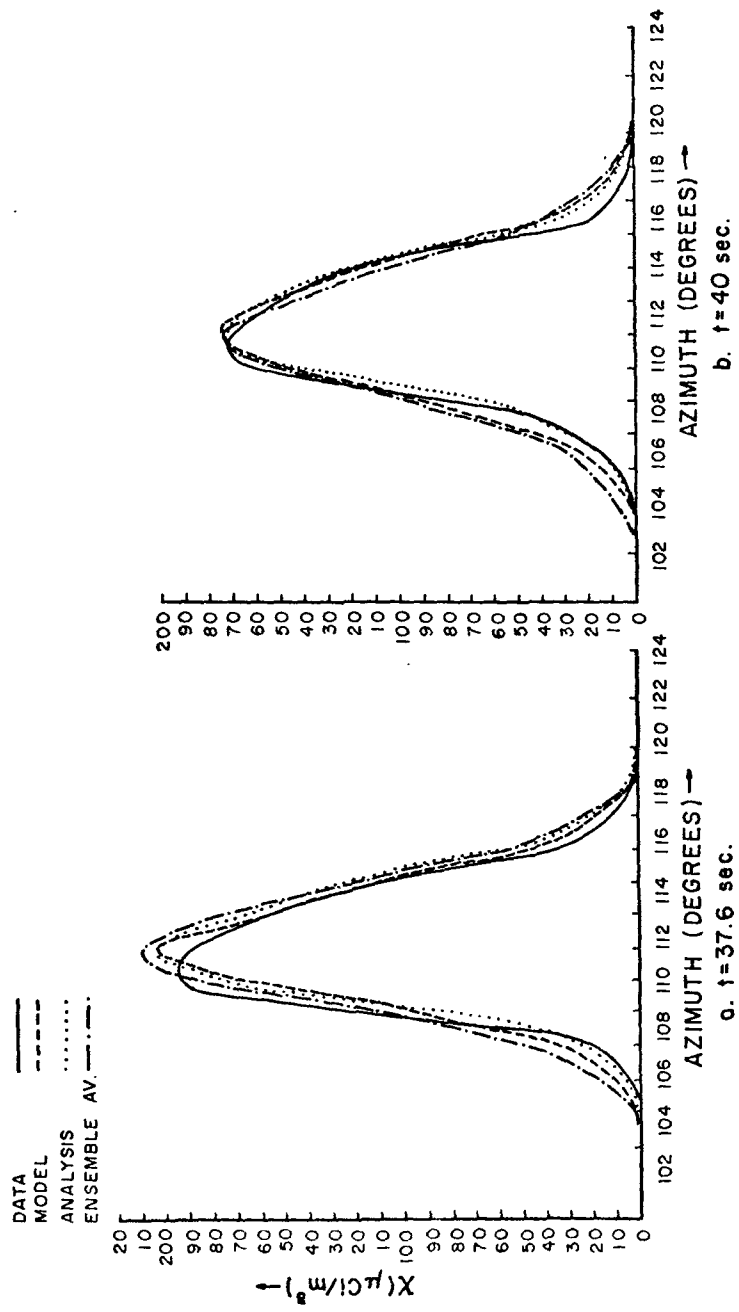
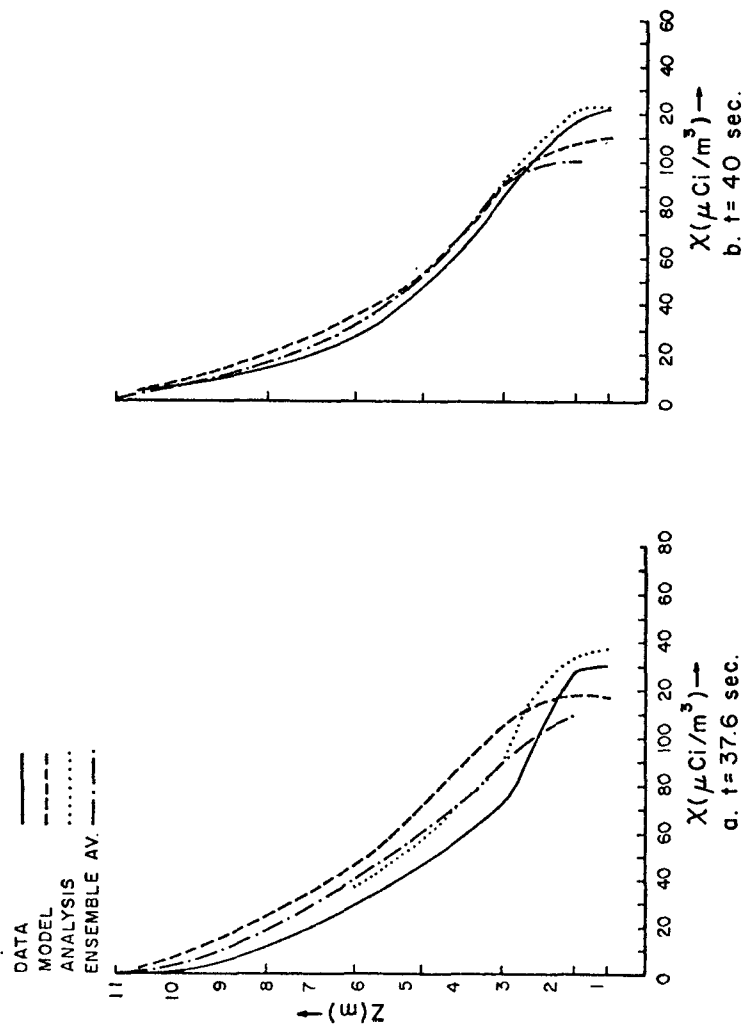Fig. 6. Concentrations at the 1.5 m level for test p5.

30

Fig. 7. Concentration profiles on the 114° azimuth for test P5. Tick marks indicate levels at which observations are taken and/or analyses are performed.
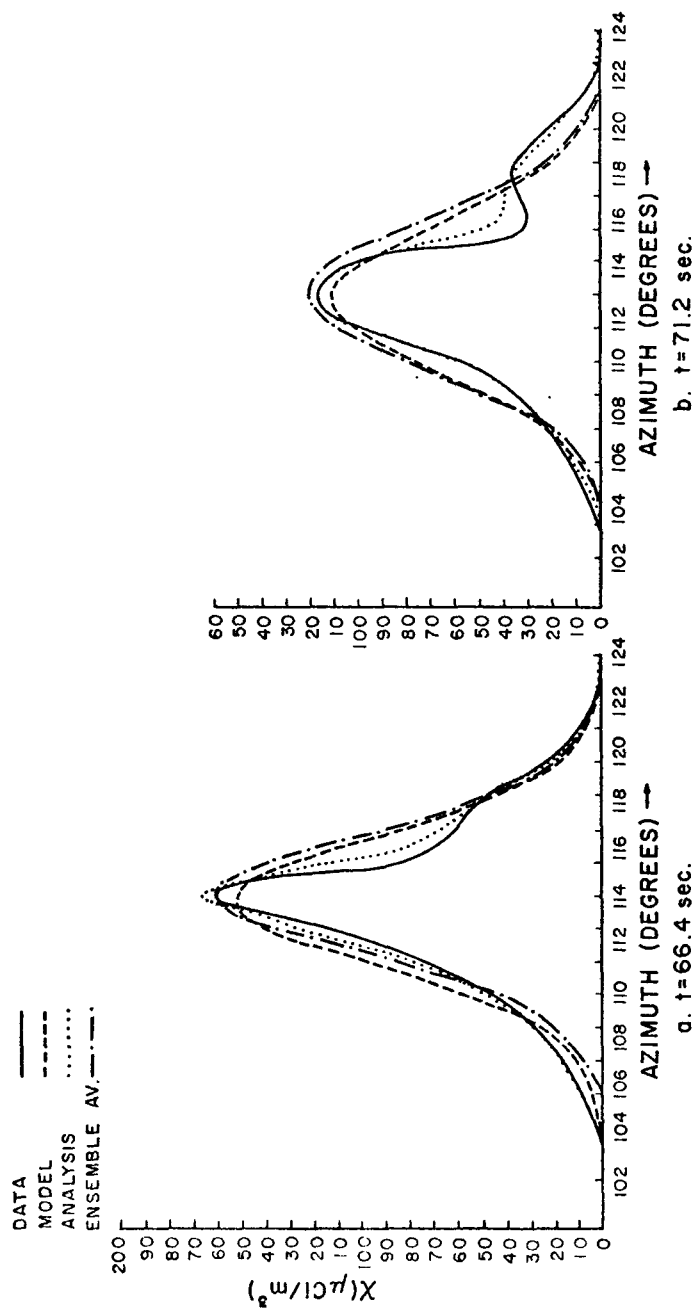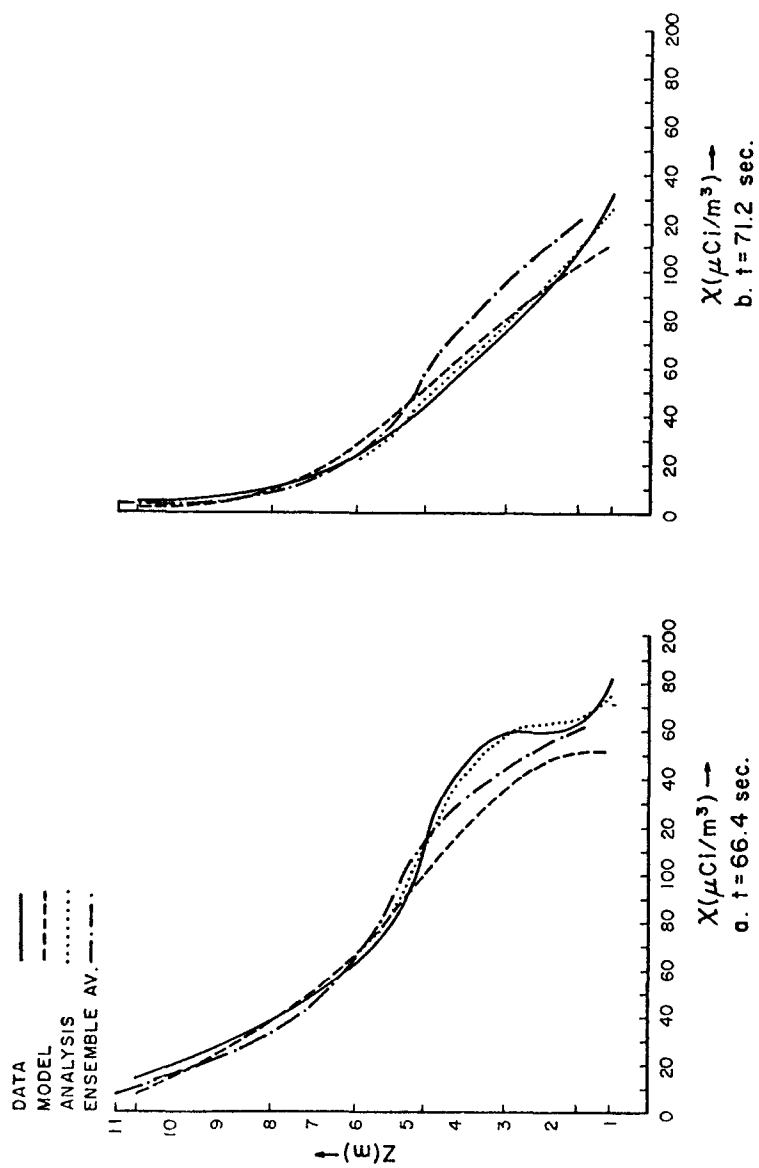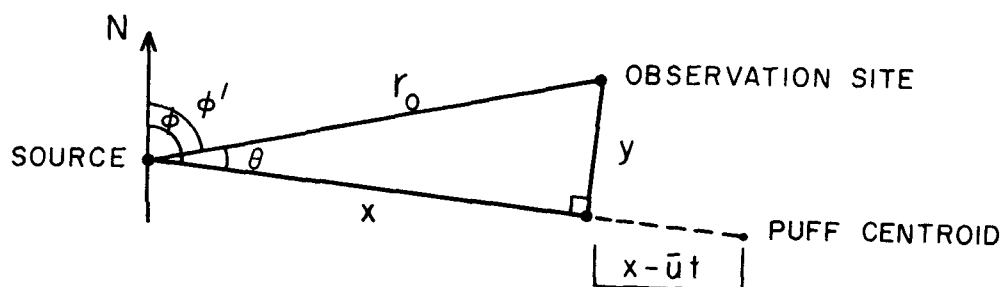
31

Fig. 8. Concentrations at the 1.5 m level for test P7.

Fig. 9. Concentration profiles on the 114° azimuth for test P7.
Tick marks indicate levels at which observations are taken and/or
analyses are performed.

Fig. 10. Relationship between observation and model coordinates. The φ represents the aximuthal angle to the puff centroid, while φ' is the azimuthal angle to the observation site and r_0 is the radial distance to the observation site.
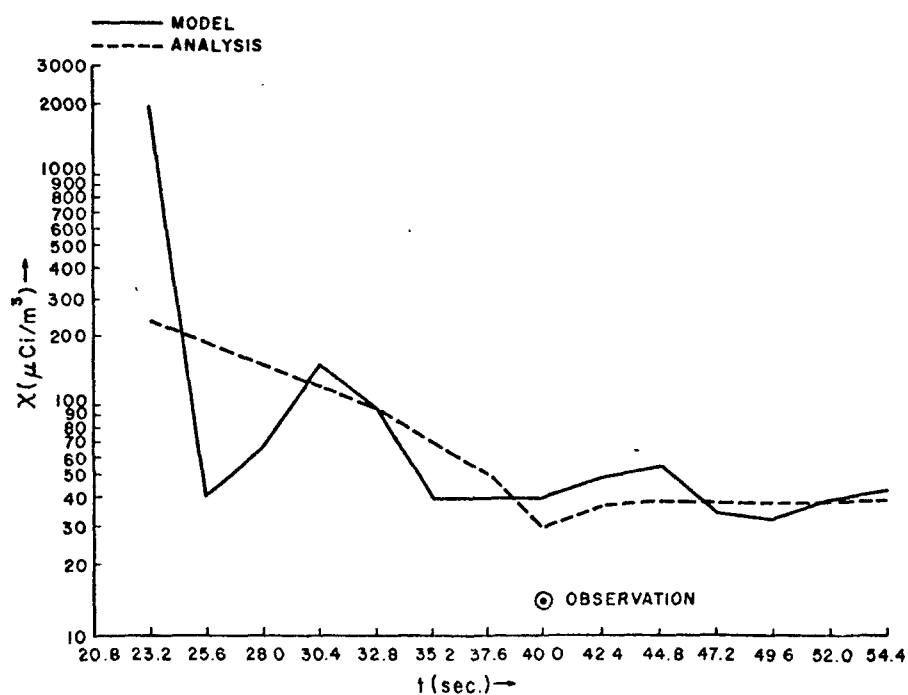

Fig. 11. Concentration profile at grid point 13, 8, 3.

Once the azimuth is evaluated, the position of the obser-
vation sites with respect to the model coordinates may be com-
puted. Therefore, the x and y distances needed in (4) may be
obtained. As shown in Fig. 10, the optimal azimuth is the direc-
tion from the source to the puff centroid. Since the azimuth and
range of the observation site is known, x and y may be determined
from the geometry depicted.

The data on the vertical tower is utilized to obtain the
mean transport wind, $\bar{u}$, as a function of height. G is determined
by the interval-halving technique using data from all the avail-
able times. Not only is it undesirable to obtain G at each time,
it is impossible. Since A(t) has not been optimized, when data
at only one time is used, the quantity $\Sigma(\chi' - \hat{\chi})^2$ is minimized
by forcing G to be either very small or very large, depending
upon whether the puff centroid has reached the measuring arc or
not.

A(t) is the final parameter to be determined. It may be
found using a least squares fit at each observation time. The
regression equation used to obtain A(t) is

$$\hat{\chi} = B(t) + A(t) \chi' , \qquad (45)$$

where χ' is given by (4) with Q' = Q and B(t) is the value of $\hat{\chi}$
on the ordinate. A comparison of Table 6 with Tables 4 and 5
shows that B(t) is very small in comparison with the observed
concentrations in the vicinity of the puff centroid, and may
therefore be ignored. As seen in Table 6, A(t) generally de-
creases with travel time. Due to the nature of A(t) (see Eq.
(2)), the decrease is most likely a result of the puff losing
mass as it proceeds downwind. However, if the puff were Gaus-
sian, residing on the surface, and totally scavenged upon en-
countering the ground, A(t) could not be less than one. When
the centroid of a Gaussian puff is on the surface, the mass flux
must be away from the surface, towards lower concentrations.
Only the concentration in the lower half of the theoretical puff
is considered scavenged. If no absorption occurs, then the
tracer is reflected from the surface and A(t) = 2.

Since the optimal A(t) is generally less than one, the
Gaussian model with the puff centroid on the surface cannot fit
the data very effectively because there must be some mass flux
towards the surface. As seen in Figs. 6 and 8, the tracer puff
is reasonably Gaussian in the horizontal. However, in the verti-
cal, the puff is somewhat non-Gaussian. The data shows that in
the forward portion of the puff there is a concentration gradient
towards the surface. This is reflected in the model, and is one
of the reasons it was decided to depart from the Gaussian verti-
cal profile.

The optimal A(t) in Table 6 decreases in a somewhat

35

irregular manner and at times actually increases. Due to irregularities in the tracer puff, A(t) is forced to behave erratically in order to fit the data as closely as possible at each observation time using the least squares procedure.

Figs. 6 to 9 show that the model does a good job of fitting the data in the horizontal; an acceptable fit in the vertical is also obtained. Since the puff is not normally distributed in the vertical, it is more difficult to model the vertical concentration profile. For example, in experiment P5, the data shows that until t = 32.8 sec, when the forward portion of the puff resided over the 200 m measuring arc, concentrations aloft consistently exceed those at the .8 m level. However at t = 35.2 sec, the concentration at the .8 m level greatly exceeds those aloft (see Table 4). The model is not capable of changing the vertical profile in such a rapid manner. However, at t = 40 sec in Fig. 7, the .8 m model concentration has become larger than those at higher levels. At longer travel times the concentration at the .8 m level is always the greatest. Therefore, the concentration in the central and rearward portions of the puff is largest near the surface while in the forward portions of the puff the concentration is largest aloft.

COMBINING MODEL DATA AND OBSERVATIONS

In order to reduce some of the irregularities in the model, an analysis combining both model and measured data is performed. The resulting concentrations are to be utilized in the determination of ensemble averaged concentration estimates. These estimates, along with estimates of the tracer fluxes will be forced to conform to the diffusion equation, Eq. (5), in which the local time rate of change of concentration is one of the most important terms. It is therefore imperative that the grid point concentrations change smoothly in time, if reasonable fluxes are to be obtained. Since the puff centroid's position fluctuates, and A(t) changes in an erratic manner, the model concentrations at a grid point exhibit a high amplitude, short period fluctuation, as shown in Figs. 11 and 12. Therefore, it is necessary to impose a low pass filter in time on the data in order to damp out the short period fluctuations.

As seen in Table 6, there are times when A(t) actually increases rather than decreases. This suggests that some source has added to the tracer mass in the puff at that time. This, however, is unreasonable, since the only source of tracer is at the initial time. Smoothing in time eliminates the bogus sources.

Figs. 6-9 show that the model does not conform to the observations exactly. Therefore, it is desirable to design the filter such that there is a tendency to force the analysis towards the collected data. This may be accomplished by using a
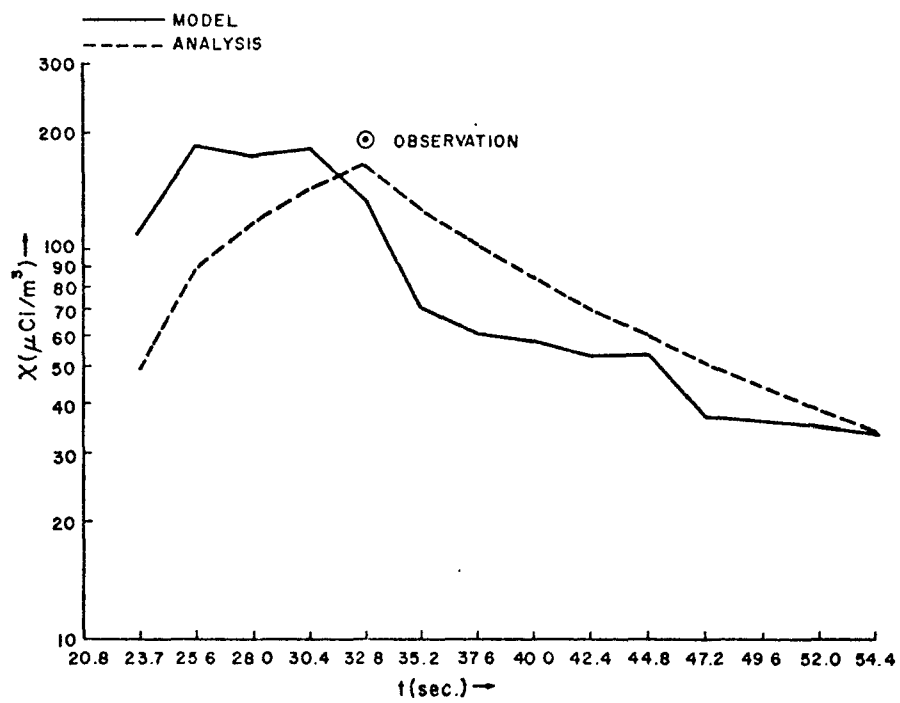
36

Fig. 12. Concentration profile at grid point 16, 7, 5.

higher observational weight at grid points where data is available. However, it is more important that the resulting analysis be smooth, rather than conform to the data. Therefore, filtering weights are chosen such that the analyses do not always conform to the data exactly. However, Figs. 6-9 show that in general the analyses are closer to the data than the model is.

The concentration model cannot account for many of the mechanisms by which a puff disperses. For example, a backing or veering wind will tilt the puff. This produces a disparity between the model and the tracer puff, which can exist for a significant length of time. Since the amount of data available is minuscule, it is desirable to equip the analysis with a "memory", so that model-data differences in a certain region of the puff are "remembered" for a short time before and after the observation time. This may be accomplished using a quasi-Lagrangian coordinate system, moving with a mean wind speed. The time filtering alters the analysis at a grid point, which maintains its relative position in the puff, at times other than the observation time. This is particularly evident in Fig. 12, where the dotted line represents the analysis with a larger weight attached to the observational constraint when data is available. The effect is also present, although not so noticeable, in Fig. 11. This effect cannot be produced in an Eulerian coordinate system, because the puff moves through the grid points, so that a specific grid point does not retain its relative position within the puff.

Since transport wind speed shear is accounted for in the model, the puff remains stationary within the Lagrangian coordinate system only at the 1.5 m level. However, because the shear is small and the time span over which the "memory" acts is generally short, the effect of the speed shear upon the analysis is negligible. Furthermore, the puff is free to move laterally within the grid system. This will also shift the puff centroid with respect to the grid points. However, the large time filtering does not allow the puff centroid to shift very rapidly. Therefore, the time filtering has the additional effect of forcing the Lagrangian coordinate system to maintain its relative position with respect to the puff centroid, and the inclusion of observations into the analysis tend to distort the analyzed puff from its Gaussian shape as well as dictate the position of the puff centroid. It is important that the puff centroid remain reasonably stationary with respect to the coordinate system, otherwise it will be impossible to separate the effects of diffusion on the puff concentration from the effects of advection.

Since measuring devices are located on vertical towers on arcs of 200 and 800 m radii from the source, a cylindrical coordinate system seems appropriate, because observation sites may then be placed on grid points in an Eulerian system. In a Lagrangian system, however, the observations can be placed closer

to grid points using a rectangular coordinate system, except near the time the puff centroid is at an observation site. As the origin of the cylindrical coordinate system moves, the range and azimuth to an observation site changes. Therefore, distances between grid points in the vicinity of a stationary measuring arc are continuously changing. At the end of the grid farthest from the origin, the grid spacing is much larger than the distance between observation sites, while at the near end the distance is much less than that between the sites.

The narrow tracer puffs may be confined to 11 observation sites on the 200 m arc. The analysis is shown observations only from these sites. Since the arc from which observations are utilized is so short, it can be approximated by a straight line. Using a properly oriented Lagrangian cartesian coordinate system with a grid row always located at 199 m from the source, the distance between the nearest grid point and an observation site are much less than a meter in the y direction, and between .3 and 1.7 m in the x direction. Therefore, observations may be assigned to the nearest grid point with little loss of validity.

In order to spread the effects of the observations and mesh them with the concentration model, smooth spatial gradients are required. Therefore, spatial as well as temporal filtering must be accomplished. The analysis system is incorporated in the variational functional:

$$J = \int_V \int_t \{\alpha_1 (\bar{\chi} - \tilde{\chi})^2 + \alpha_2 (\frac{\partial \bar{\chi}}{\partial x})^2 + \alpha_3 (\frac{\partial \bar{\chi}}{\partial y})^2$$

$$+ \alpha_4 (\frac{\partial \bar{\chi}}{\partial z}) + \alpha_5 (\frac{\partial \bar{\chi}}{\partial t})^2 \} \, dv \, dt \, . \qquad (46)$$

The functional is minimized and appropriate boundary conditions are applied to obtain the second order linear partial differential equation

$$\alpha_2 \frac{\partial^2 \bar{\chi}}{\partial x^2} + \alpha_3 \frac{\partial^2 \bar{\chi}}{\partial y^2} + \alpha_4 \frac{\partial^2 \bar{\chi}}{\partial z^2} + \alpha_5 \frac{\partial^2 \bar{\chi}}{\partial t^2} - \alpha_1 \bar{\chi} + \alpha_1 \tilde{\chi} = 0 \, . \qquad (47)$$

Since this Euler equation is elliptic, it may be finite-differenced and solved numerically using an over-relaxation technique. Because the measuring devices are not equally spaced on the towers, the finite-difference scheme must take into account the non-equal grid spacing. The finite-differencing schemes used in this research are reviewed in Appendix B, and the derivation and solution of the finite-difference form of (47) is discussed in Appendix C.

FILTERING CHARACTERISTICS

The filtering characteristics of (47) may be examined by

defining a response function, R, where

$$R \equiv \bar{A}/\tilde{A} \ . \tag{48}$$

$\bar{A}$ is the amplitude of the filtered analysis, and $\tilde{A}$ is the amplitude of the observations.

Using

$$\bar{\chi} \equiv \bar{A} \ e^{i(kx \ + \ \ell y \ + \ \ell z \ + \ \nu t)}$$

and

$$\tilde{\chi} \equiv \tilde{A} \ e^{i(kx \ + \ \ell y \ + \ \ell z \ + \ \nu t)} \ , \tag{49}$$

where $k \equiv \dfrac{2\pi}{L_x}$, $\ell \equiv \dfrac{2\pi}{L_{y \ or \ z}}$,   and $\nu \equiv \dfrac{1}{T_o}$,

$L_x \equiv$ wavelength, downwind direction, $L_{y \ or \ z} \equiv$ wavelength in the transverse directions and $T_o \equiv$ period, a response function may be obtained by substitution of (49) into (47), using the definition (48); thus,

$$R = 1/(1 \ + \ \alpha_2/\alpha_1 \ k^2 \ + \ 2 \ \alpha_3/\alpha_1 \ell^2 \ + \ \alpha_4/\alpha_1 \ \nu^2) \ . \tag{50}$$

The filter's response is shown in Figs. 13 and 14. The weight ratios in Fig. 13 are those used when the observation consists of model data, and those in Fig. 14 are utilized when measured concentrations are available. As shown in Fig. 13a, long wavelength, low frequency waves pass through the filter relatively undamped. The period of the "large scale" tracer distribution in a Lagrangian coordinate system is nearly infinite, since the coordinate system moves with the puff as it diffuses. The wavelength of the large scale distribution is about 400 m in the downwind direction when the puff is 200 m from the source. (The Gaussian distribution is about half this size.) In the transverse directions the wavelength is about 100 m.

Fig. 13a shows that long wavelength, high frequency (short period) waves are considerably damped. The high frequencies are caused by the method of determining the puff's azimuthal position and the least square coefficient, and should be minimized. High frequency waves are of small amplitude in the observations, due to the incremental averaging time. A comparison of Figs. 13a-d show that the shorter the transverse wavelength, the more the wave's amplitude is damped. Short waves are created by differences between the observed and model values, and must be eliminated, to the extent possible, by changing the model values.

The response obtained when measured concentrations are available shows that comparatively little damping occurs. Fig. 14a shows little amplitude decrease for waves considerably
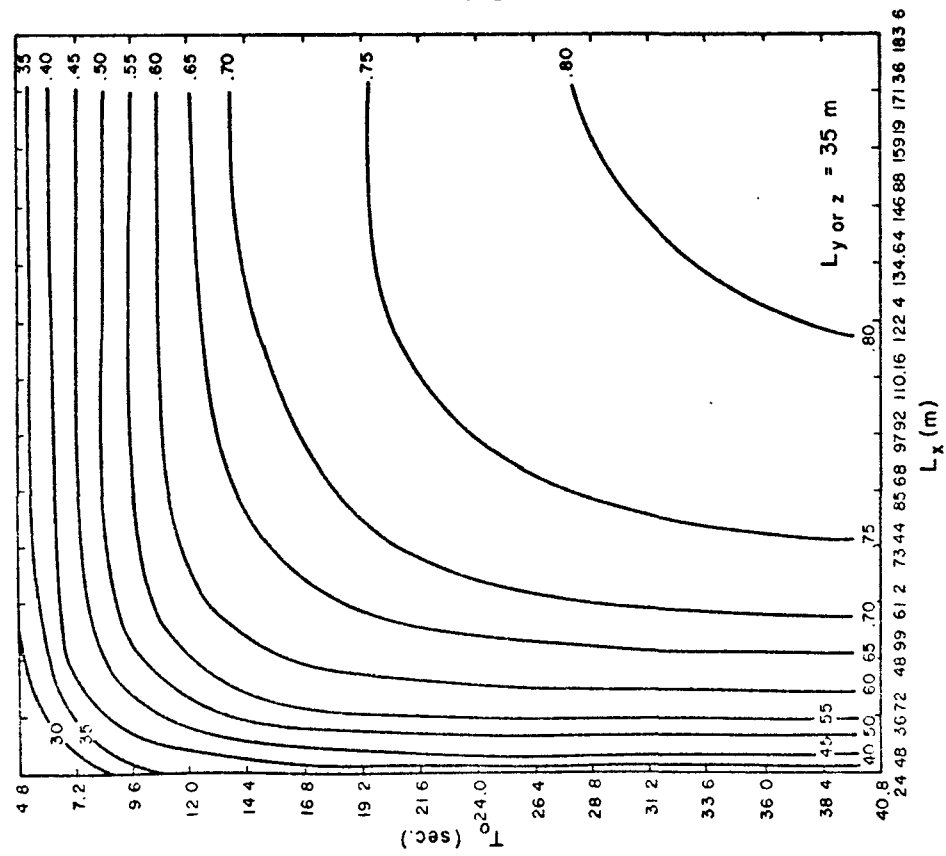
40

Fig. 13a. Response function using $\alpha_2/\alpha_1 = 20$, $\alpha_3/\alpha_1 = 2.5$ and $\alpha_4/\alpha_1 = 50$.
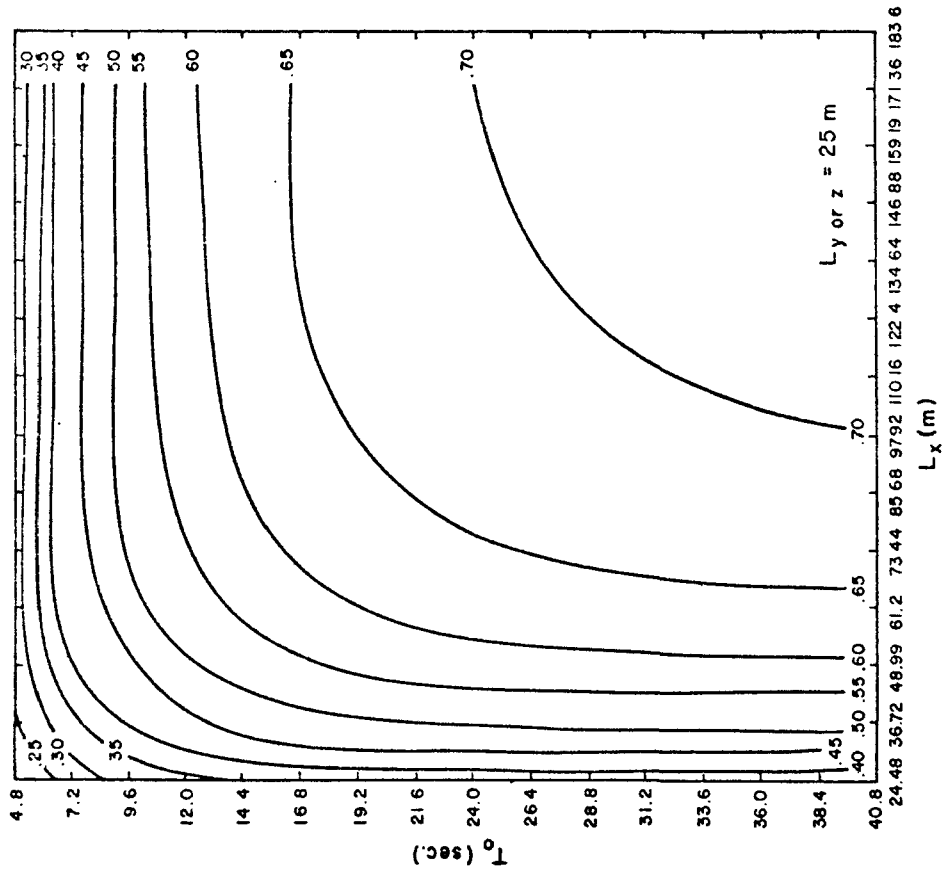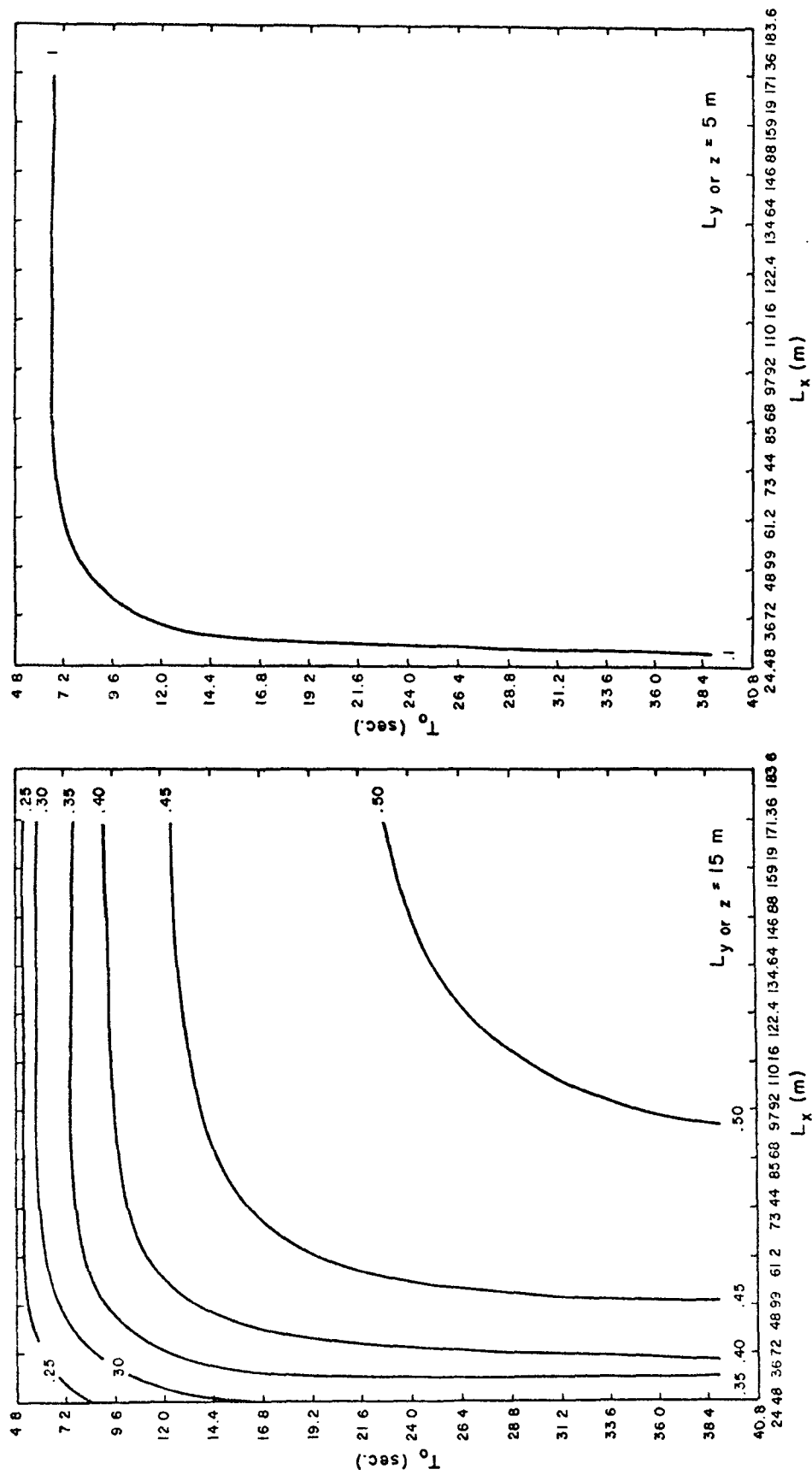
Fig. 13b. Same as Fig. 13a except $L_{y \text{ or } z} = 25m$.

41

Fig. 13c. Same as Fig. 13a except $L_{y \text{ or } z}$ =15m. Fig. 13d. Same as Fig. 13a except $L_{y \text{ or } z}$ = 5m.
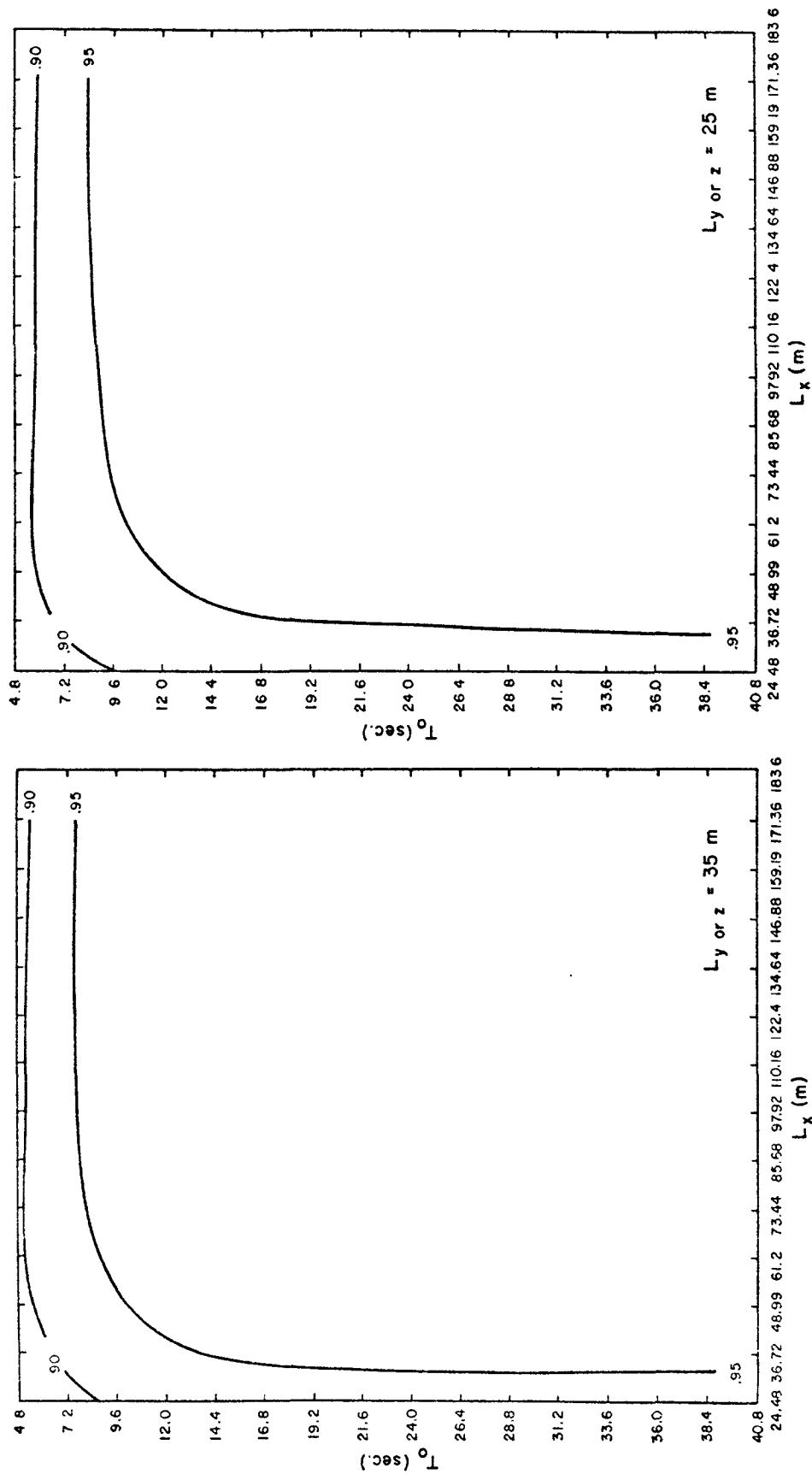
42

Fig. 14a. Response function using $\alpha_2/\alpha_1 = 1.$, Fig. 14b. Same as Fig. 14a except L_y or $z = 25m$. $\alpha_3/\alpha_1 = .125$ and $\alpha_4/\alpha_1 = 2.5$.
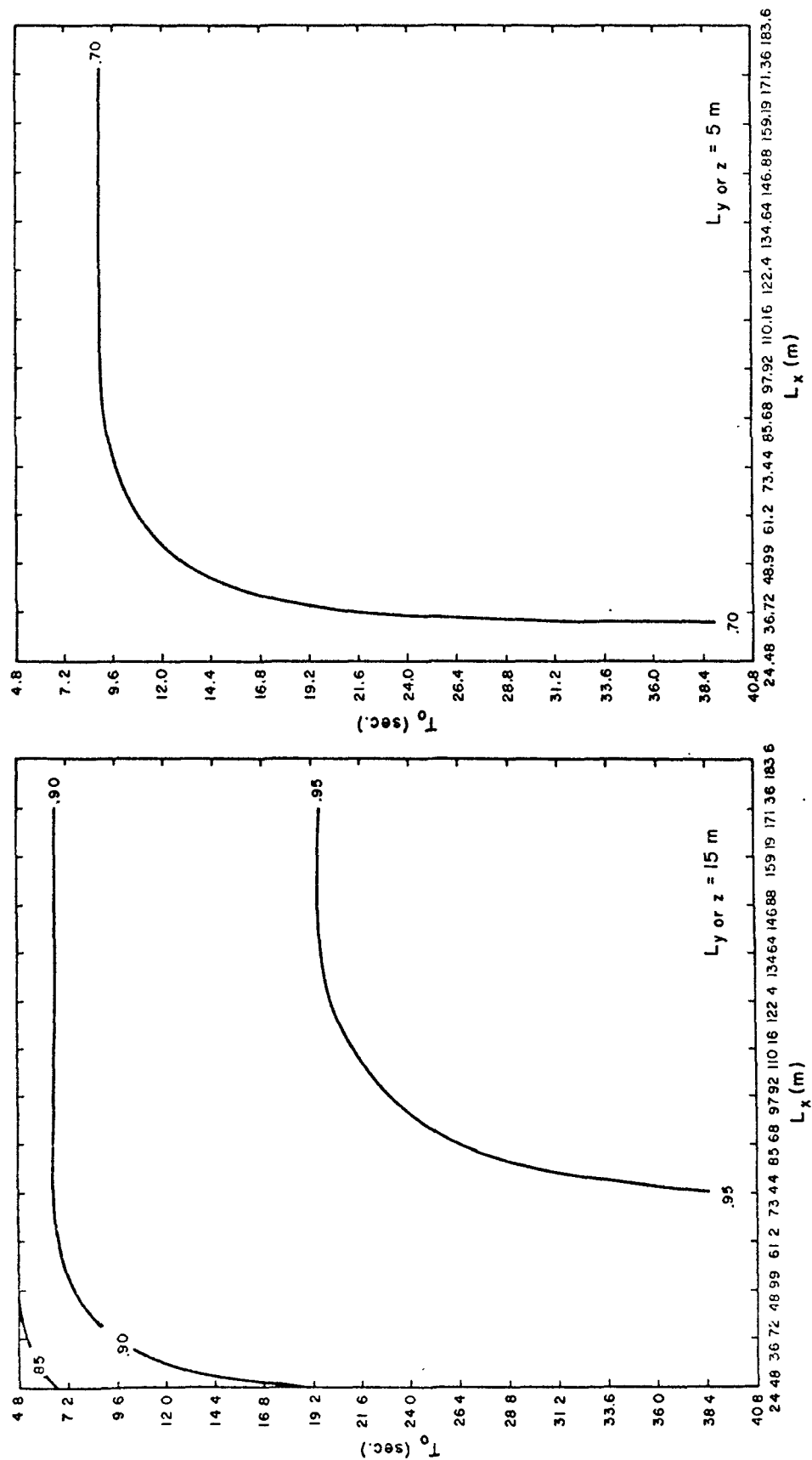
43

Fig. 14c. Same as Fig. 14a except $L_{y \text{ or } z}$ = 15m. Fig. 14d. Same as Fig. 14a except $L_{y \text{ or } z}$ = 5m.

44

smaller than the large scale distribution. This allows the anal-
ysis to conform to the observations more closely. A comparison
of Figs. 14a-d show that as the transverse wavelength decreases
the filtered amplitude also diminishes. This is desirable, since
the observed data shows short wave fluctuations which should be
damped to a certain extent in order to produce a smoother anal-
ysis.

BOUNDARIES

The concentration boundaries utilized in this analysis
technique are composed of generated data. The top and side
boundaries cause no problem, because the puff is completely con-
tained within these boundaries. However, the temporal and bottom
boundaries have a noticeable effect upon the analysis. The ef-
fect of the initial time boundary, computed at a travel time of
20.8 seconds, may be seen in Figs. 11 and 12. The heavy temporal
filtering forces the analysis away from the model value, towards
the boundary value. This is one of the reasons that further
analyses are performed at times as far from the temporal bound-
aries as possible. The high amplitude, short period fluctuations
observed in Fig. 11 near the initial time indicates that the op-
timal azimuth obtained when the puff centroid is far from the
measuring arc may not be a good estimate of the centroids true
position. A considerable amount of puff meander would be re-
quired to produce this effect. This is another reason for not
using the analyses close to the boundaries.

ANALYZED CONCENTRATIONS

The analyzed concentrations are reasonably close to those
observed during the time period of interest. This may be seen
by a comparison of Tables 7 and 8 with 4 and 5, respectively.
However, the azimuth of maximum concentration changes more rap-
idly in the data than in the analysis in test P5, a result of
the temporal filtering. The analyzed concentrations are closer
to those observed in test P7. One reason is the aximuth of max-
imum concentration changes more slowly in this case.

The analyzed concentrations differ from the model values
in several respects. The shape of the distributions in both the
horizontal and the vertical are very similar, but differences due
to the inclusion of observations are evident. Fig. 15 shows the
analyzed concentration on the 1.5 m level, where most of the ob-
servations were taken, for the six central time periods in test
P5. In each of these analyses, observations were available on
one entire grid row. At t = 32.8 sec, the data is on the third
grid row downwind of the puff center. At t = 44.8 sec, the data
is on the third grid row upwind of the puff center. The grid
length is chosen such that data is assigned to consecutive grid
rows at each new time. Since the weight assigned to data obser-
vations is much larger than that assigned to model observations,

45

Table 7. Analyzed concentrations for test P5 when the puff centroid is near the 200 m measuring arc.

a. Concentrations $(\mu Ci/m^3)$ at the 1.5 m level

	Azimuth (degrees)										
Time	104	106	108	110	112	114	116	118	120	122	124
32.8	1	5	48	115	184	190	63	9	3	2	0
35.2	1	6	51	151	220	144	56	8	3	1	0
37.6	1	6	40	171	194	134	41	7	1	1	0
40.0	2	13	51	150	167	121	30	6	1	1	0
42.4	2	7	23	95	114	93	33	6	2	1	0
44.8	2	6	20	75	106	63	45	9	3	1	0

b. Concentrations $(\mu Ci/m^3)$ at the 114° azimuth

	Level (m)		
Time	.8	3	6.1
32.8	193	191	164
35.2	159	111	61
37.6	137	89	37
40.0	123	91	31
42.4	105	77	34
44.8	76	40	18

Table 8. Analyzed concentration for test P7 when the puff centroid is near the 200 m measuring arc.

a. Concentrations ($\mu Ci/m^3$) at the 1.5 m level

					Azimuth (degrees)						
Time	104	106	108	110	112	114	116	118	120	122	124
56.8	0	0	3	35	134	212	123	26	13	5	0
61.6	0	1	6	24	101	216	109	55	23	8	1
66.4	1	11	22	52	101	165	80	49	18	4	0
71.2	2	12	26	55	109	110	43	36	18	3	0
76.0	2	7	25	59	70	72	36	22	6	1	0
80.8	1	3	9	32	33	44	22	12	6	2	1

b. Concentrations ($\mu Ci/m^3$) at the 114° azimuth

	Level		
Time	.8m	3m	6.1m
56.8	216	223	231
61.6	223	214	89
66.4	174	158	65
71.2	126	79	22
76.0	86	45	18
80.8	47	36	7
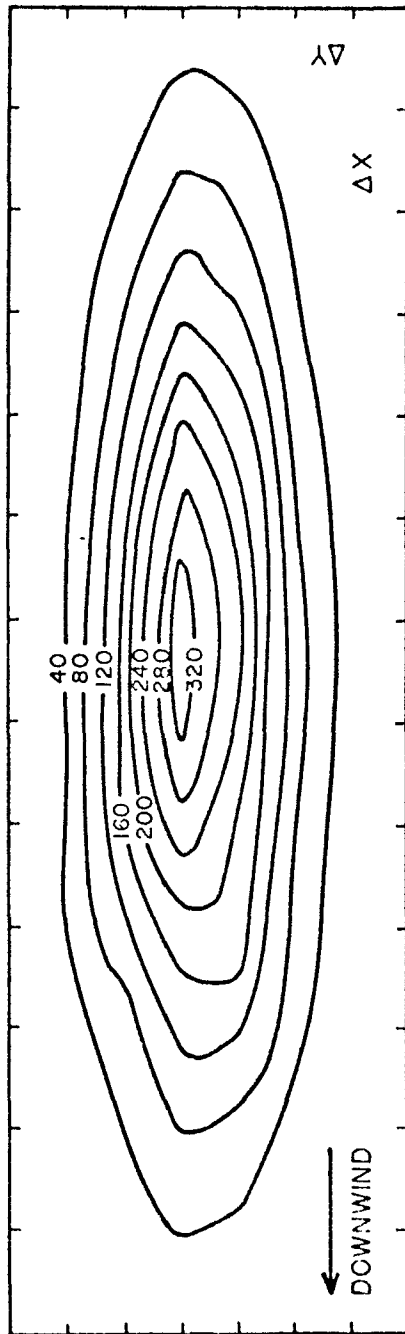
Fig. 15a. Analyzed concentration at the 1.5m level for puff P5. The maximum concentration is 344 $\mu Ci/m^3$, t = 32.8 seconds, Δx = 12.24 m and Δy = 6.95 m.
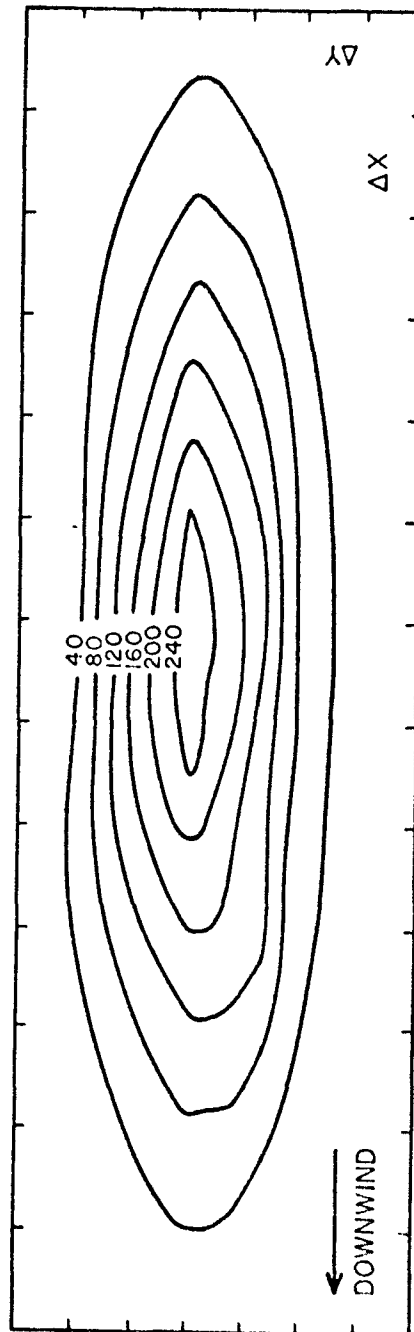
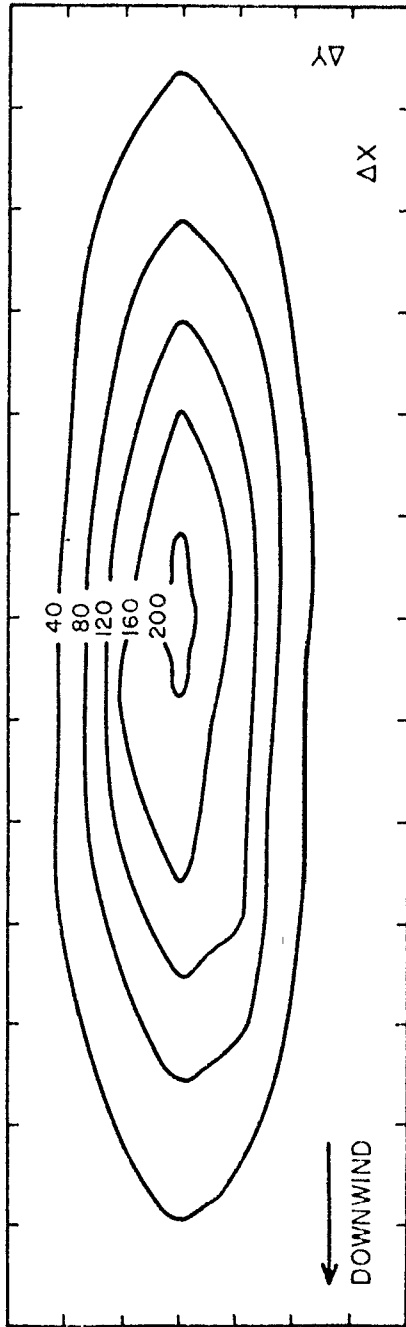Fig. 15b. Same as Fig. 15a except the maximum concentration is 275 $\mu Ci/m^3$ and t = 35.2 seconds.

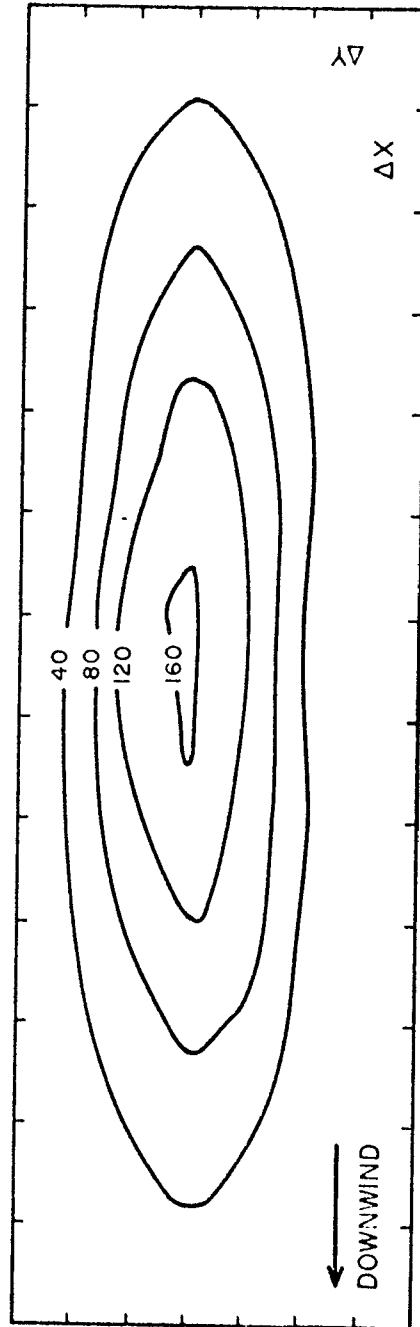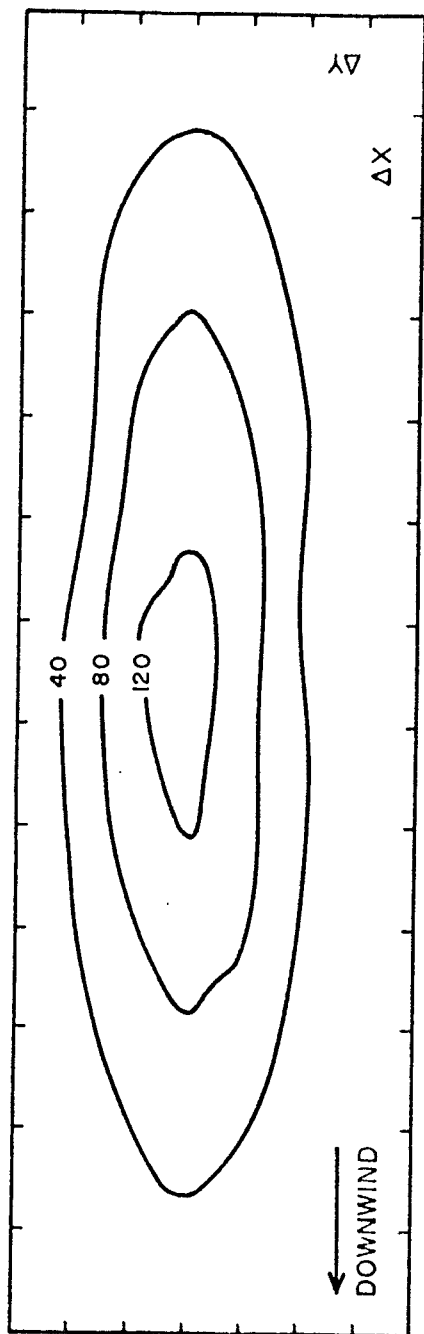Fig. 15c. Same as Fig. 15a except the maximum concentration is 217 μCi/m^3 and t = 37.6 seconds.

Fig. 15d. Same as Fig. 15a except the maximum concentration is 167 μCi/m^3 and t = 40.0 seconds.

Fig. 15e. Same as Fig. 15a except the maximum concentration is
138 $\mu Ci/m^3$ and t = 42.4 seconds.
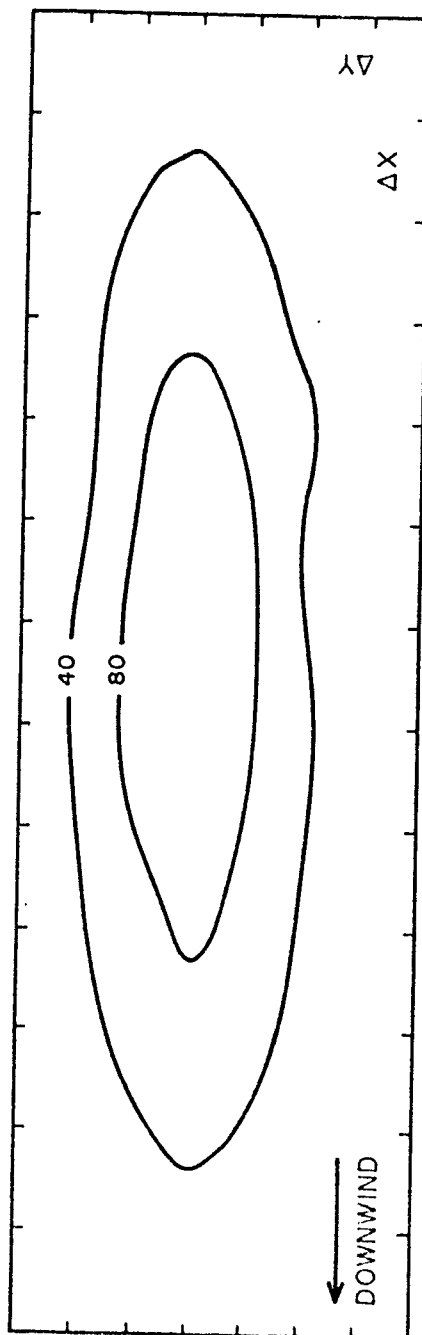
Fig. 15f. Same as Fig. 15a except the maximum concentration is
114 $\mu Ci/m^3$ and t = 44.8 seconds.

there is a tendency to induce short waves in the analysis. However, inspection of Figs. 15a-f shows that with the weighting system used this effect is not very noticeable.

Fig. 16 contains the analyses for the six central times at the 6.1 m level. A comparison with Fig. 15 shows the effect of wind speed shear. In Fig. 16 the maximum concentration is displaced considerably windward. A comparison of the two figures further shows that the maximum concentration at the 6.1 m level is displaced towards the right with respect to the maximum concentration at the 1.5 m level. This is due to the extremely high concentration observed at the 6.1 m height on the 114° tower at t = 32.8 sec. Fig. 12 shows that this observation forces the analyzed concentration to be much larger than the model concentration at times later than 32.8 sec at this quasi-Lagrangian grid point. However, Table 4 shows that at later times the concentration is much lower at this observation site. Therefore, at positions nearer to and upwind from the puff centroid, the concentration is much smaller, so the combined observations produce a distinct bulge in the right front quadrant of the puff.

These analyses are consistent with the concept under which the analysis scheme was devised: namely, that the abrupt changes in concentration distribution are due to a combination of meander of the puff centroid and irregularities in the puff distribution. Fig. 16 indicates that the analysis exhibits a distinct departure from the Gaussian distribution, especially at the shorter travel times. Furthermore, the puff centroid is still allowed to meander, as shown in Table 9a. Comparison with Table 6a shows that the meander is considerably damped by the analysis scheme, however.

Figs. 17 and 18 show that the analyses for the six observation times closest to the time that the puff P7 centroid passes the measuring arc, at the 1.5 and 6.1 m levels, respectively. Note that the tracer is more nearly normally distributed in this case. As with puff P5, the concentration aloft is greatest forward of the puff centroid. This is demonstrated again in Table 5. The observed concentration at the 6.1 m level is much larger at t = 56.8 sec than at the following times. The combined effect of wind shear and surface scavenging has again distorted the puff so that its distribution is no longer Gaussian in the vertical.

Even though puff P7 traveled for a much longer time to reach the 200 m measuring arc, its concentration is comparable to that of puff P5, because the puff is diffusing more slowly in the former case. The puff appears to be losing mass due to more rapid scavenging in test P7, but this is partly due to the fact that the time interval between observations is twice as large as in the other case.
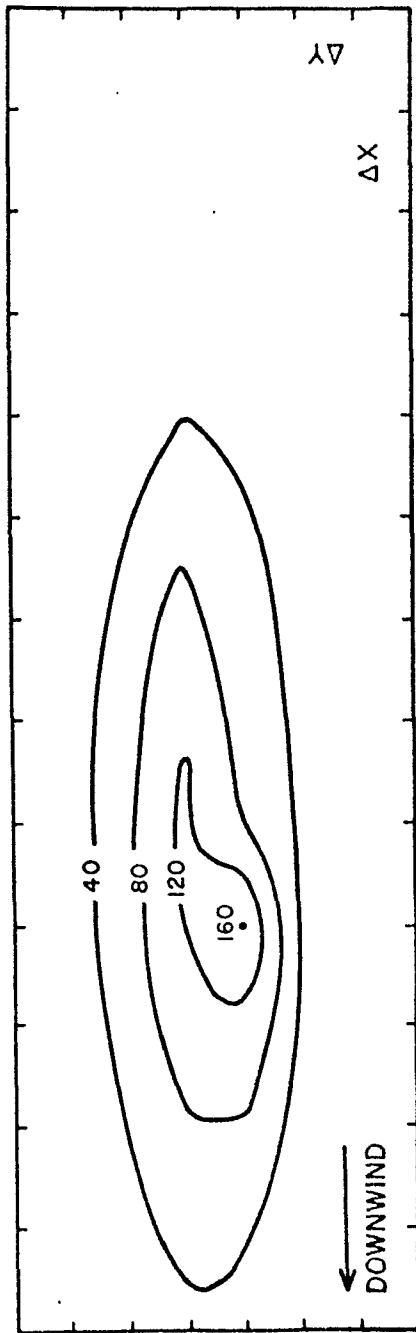
Fig. 16a. Analyzed concentration at the 6.1m level for puff P5. The maximum concentration is **164** $\mu Ci/m^3$, t = 32.8 seconds, $\Delta x = 12.24m$ and $\Delta y = 6.95m$.

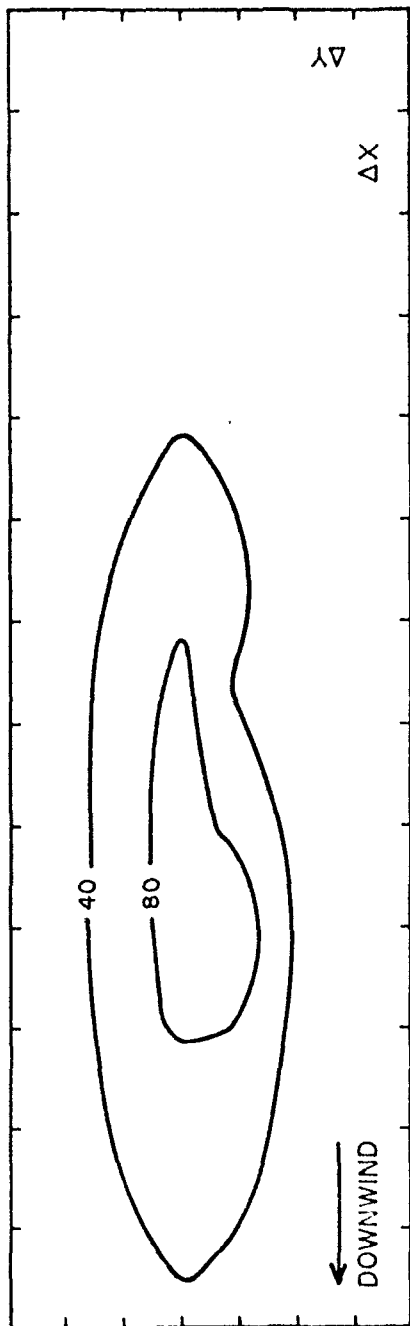Fig. 16b. Same as Fig. 16a except the maximum concentration is 129 $\mu Ci/m^3$ and t = 35.2 seconds.

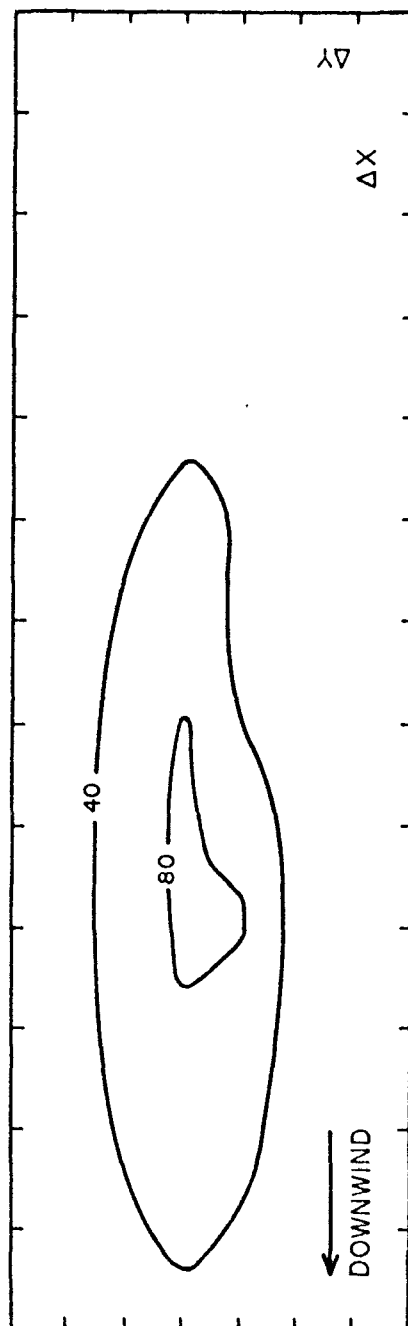Fig. 16c. Same as Fig. 16a except the maximum concentration is 103 μCi/m³ and t = 37.6 seconds.

Fig. 16d₃ Same as Fig. 16a except the maximum concentration is 87 μCi/m³ and t = 40.0 seconds.
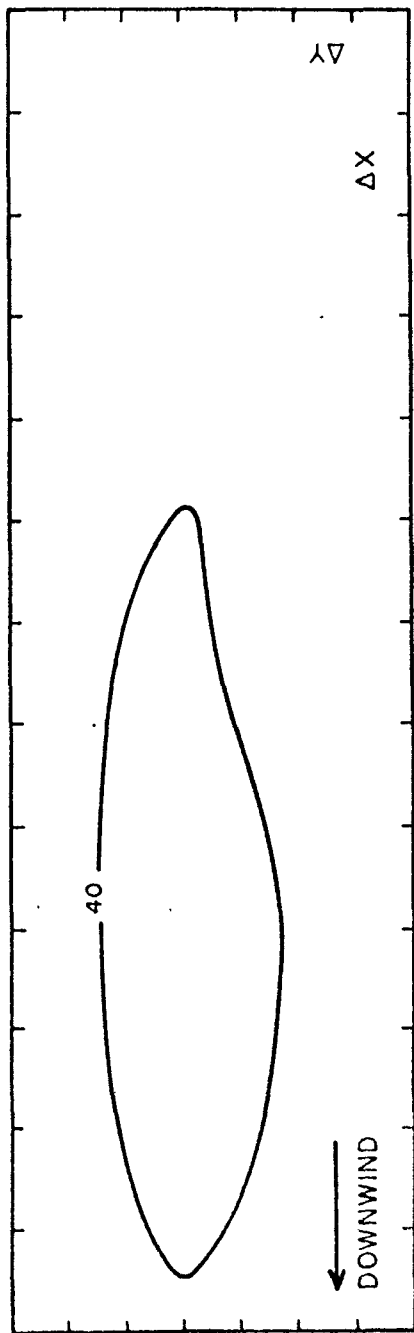
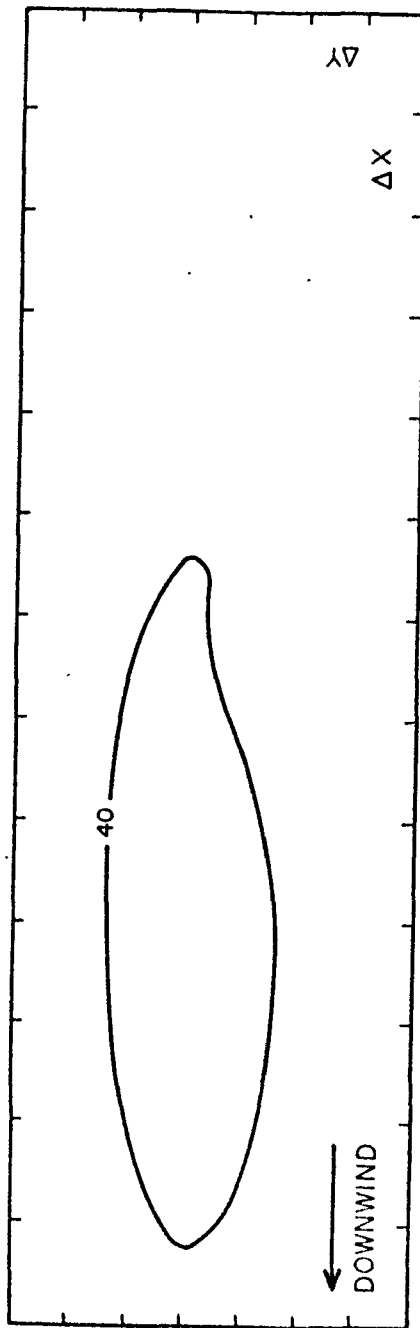Fig. 16e. Same as Fig. 16a except the maximum concentration is 75 $\mu Ci/m^3$ and t = 42.4 seconds.

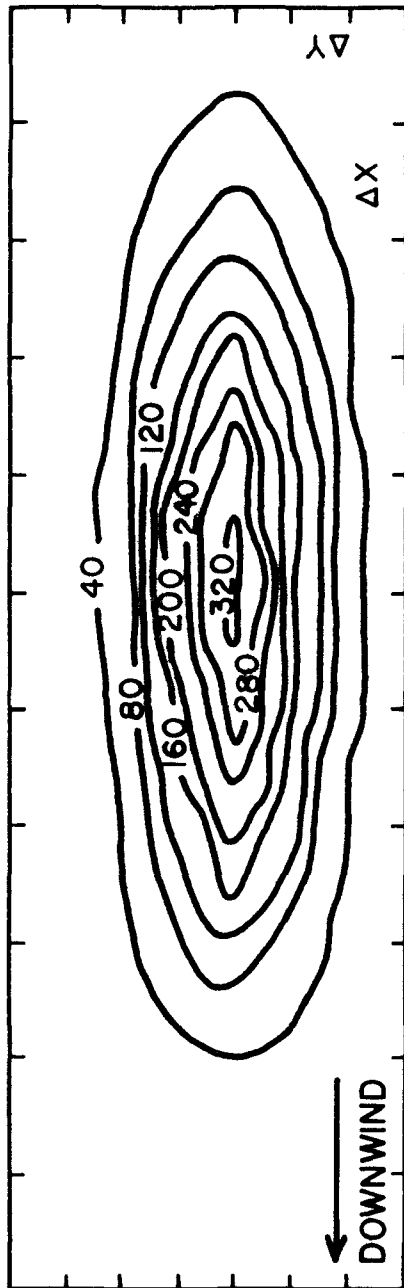Fig. 16f. Same as Fig. 16a except the maximum concentration is 65 $\mu Ci/m^3$ and t = 44.8 seconds.

Fig. 17a. Analyzed concentration at the 1.5m level for puff P7. The maximum concentration is 347 μCi/m^3, t = 56.8 seconds, Δx = 14.4m and Δy = 6.95m.
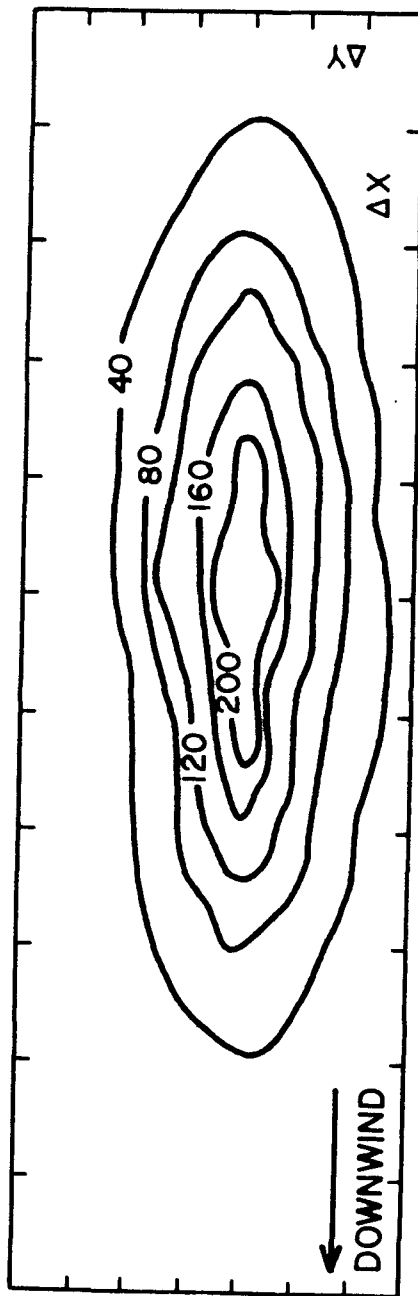

Fig. 17b. Same as Fig. 17a except the maximum concentration is 238 μCi/m^3 and t = 61.6 seconds.

Fig. 17c. Same as Fig. 17a except the maximum concentration is 165 µCi/m³ and t = 66.4 seconds.

Fig. 17d. Same as Fig. 17a except the maximum concentration is 122 µCi/m³ and t = 71.2 seconds.

Fig. 17e. Same as Fig. 17a except the maximum concentration is 94 μCi/m^3 and t = 76 seconds.

Fig. 17f. Same as Fig. 17a except the maximum concentration is 74 μCi/m^3 and t = 80.8 seconds.

Fig. 18a. Analyzed concentration at the 6.1 m level for puff P7. The maximum concentration is 231 $\mu Ci/m^3$, t = 56.8 seconds, Δx = 14.4 m and Δy = 6.95 m.
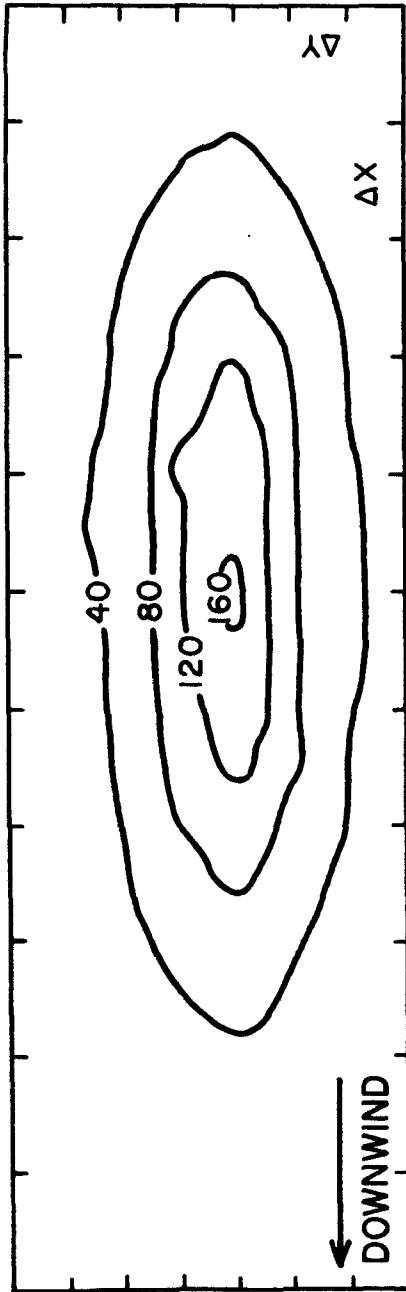
Fig. 18b. Same as Fig. 18a except the maximum concentration is 163 $\mu Ci/m^3$ and t = 61.6 seconds.

58

Fig. 18c. Same as Fig. 18a except the maximum concentration is 117 μCi/m^3 and t = 66.4 seconds.
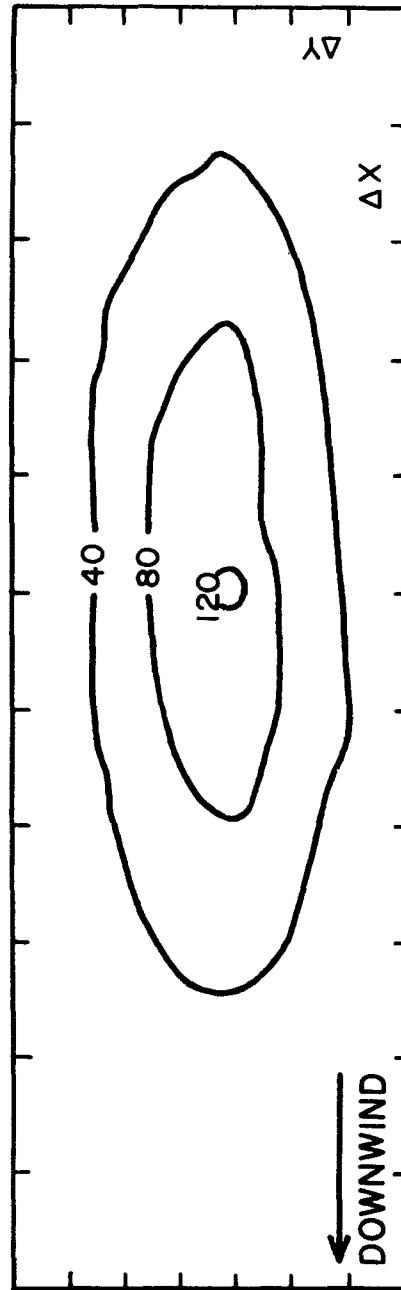
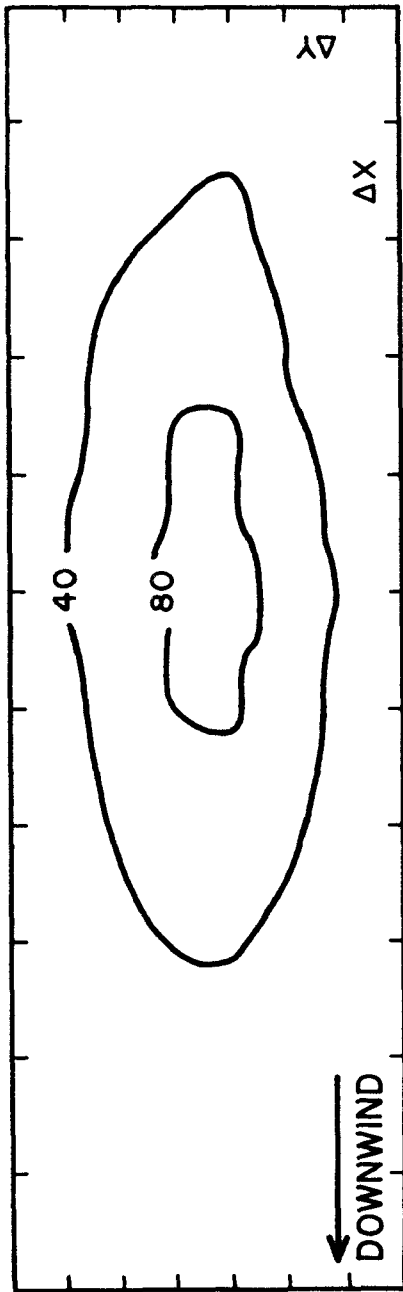Fig. 18d. Same as Fig. 18a except the maximum concentration is 81 μCi/m^3 and t = 71.2 seconds.

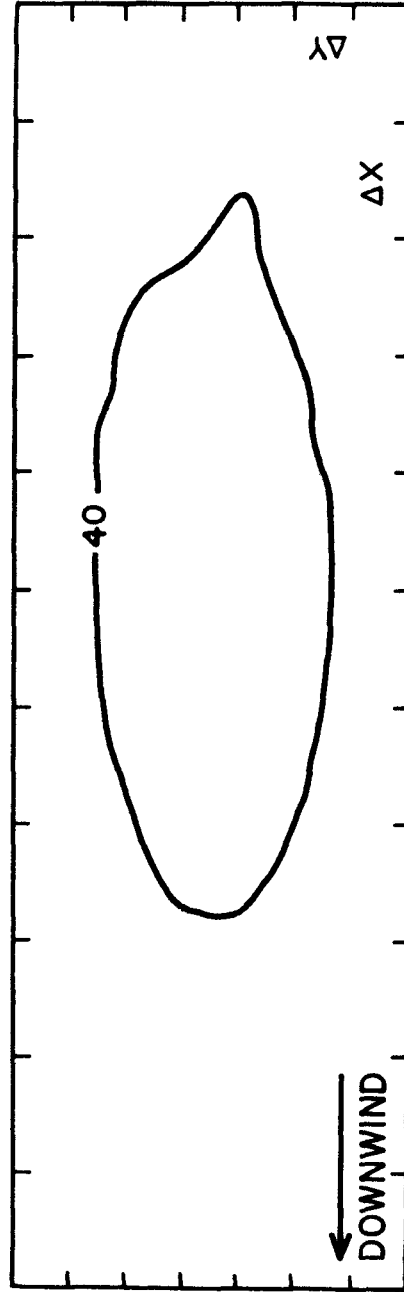Fig. 18e. Same as Fig. 18a except the maximum concentration is 68 $\mu Ci/m^3$ and t = 76 seconds.

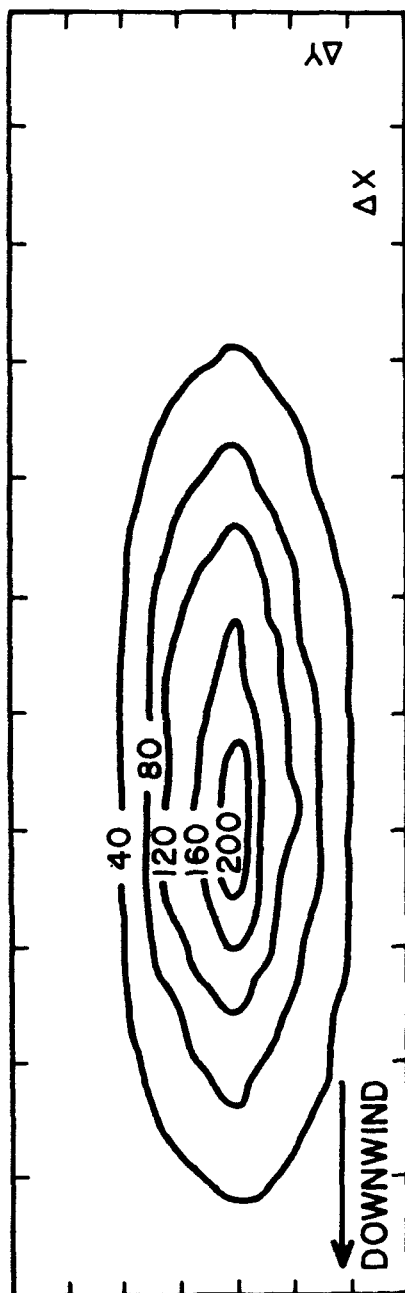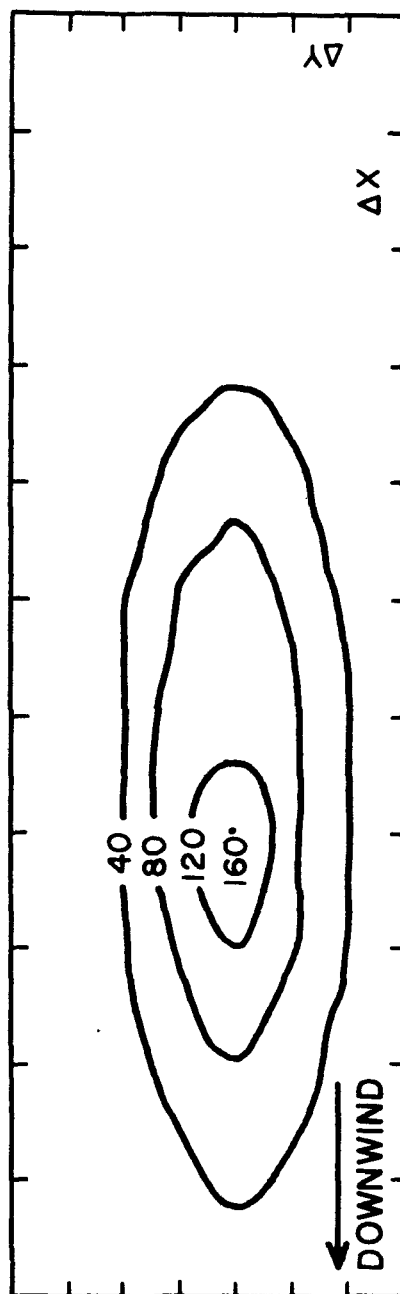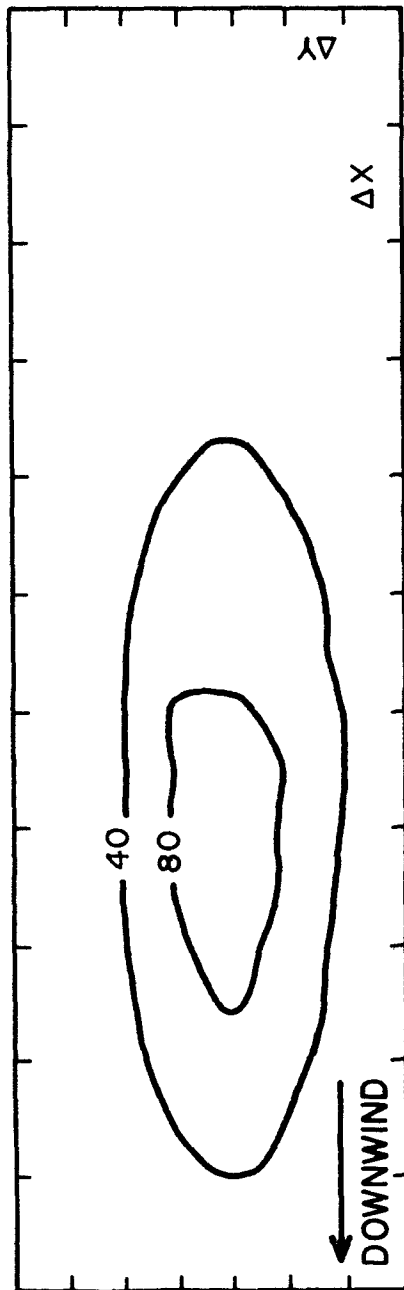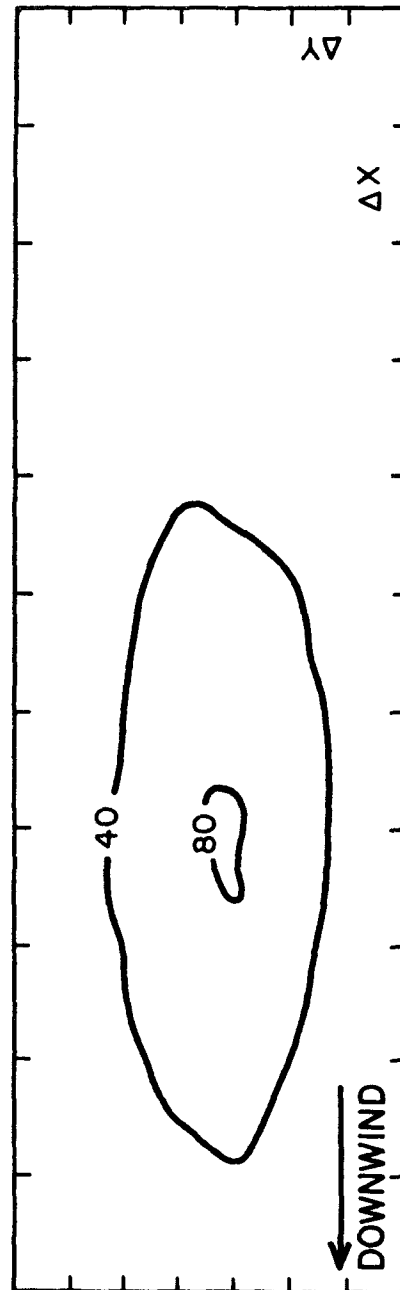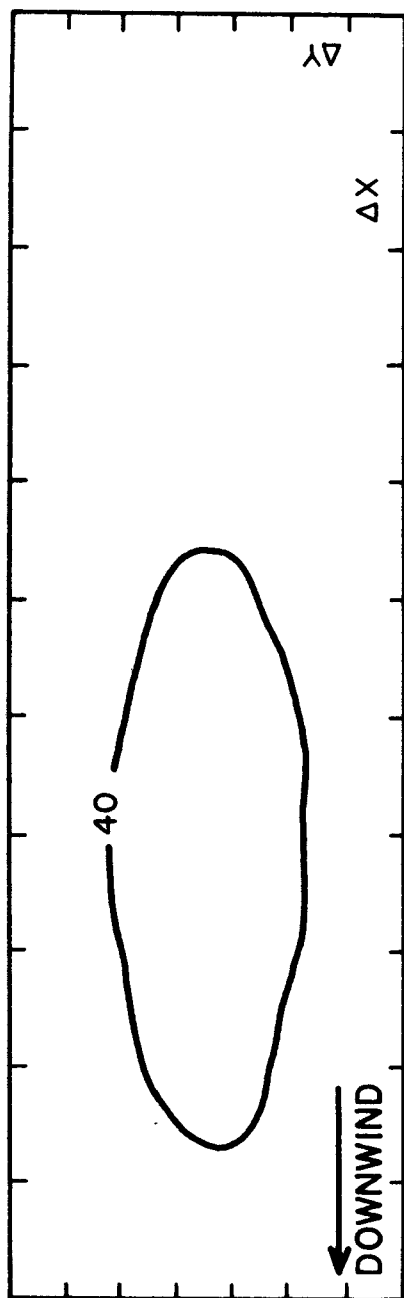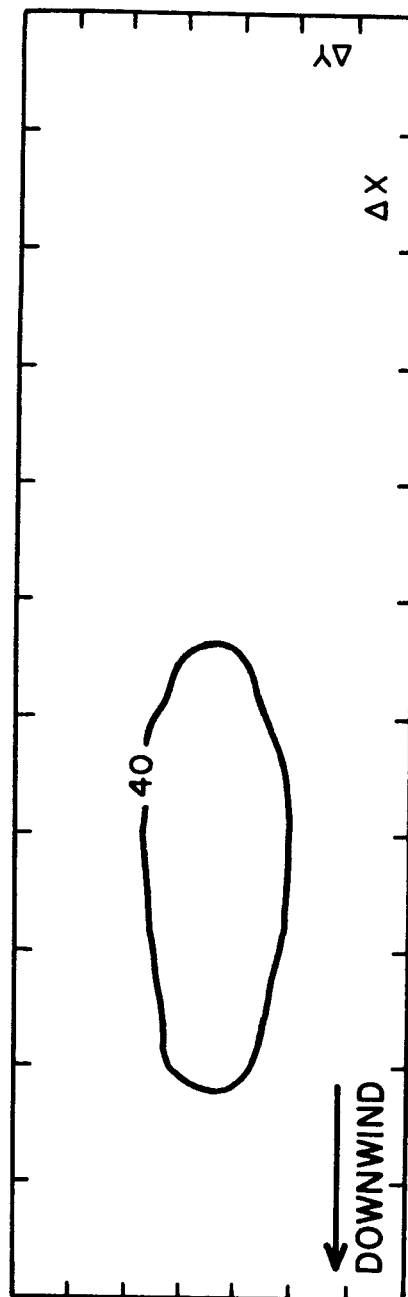Fig. 18f. Same as Fig. 18a except the maximum concentration is 53 $\mu Ci/m^3$ and t = 80.8 seconds.

60

The parameters optimized to fit the initial concentration model to the analysis are shown in Table 9. The optimal $\varphi(t)$ and $A(t)$ in Table 9 are obtained in the same manner as those in Table 6, except the analyzed concentrations have been utilized. The scavenging coefficient, β, is on the same order for both tests, but is more variable in test P7. Since $B(t)$ is very small, it may be ignored.

The analysis presented here using the indicated weights has many desirable features. Filtering in time produces smooth temporal changes in concentration and tends to allow model-data differences to be preserved for short periods of time. The use of larger observational weights when measured concentrations are available forces the analysis toward the observed puff and away from the model. The spatial filtering reduces the amplitude of short waves and therefore helps blend the model and data together.

The analysis scheme is designed to yield concentration patterns with the high frequency waves filtered out. This is consistent with the observations used, which were averaged over the collection interval. However, the analysis cannot be used directly as an estimate of the ensemble averaged concentration.

CONCENTRATION ESTIMATES

The ensemble average concentration estimate is based on the concentration model developed at the beginning of the section. The assumption that the ensemble average concentration is approximately normal in the horizontal is reasonable since puff irregularities are eliminated when puffs diffusing under identical conditions are averaged, due to the random nature of turbulence. In the vertical, the ensemble average concentration profile will still be affected by the combined effects of wind shear and scavenging occurring only at the surface. As seen in Figs. 16 and 18, the positions of the concentration maxima at the 6.1 m level change very slowly with time. Therefore, for the six central times in each test, the average position for the concentration maximum at each height is computed with respect to the position of the maximum at the 1.5 m level, using (44) with $u_o = 0$ for the effective transport speed. This allows for the generation of the ensemble average estimates in a true Lagrangian coordinate system, since the azimuthal variation of the puff centroid may also be eliminated using an ensemble average model.

The quantity $A(t)$ has already been computed using the analyses and is shown in Table 9. This represents an improved estimate for use in an ensemble average over estimates given in Table 6, since $A(t)$ decreases with time in a reasonably smooth manner. However, the scavenging coefficient, $\beta(t)$, which is computed using $A(t)$, displays a somewhat erratic nature. Therefore, for an ensemble average, further smoothing of $A(t)$ may be desirable. Because so little is known about the nature of the

Table 9. Parameters optimized to fit an ensemble averaged estimate to the analysis.

Travel time	B(t)	A(t)	φ(t)	β(t)
	a.	Test P5		
32.8	1.072	.6168	112.5	
35.2	.5611	.5855	112.3	− .0198
37.6	.2351	.5608	112.1	− .0154
40.0	.0338	.5438	111.9	− .0172
42.4	.0354	.5163	112.0	− .0168
44.8	.0516	.5017	112.1	
	b.	Test P7		
56.8	.1309	.7479	113.9	
61.6	.1854	.6156	114.0	− .0372
66.4	.2930	.5234	113.8	− .0266
71.2	.2965	.4769	113.2	− .0140
76.0	.1952	.4574	112.9	− .0144
80.8	.1095	.4153	113.0	

φ(t) = optimal azimuthal angle
A(t) = coefficient obtained from least squares fit
B(t) = constant obtained from least squares fit
β(t) = scavenging coefficient

scavenging in the diffusion puffs or the effect of wind shear, further smoothing is forgone.

In spite of a lack of knowledge concerning the precise manner in which wind shear and scavenging affect an ensemble averaged puff, reasonable estimates of the ensemble averaged concentration may be obtained using the model described above. The effect of wind shear and scavenging was examined for the data available; Figs. 7 and 9 show that the modeling used to describe these effects, though crude, is reasonably effective. The assumption that the ensemble averaged concentration is nearly normally distributed in the horizontal is a good one, because of the random nature of turbulent flows. Puff P5 shows some displacement in the transverse direction with height, possibly due to wind direction shear. However, this effect is not included in the ensemble averaged estimate, because, on the average, wind direction shear is negligible in the atmospheric surface layer. Concentration estimates obtained above will be used in the variational formalism developed in the next section.

SECTION 6

COMBINING FLUX AND CONCENTRATION ESTIMATES

A variational technique has been developed to combine the ensemble average concentration estimates and the analytical fluxes such that the diffusion equation is satisfied. This is not the first variational technique to use the diffusion equation. Wilkins (1971, 1972) developed a technique for the purpose of optimizing objectively contoured patterns of air pollution concentrations. He used the diffusion equation as a dynamical constraint in a numerical objective analysis technique to remove pattern inconsistencies between successive isopleth pattern presentations.

THE VARIATIONAL FORMALISM

The diffusion equation is used here as a strong constraint, so it is satisfied as closely as the numerical methods allow, by adjusting both the concentration and flux estimates. This approach is similar to that employed by McFarland (1975) when he used the continuity equation to obtain dynamically consistent wind fields. As shown by Sasaki et al. (1977), the proper finite-difference scheme must be used in order to satisfy the strong constraint.

In a Lagrangian coordinate system the diffusion equation may be written as

$$\frac{\partial \chi}{\partial t} + \frac{\partial F_x}{\partial x} + \frac{\partial F_y}{\partial y} + \frac{\partial F_z}{\partial z} + \beta \chi = 0 , \tag{51}$$

where $F_x \equiv \overline{\chi' u'}$, $F_y \equiv \overline{\chi' v'}$, $F_z \equiv \overline{\chi' w'}$ and β is defined in Section 2. The fluxes and concentrations all represent ensemble averaged quantities.

The variational functional which incorporates the concentration, fluxes and diffusion equation is

$$J = \int_V \int_t \{ \gamma_1 (\chi - \langle \chi \rangle)^2 + \gamma_2 (F_x - \hat{F}_x)^2 + \gamma_3 (F_y - \hat{F}_y)^2$$
$$+ \gamma_4 (F_z - \hat{F}_z)^2 + \lambda (\frac{\partial \chi}{\partial t} + \frac{\partial F_x}{\partial x} + \frac{\partial F_y}{\partial y} + \frac{\partial F_z}{\partial z} + \beta \chi) \} dVdt . \tag{52}$$

64

The $\langle \chi \rangle$ is the ensemble averaged concentration estimate. The fluxes which were shown in Section 3 to be the true ensemble averaged fluxes in the case of a puff diffusing in the absence of wind shear and with uniform scavenging are used as estimates of the fluxes for the case when the puff is diffusing in a sheared flow with scavenging occurring only at the surface. Therefore, $\hat{F}_x$, $\hat{F}_y$ and $\hat{F}_z$ are obtained using (41) with the estimated ensemble averaged concentrations.

The Euler equations obtained from the functional using appropriate boundary conditions are

$$2\gamma_1(\chi - \langle \chi \rangle) - \frac{\partial \lambda}{\partial t} + \beta \lambda = 0 , \tag{53}$$

$$2\gamma_2(F_x - \hat{F}_x) - \frac{\partial \lambda}{\partial x} = 0 , \tag{54}$$

$$2\gamma_3(F_y - \hat{F}_y) - \frac{\partial \lambda}{\partial y} = 0 , \tag{55}$$

$$2\gamma_4(F_z - \hat{F}_z) - \frac{\partial \lambda}{\partial z} = 0 , \tag{56}$$

and

$$\frac{\partial \chi}{\partial t} + \frac{\partial F_x}{\partial x} + \frac{\partial F_y}{\partial y} + \frac{\partial F_z}{\partial z} + \beta \chi = 0 . \tag{57}$$

The derivation of the finite-difference form of these equations, a discussion of boundary conditions and the solution of the equations are included in Appendix D.

The above equations may be combined to obtain a second order elliptic partial differential equation in λ, the Lagrange multiplier. Once λ is determined χ, F_x, F_y and F_z may be obtained by substitution into (53)-(56). These quantities satisfy the diffusion equation and are as close to χ, $\hat{F}_x$, $\hat{F}_y$ and $\hat{F}_z$, respectively, as the weight ratios γ_2/γ_1, γ_3/γ_1 and γ_4/γ_1 allow, except at grid points adjacent to or on the boundaries. Therefore, the outermost three grid points in each spatial dimension are not available for the final concentration analysis, since the consistent finite difference scheme for second order partial differentials involves two rows of boundary values. In Appendix D, second order differentials of the concentration estimate appear in the equation for λ. Because it is desirable to obtain good results at the 1.5 m level, where most of the data is located, the first three levels of the ensemble averaged concentration estimate are generated below the surface. The levels at which concentration estimates are computed are -8.1 m, -4.9 m, -1.7 m, 1.5 m, 4.7 m, 7.9 m, 11.1 m, 14.3 m, 17.5 and 20.7 m. The grid spacing was chosen to permit convenient computer output. In order to reduce the truncation error in the finite-difference scheme, the grid intervals used here are smaller than those used in the preceding section. In the downwind and crosswind directions the grid intervals used are 8 and 4.8 m, respectively.

ANALYSIS OF A GAUSSIAN PUFF

To analyse the results obtained from the variational technique, two different cases are considered for test P5. In Case 1, χ is generated such that it is as close to the ensemble averaged concentration estimate as possible, except that no wind shear or non-uniform scavenging is allowed so that the concentration distribution is Gaussian. It was shown in Section 3 that the estimated fluxes and concentrations satisfy the diffusion equation exactly in this case. Therefore, errors in the final analysis will be numerical, such as truncation errors in the finite-difference schemes. These numerical errors are not small, although they have been reduced considerably by using the smaller grid spacing. A measure of the finite-difference errors is the variance of the residual of the diffusion equation (51), VR. The variance is .533 for test P5, Case 1. This variance is unacceptable, because it indicates that the residuals are of the same order of magnitude as the terms in the diffusion equation. However, when the variational technique is applied the variance is greatly reduced to .000008. This indicates that the residuals were reduced more than two orders of magnitude. While this is a satisfactory reduction in the residual, it is not reduced to the limit of accuracy of the computer. If the last term on the left hand side of (51) is omitted, then the residual is further reduced.

The concentrations and fluxes for the two central times have been examined. They are displayed for the 1.5 m level at the 37.6 sec travel time in Figs. 19-22. At this level the vertical flux is much less than the horizontal. However, at the top of the puff the two are the same order of magnitude. The vertical concentration profile is shown in Fig. 23. Since there is no wind shear or non-uniform scavenging allowed in Case 1, the concentration distribution is Gaussian in the vertical as well as in the horizontal.

The analysis performed above could also have been applied to test P7. However, as shown in Section 4, the vertical spread of the puff in this test occurs so slowly that it violates one of the boundary conditions which is shown in Section 3 to be valid for a Gaussian puff. Therefore, it makes little sense to generate a Gaussian puff which conforms to the diffusion rates of puff P7.

Diffusivities may be computed from the final fluxes and concentrations. The averaged results for grid points where reasonably large concentration gradients exist in Case 1 are shown in Table 10. Note that, at the 37.6 and 40.0 sec travel times, the averaged diffusivities are very close to the true diffusivities, which are given by (25) for the non-sheared, uniform scavenging case. This is to be expected, since the flux and concentration estimates satisfy the diffusion equation exactly in this case.

66

Fig. 19. Ensemble averaged concentration for Case 1, test P5, at the 1.5 m level. The maximum concentration is 209 μCi/m³, t = 37.6 seconds Δx = 8.0 m and Δy = 4.8 m.

Fig. 20. Ensemble averaged downwind flux for Case 1, test P5, at the 1.5 m level. The maximum flux is 106 μCi/m² sec, the minimum flux is -106 μCi/m² sec, t = 37.6 seconds, Δx = 8.0 m and Δy = 4.8 m.
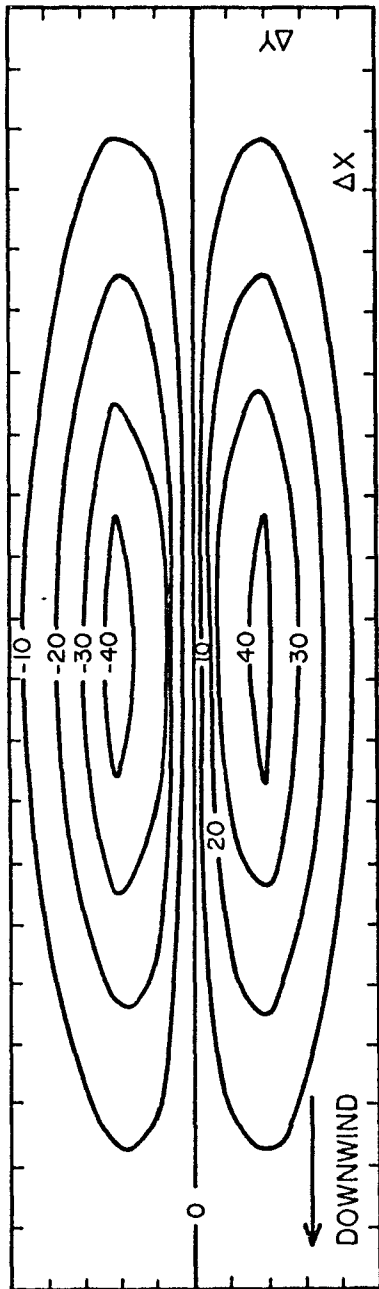
Fig. 21. Ensemble averaged crosswind flux for Case 1, test P5, at the 1.5 m level. The maximum flux is 43.9 $\mu Ci/m^2$ sec, the minimum flux is -43.9 $\mu Ci/m^2$ sec, t = 37.6 seconds, Δx = 8.0 m and Δy = 4.8 m.
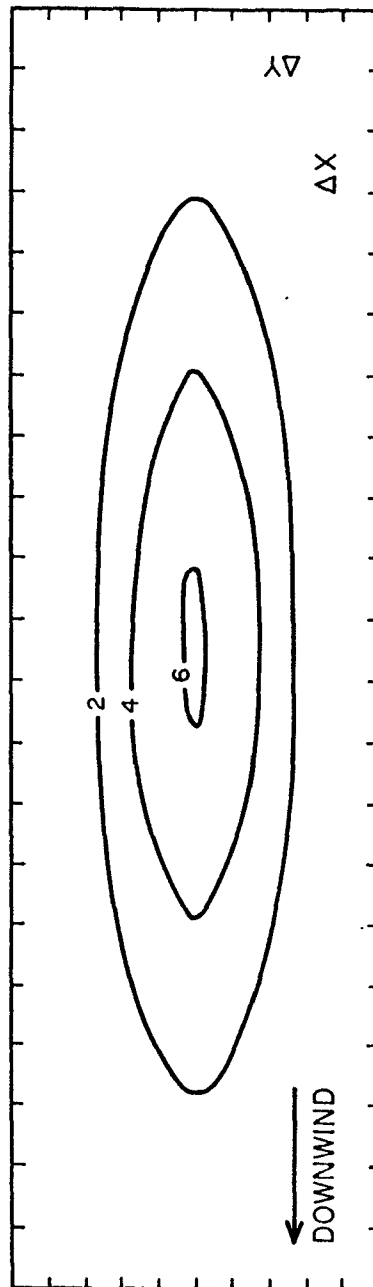
Fig. 22. Ensemble averaged vertical flux for Case 1, test P5, at the 1.5 m level. The maximum flux is 6.1 $\mu Ci/m^2$ sec, t = 37.6 seconds, Δx = 8.0 m and Δy = 4.8 m.

Fig. 23. Ensemble averaged concentration profile for Case 1, test P5. The maximum concentration is 209 $\mu Ci/m^3$, t = 37.6 seconds, Δx = 8.0 m, Δy = 4.8 m, and Δz = 3.2 m.

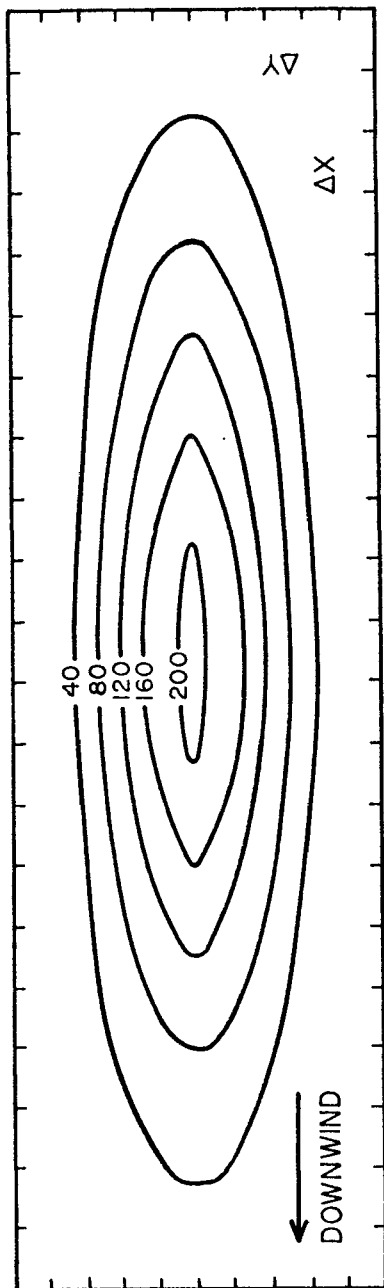
Fig. 24. Ensemble averaged concentration for Case 2, test P5, at the 1.5 m level. The maximum concentration is 208 $\mu Ci/m^3$, t = 37.6 seconds, Δx = 8.0 m and Δy = 4.8 m.

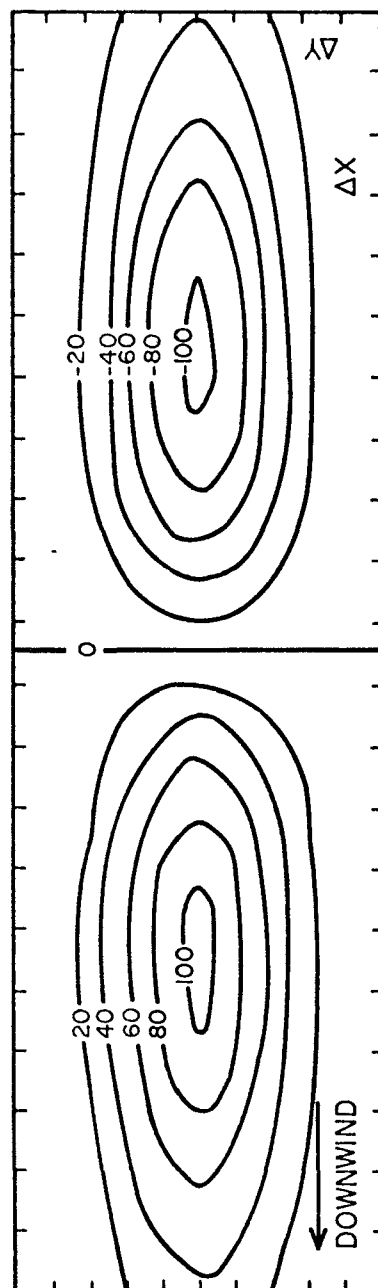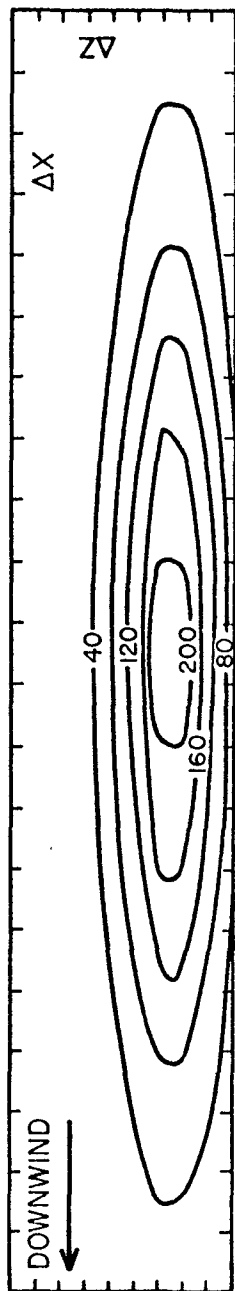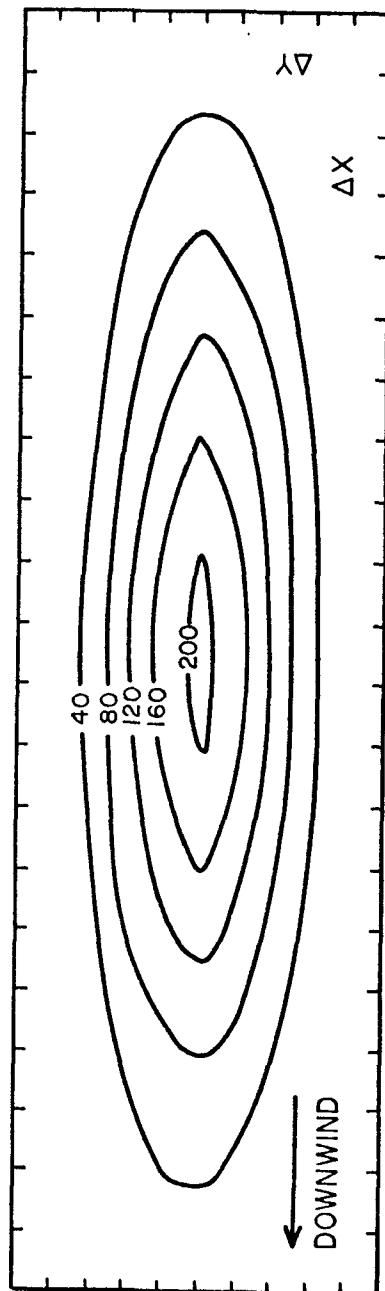The weight ratios are chosen so that the variance of the diffusivities, V_x, V_y and V_z, respectively, remain at least an order of magnitude smaller than the diffusivities, while still forcing the final concentration to be very close to the esti-mate. For Case 1 we know that the diffusivities are constant in space, so the variances should be zero. Using the weight ratios $\gamma_2/\gamma_1 = .2$, $\gamma_3/\gamma_1 = 1.$ and $\gamma_4/\gamma_1 = 5.9$, the variances displayed in Table 10 are sufficiently small. The correlation between the final and estimated concentrations is almost perfect. Spot checks were made to ensure that the magnitudes of the two were also nearly identical.

If the variance of the diffusivities is small enough, then the fluxes obtained using the average diffusivities and final concentrations must be highly correlated with the final fluxes. As seen from Table 11, the correlation between the fluxes is very high in Case 1. This result is anticipated, since we already knew that in this case the concept of down-gradient flux is a good one.

When the correlations in Table 11 are good and the vari-ances are small in Table 10, then the fluxes are proportional to the concentration gradients, and the constants of proportionality are the mean diffusivities. If the mean diffusivities are such that (25) represents a good approximation, then the diffusivities are the diffusion rates for the puff. The results displayed for Case 1, a situation where we have an a priori knowledge of the diffusivities and fluxes, indicates that the fluxes are propor-tional to the concentration gradients and the diffusivities are the diffusion rates for the puff.

ANALYSIS OF PUFFS P5 AND P7

In Case 2 $\langle \chi \rangle$ is generated as described in the last section, so that it is an estimate of the ensemble average concentration for puffs P5 and P7. The same type of analysis of the results of the variational technique used in Case 1 is performed here. How-ever, in this case we do not have an a priori knowledge of the results.

The variance of the residual of the diffusion equation is caused by finite-difference errors and possibly because the flux and concentration estimates do not satisfy the diffusion equa-tion exactly in this case. However, VR is not increased over that obtained in Case 1, being .601 for test P5 and .106 for test P7. The residuals are again the same order of magnitude as the terms in the diffusion equation. When the variational technique is applied, VR is again greatly reduced, to .000008 for test P5 and to .00001 for test P7. Therefore, the residuals are reduced more than two orders of magnitude for both tests.

The concentrations and fluxes have been examined for the

Table 10. Diffusivities and their variances.

Time	$\hat{K}_x$	$\bar{K}_x$	V_x	$\hat{K}_y$	$\bar{K}_y$	V_y	$\hat{K}_z$	$\bar{K}_z$	V_z	C	Case
37.6	32.6	32.8	.053	3.09	3.08	.0469	.547	.542	.004	.998	1
40.0	33.9	34.2	.093	3.54	3.60	.0604	.568	.586	.004	1.00	1
37.6	32.6	32.0	1.33	3.09	3.19	.188	.547	.453	.024	.991	2
40.0	33.9	33.2	2.01	3.54	3.70	.194	.568	.488	.034	.994	2
66.4	11.7	10.7	1.25	2.21	2.37	.032	.232	.181	.003	.999	2
71.2	12.2	11.0	1.38	2.55	2.80	.029	.227	.167	.006	1.00	2

$$\hat{K}_x \equiv \frac{1}{2}\frac{d\sigma_x^2}{dt} , \bar{K}_x \equiv \frac{-\sum_{i=1}^{\ell} F_x/\nabla_x\chi}{\ell} , V_x \equiv \text{variance of } K_x$$

$$\hat{K}_y \equiv \frac{1}{2}\frac{d\sigma_y^2}{dt} , \bar{K}_y \equiv \frac{-\sum_{i=1}^{m} F_y/\nabla_y\chi}{m} , V_y \equiv \text{variance of } K_y$$

$$\hat{K}_z \equiv \frac{1}{2}\frac{d\sigma_z^2}{dt} , \bar{K}_z \equiv \frac{-\sum_{i=1}^{n} F_z/\nabla_z\chi}{n} , V_z \equiv \text{variance of } K_z$$

ℓ, m and n are no. grid points at which $|\frac{\partial\chi}{\partial x}|$, $|\frac{\partial\chi}{\partial y}|$ and $|\frac{\partial\chi}{\partial z}| > 0$, respectively.

C $\equiv$ correlation between χ and $\hat{\chi}$

Table 11. Correlation between fluxes.

Time	c_x	c_y	c_z	Case
37.6	1.000	.9994	.9992	1
40.0	1.000	.9988	.9984	1
37.6	.9995	.9986	.9976	2
40.0	.9993	.9979	.9965	2
66.4	.9960	.9966	.9892	2
71.2	.9939	.9959	.9834	2

$c_x \equiv$ correlation between F_x and $\bar{K}_x \nabla_x \chi$

$c_y \equiv$ correlation between F_y and $\bar{K}_y \nabla_y \chi$

$c_z \equiv$ correlation between F_z and $\bar{K}_z \nabla_z \chi$

Fig. 25. Ensemble averaged downwind flux for Case 2, test P5, at the 1.5 m level. The maximum flux is 104 $\mu Ci/m^2$ sec, the minimum flux is -103 $\mu Ci/m^2$ sec, t = 37.6 seconds, Δx = 8.0 m and Δy = 4.8 m.
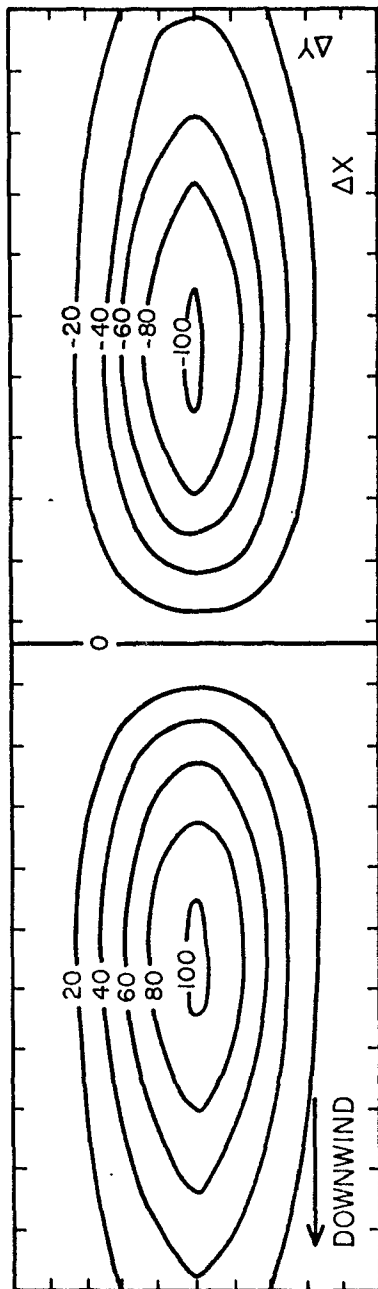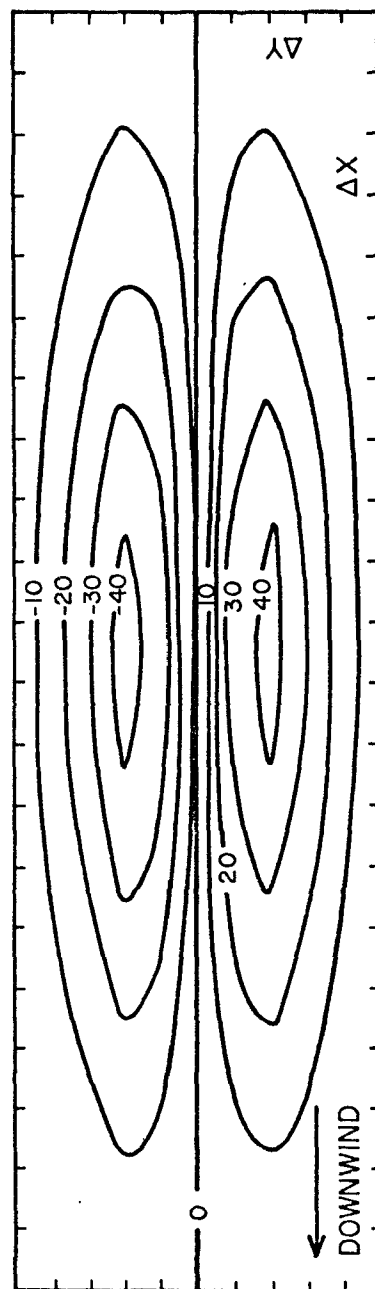

Fig. 26. Ensemble averaged crosswind flux for Case 2, test P5, at the 1.5 m level. The maximum flux is 43 $\mu Ci/m^2$ sec, the minimum flux is -43 $\mu Ci/m^2$ sec, Δx = 8.0 m and Δy = 4.8 m.

73

two central times in each test. They are displayed for the 1.5 m level at the 37.6 and 66.4 sec travel times in Figs. 24-33. Since the variational technique leaves the concentration virtually unchanged, Figs. 24 and 19 are nearly identical. The downwind flux for puff P5, in Fig. 25, is virtually the same as the flux in Fig. 20. The cross-wind fluxes in Figs. 26 and 21 are again nearly identical. The horizontal fluxes and concentrations also compare very well for the other travel times and levels examined. Of course the flux and concentration patterns at higher levels in Case 2 are displaced downwind from those in Case 1, due to the effect of wind shear and surface scavenging. Some deterioration in the comparison of downwind flux was observed at the highest level examined, 11.1 m, near the top of the puff.

While the horizontal fluxes did not change much from Case 1 to Case 2, the same cannot be said for the vertical fluxes. A comparison of Fig. 27 with 22 shows that the maximum flux more than doubled for Case 2 at the 1.5 m level. Furthermore, the pattern is completely different. Rather than a symetric upward flux with the maximum at the center of the grid, the maximum upward flux is displaced well upwind in Case 2. The downwind portion of the puff is dominated by downward flux in this case.

The vertical flux pattern has changed completely from Case 1 to Case 2 because the vertical concentration profile is very different in the two cases. The vertical profiles for Case 2 at the 37.6 and 66.4 sec travel times are in Figs. 32 and 33. A comparison of Figs. 32 and 23 shows how wind shear and surface scavenging change the vertical profile. While the maximum concentration remains relatively unchanged, the largest concentration in the downwind portion of the puff in Case 2 is aloft, while in Case 1 it is at the surface. Therefore, the concentration gradient in the downwind portion of the puff at the 1.5 m level is directed downward in Case 2, but upward in Case 1. Since the flux is down-gradient, F_z also changes direction in this portion of the puff. In the upwind portion of the puff, the concentration gradient is larger in Case 2 at the 1.5 m level. This accounts for the smaller upward flux in Case 1 in this region.

An examination of Figs. 24 and 28 shows that while the travel time for puff P7 is much longer, the concentration in this puff is only slightly less than in puff P5, because this puff is diffusing at a much slower rate. This may be seen from a comparison of the fluxes. While the shape of F_x is similar in Figs. 25 and 29, the magnitude is much larger in Fig. 25. The magnitudes of F_y in Figs. 26 and 30 are closer, which accounts for the difference in the shape of the puff. Puff P5 is elongated more than puff P7 because the downwind flux is relatively larger in test P5. The vertical fluxes in Figs. 27 and 31 have a similar pattern, because the vertical concentration profiles in Figs. 32 and 33 are very similar.
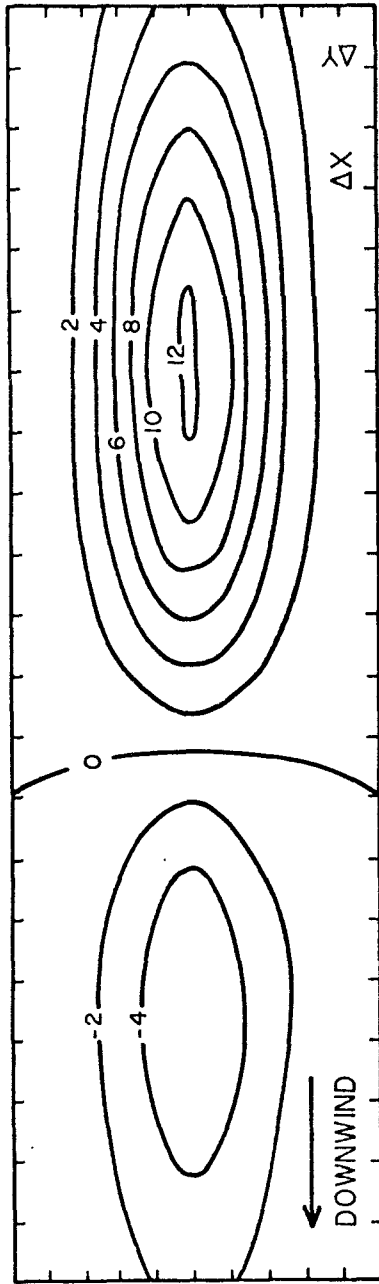
Fig. 27. Ensemble averaged vertical flux for Case 2, test P5, at the 1.5 m level. The maximum flux is 12.6 μCi/m² sec, the minimum flux is -5.57 μCi/m² sec, t = 37.6 seconds, Δx = 8.0 m and Δy = 4.8 m.
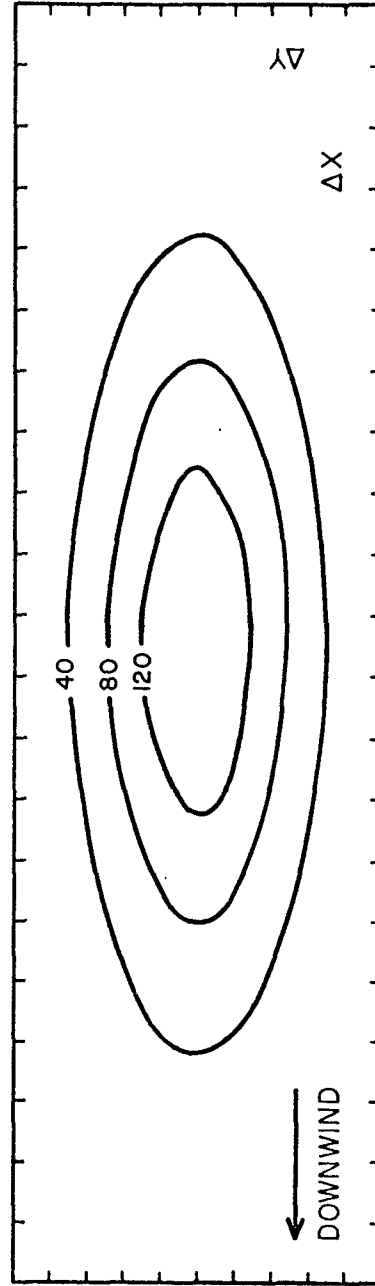

Fig. 28. Ensemble averaged concentration for Case 2, test P7, at the 1.5 m level. The maximum concentration is 157 μCi/m³, t = 66.4 seconds, Δx = 8.0 m and Δy = 4.8 m.

The mean diffusivities and the diffusivity variances for Case 2 are given in Table 10. The correlation between the fluxes obtained using the average diffusivities and the final fluxes for Case 2 are shown in Table 11. The variances in Table 10 are low and the correlations in Table 11 are high. Therefore, the fluxes are nearly proportional to the concentration gradients, and the constants of proportionality are the mean diffusivities. This result could be anticipated for the horizontal fluxes, because the ensemble average concentration maintains a near Gaussian distribution in the horizontal. Furthermore, it has already been shown in Section 2 that the diffusivity concept has a physical validity for the vertical flux near the surface. However, this conclusion is not valid for all fluxes; for example, it may be shown that the heat flux can be counter-gradient in the planetary boundary layer (Businger, 1973).

Table 10 shows that the mean horizontal diffusivities for Case 2 are close to the diffusivities computed using (36). Therefore, $\bar{K}_x$ and $\bar{K}_y$ may be reliably estimated using the horizontal diffusion rates for the puffs. However, this is not true for the vertical diffusivities. In Case 2 $\bar{K}_z$ is consistently smaller than $\hat{K}_z$, and for test P7 $\bar{K}_z$ decreases with increasing travel time. This result is not surprising since, when the puff is not Gaussian, there is no physical reason why $\bar{K}_z$ should be the vertical diffusion rate.

The magnitude of $\bar{K}_z$ varies as the weight ratio γ_4/γ_1 changes. If γ_4/γ_1 is made infinitely large, then $\bar{K}_z$ will conform to $\hat{K}_z$ exactly, provided the concentration distribution remains unchanged. Since the weight ratios used are very reasonable, because the concentration is relatively unchanged, and the expected diffusivities are obtained in Case 1, the $\bar{K}_z$'s computed for Case 2 must be reasonably accurate. This is born out in a comparison of the vertical diffusivities in Fig. 1 and Table 10. An average of the analytical diffusivities in the lowest levels compares favorably with the $\bar{K}_z$'s, which may be regarded as average diffusivities over the first few meters of the surface layer.

ENSEMBLE AVERAGE CONCENTRATIONS

The ensemble average concentrations obtained are very close to the analyzed concentrations. A comparison of Fig. 24 with Fig. 15c and Fig. 28 with Fig. 17c shows that at the 1.5 m level, where a majority of the data is found, the concentration patterns displayed agree very well. At levels where the analyzed concentrations are not so close to a Gaussian distribution, larger discrepancies exist.

The comparison of the ensemble averaged concentration and the data may be made in Figs. 6-9. The ensemble average concentrations are at grid points which do not coincide with the observation sites. In general, grid points are close enough so that

76
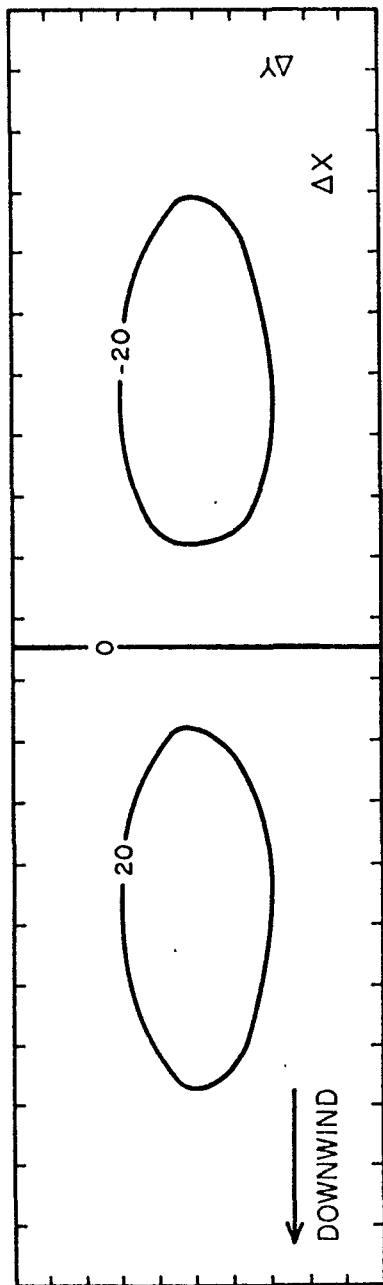
Fig. 29. Ensemble averaged downwind flux for Case 2, test P7, at the 1.5 m level. The maximum flux is 34.8 $\mu Ci/m^2$ sec, the minimum flux is -33.8 $\mu Ci/m^2$ sec, $t = 66.4$ seconds, $\Delta x = 8.0$ m and $\Delta y = 4.8$ m.
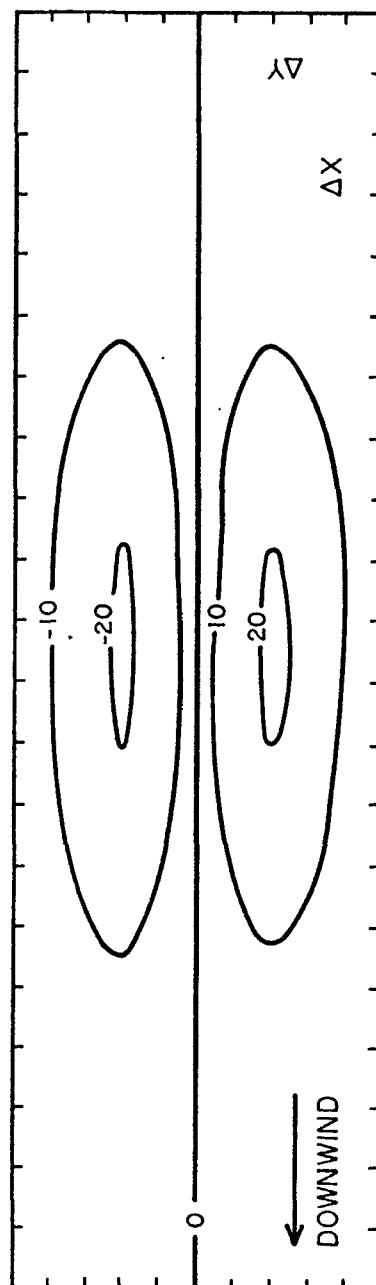
Fig. 30. Ensemble averaged crosswind flux for Case 2, test P7, at the 1.5 m level. The maximum flux is 21.7 $\mu Ci/m^2$ sec, the minimum flux is -21.7 $\mu Ci/m^2$ sec, $t = 66.4$ seconds, $\Delta x = 8.0$ m and $\Delta y = 4.8$ m.
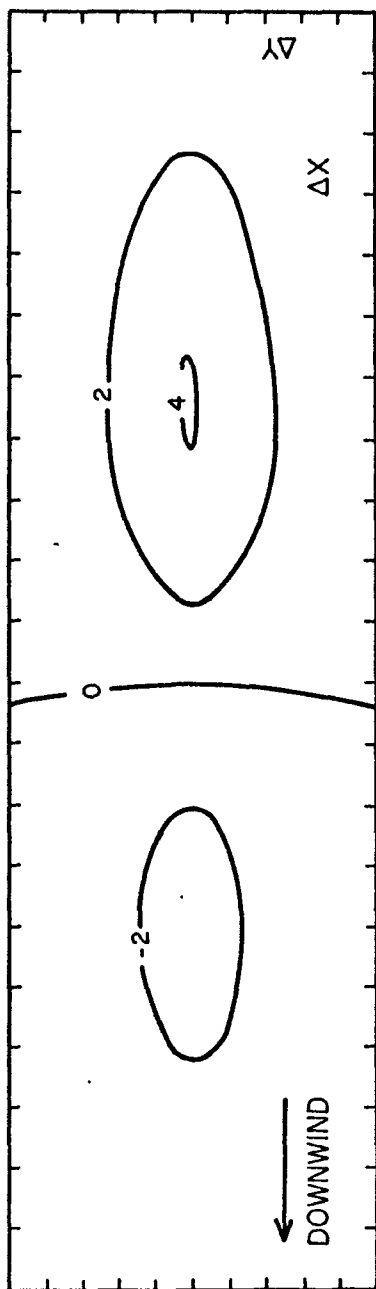
Fig. 31. Ensemble averaged vertical flux for Case 2, test P7, at the
1.5 m level. The maximum flux is 4.07 μCi/m^2 sec, the minimum flux
is -2.74 μCi/m^2 sec, t = 66.4 seconds, Δx = 8.0 m and Δy = 4.8 m.
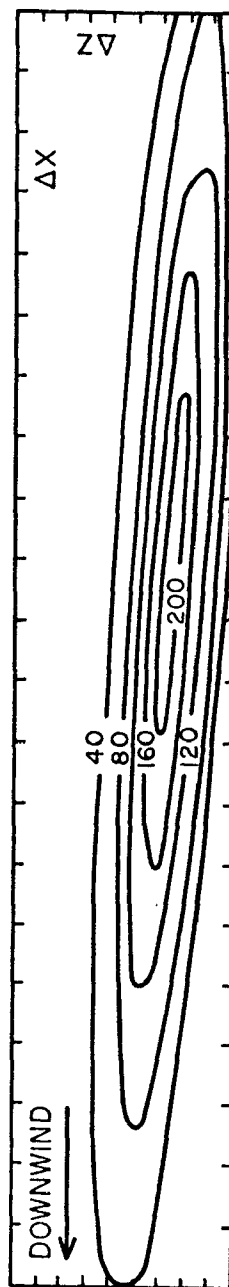
Fig. 32. Ensemble averaged concentration profile for Case 2, test P5.
The maximum concentration is 208 μCi/m^{3}m t = 37.6 seconds, Δx = 8.0 m,
Δy = 4.8 m, and Δz = 3.2 m.
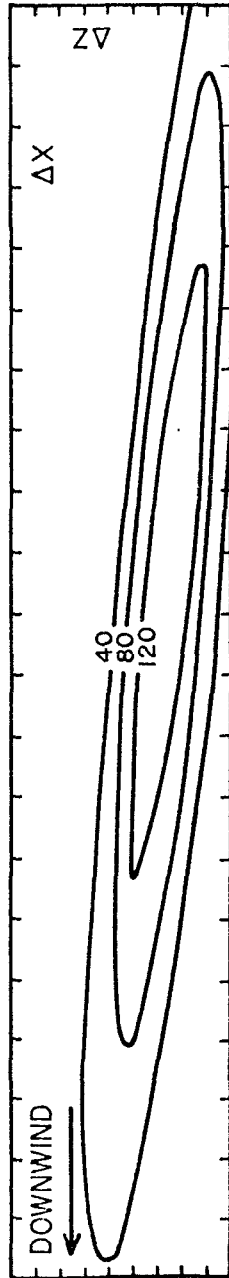
Fig. 33. Ensemble averaged concentration profile for Case 2, test P7. The maximum concentration is 157 $\mu Ci/m^3$, t = 66.4 seconds, Δx = 8.0 m, Δy = 4.8 m, and Δz = 3.2 m.

discrepancies caused by this procedure are small. The concentrations at the 1.5 m level in Figs. 6 and 8 are very close to the observations. Fortunately, grid points and observation towers coincided very well in both tests, and the vertical concentration profiles also agreed with the data in Figs. 7 and 9. By using the concentration estimate described in the last section, the final concentration is constrained to fit the data.

The results obtained above are not affected by the use of an average centroid position at each level. If such an approach were not taken, then an advection term would have to be included in the diffusion equation, as in (5). However, for the wind shear observed in tests P5 and P7, this term is an order of magnitude smaller than the other terms at most levels, and may therefore be neglected.

SECTION 7

CONCLUSIONS

The ultimate value of the K-theory approach discussed in the previous sections rests on the physical validity of the concept of diffusivity. Lacking this, the prediction of concentration distributions, which is the ultimate goal of K-theory, reduces to rather arbitrary formula-fitting. It is evident that a puff will be acted upon by a whole spectrum of turbulent fluctuations. Only those fluctuations which are small compared with the existing distribution of material can be represented by the diffusivity concept. The fluctuations which are on a scale similar to or greater than that of the puff itself will exert effects ranging from distortion to bodily movement of the tracer distribution. Therefore, the diffusivity concept alone cannot account for the dispersion of an individual puff released from an instantaneous point source.

In light of this, the research performed has answered several important questions, the most important being under what conditions the diffusivity concept does have physical validity. It is shown in Section 3 that if the diffusivity is considered to be proportional to the product of a characteristic length and a characteristic velocity, the physical interpretation is that the tracer is spread over the characteristic length by the turbulent eddies. It is further shown that the diffusivities satisfy the diffusion equation and a meaningful set of boundary conditions when the puff distribution is defined by the Gaussian model. Therefore, the concept of the tracer fluxes being equivalent to the negative of the product of the time dependent diffusivity derived in Section 3 and the concentration gradient is valid under the conditions for which the concentration has a normal distribution; a stationary homogeneous flow in the absence of external boundaries. The concentration under these conditions is the ensemble averaged concentration one would expect to observe in a non-sheared turbulent flow with uniform scavenging near the surface.

A second important question is whether or not the diffusivity can be identified with some other physical quantity which may be determined from easily measured atmospheric variables. It was shown in Section 3 that, under the described conditions, the diffusivity is the rate of spread of the puff. This is fortunate, since much work has been accomplished in the determination of

81

diffusion rates, by Lin (1960), and Smith and Hay (1961), for example. There is, of course, too little data currently available to determine if these results are directly applicable; however, a valuable foundation for further research has been laid.

A stationary homogeneous flow, required for a normally distributed puff, is unrealistic in the atmospheric surface layer, and there exists an external boundary in the form of the earth's surface. Therefore, an ensemble averaged concentration analysis is developed which is decidedly non-Gaussian in the vertical. A comparison with the data shows that the vertical concentration profile adequately describes both the effect of wind shear and also that of surface scavenging. Furthermore, the near normal ensemble averaged concentration distribution in the horizontal is shown to conform to the available data. Therefore, the flow conditions implied by the ensemble averaged concentration, i.e., stationary, horizontally homogeneous turbulence, appear to be a reasonable enough approximation of the true ensemble averaged flow in the surface layer. This is not surprising since the assumptions of horizontal homogeneity and stationarity are routinely used in the study of the structure of the surface layer.

Due to the assumption of horizontal homogeneity, the horizontal diffusivity may still be identified with the rate of spread of the puff. Therefore, horizontal diffusivities which are time dependent only are likely to have the same physical validity as in the case of a vertically homogeneous flow for the shallow puff considered here.

When the concentration is not normally distributed in the vertical, equating diffusivity to the diffusion rate, as in (25), has little physical validity, since the vertical concentration profile can no longer be specified by a standard deviation. Therefore, it is not surprising that the $\bar{K}_z$'s obtained in Section 6 do not agree with their estimates, even though a large weight ratio is employed for the vertical flux. The variational technique employed in the preceding section guarantees that the ensemble averaged concentration and fluxes satisfy the diffusion equation (Eq. 51). Since the concentration and horizontal fluxes are shown to be close to their estimates, as expected, it may be assumed that the vertical fluxes are also correct. Therefore, the vertical diffusivities obtained are reasonable approximations of the average vertical diffusivities in the layer occupied by the puff.

Because of the good comparison between the $\bar{K}_z$'s and the diffusivities in Fig. 1, it may be that the vertical diffusivity is well defined by (14). The physical validity of this form for the vertical diffusivity has already been established for a puff released on the surface. However, the variance of $\bar{K}_z$ is smaller than it should be if (14) represents the actual diffusivity. As seen in Fig. 1, the diffusivity varies rapidly with height close

to the surface. Furthermore, in the neutral case the diffusivity is less than that in the unstable case. However, $\bar{K}_z$ was found to be less in the unstable than in the neutral case. Eq. (14) does not allow a time dependence for K_z. It may not be necessary, however, since the dependence upon time obtained from the available data is ambiguous. In test P5 $\bar{K}_z$ increased with time, while in test P7 $\bar{K}_z$ decreased. It is, therefore, evident that this research did not reveal the precise nature of the vertical diffusivity in the atmospheric surface layer.

Since ambient data upon which the profiles in Fig. 1 are based is very limited, these profiles are subject to change. It may be possible to obtain improved profiles by using (14) to estimate vertical fluxes, employ the variational technique described in the last section, and determine $\bar{K}_z$ at each available level.

The diffusivity concept appears to be valid for an ensemble averaged tracer puff diffusing on the surface. Furthermore, the diffusivities can be identified with other physical quantities which may be determined from measurable atmospheric variables.

The diffusivities may be used to estimate fluxes, which, together with the concentration estimates, can be employed in the variational technique to obtain fluxes and concentrations which satisfy the diffusion equation. These quantities are assumed to be the true ensemble average concentrations and fluxes.

SECTION 8

BIBLIOGRAPHY

Businger, Joost A., 1973: Turbulent transfer in the atmospheric surface layer. Workshop on Micrometeorology, American Meteorological Society, Boston, Mass.

Gifford, F. A., Jr., 1957: Relative atmospheric diffusion of smoke puffs. J. Meteorol., 14(5), 245-251.

_____, 1968: An outline of theories of diffusion in the lower layers of the atmosphere. Meteorology and Atomic Energy, 1968, TID-24190. Clearinghouse for Federal Scientific and Technical Information, 65-116.

Hildebrand, Peter H., 1977: A radar study of turbulent diffusion in the lower atmosphere. J. Appl. Meteor., 16, 493-510.

Lewellen, W. S., M. Teske, and C. duP. Donaldson, 1974: Turbulence model of diurnal variations in the planetary boundary layer. Proceedings of the 1974 Heat Transfer and Fluid Mechanics Institute. Stanford University Press.

Linn, C. C., 1960: On a theory of dispersion by continuous movements. Proc. Natl. Acad. Sci., 46, 566-570.

_____, and W. H. Reid, 1963: Turbulent flow, theoretical aspects. Handbuch der Physik, 8, Part 2, 438-523, Springer-Verlag, Berlin.

McFarland, M. J., 1975: Variational optimization analysis of temperature and moisture in a severe storm environment. Ph.D. Dissertation, University of Oklahoma, Dept. of Meteorology, Norman.

Mood, A. M., and F. A. Graybill, 1963: Introduction to the Theory of Statistics. McGraw-Hill, New York.

Nickola, P. W., 1971: Measurement of the movement, concentration and dimension of clouds resulting from instantaneous point sources. J. Appl. Meteor., 10, 962-973.

_____, J. V. Ramsdell, Jr., and J. D. Ludwick, 1970a: An inert gas tracer system for monitoring the real time history of a diffusing plume or puff. J. Appl. Meteor., 9, 621-626.

_____, 1970b: Detailed Time - Histories of Concentrations Re-
sulting From Puff and Short Period Releases of an Inert
Radioactive Gas: A Volume of Atmospheric Diffusion Data,
BNWL - 1272. National Technical Information Service.

Pasquill, F., 1970: Prediction of diffusion over an urban area-
current practice and future prospects. Proceedings of
Symposium On Multiple-Source Urban Diffusion Models, Air
Pollution Controle Office Publication, AP-86, Sec. 3.

_____, 1974: Atmospheric Diffusion. John Wiley and Sons, New
York.

Richardson, L. F., 1926: Atmospheric diffusion shown on a dis-
tance-neighbor graph. Proc. Roy. Soc. (London), A110,
709-737.

Roberts, J. J., E. S. Croke, and A. S. Kennedy, 1970: An urban
atmospheric dispersion model. Proceedings of Symposium on
Multiple-Source Urban Diffusion Models, Air Pollution Con-
trol Office Publication, AP-86, Sec 6.

Roberts, O. F. T., 1923: The theoretical scattering of smoke in
a turbulent atmosphere. Proc. Roy. Soc. (London), A104,
640-654.

Sasaki, Y., 1970a: Some basic formalisms in numerical varia-
tional analysis. Mon. Wea. Rev., 98, 875-883.

_____, 1970b: Numerical variational analysis formulated under
the constraints as determined by longwave equations and
low-pass filter. Mon. Wea. Rev., 98, 884-898.

_____, 1970c: Numerical variational analysis with weak con-
straint and application to surface analysis of severe storm
gusts. Mon. Wea. Rev., 98, 899-910.

_____, P. S. Ray, J. S. Goerss, and P. Soliz (1977): Errors due
to inconsistency of finite difference schemes. Submitted
to Monthly Weather Review.

Smith, F. B., and J. S. Hay, 1961: The expansion of clusters of
particles in the atmosphere. Quart. J. R. Met. Soc., 87,
82-101.

Sutton, O. G., 1953: Micrometeorology. McGraw-Hill, New York.

Taylor, G. I., 1921: Diffusion by continuous movements. Proc.
London Math. Soc., (2) 20, 196-202.

Tennekes, H., and J. L. Lumley, 1972: A First Course In Turbu-
lence. The MIT Press, Cambridge, Mass.

Van der Hoven, I., 1968: Deposition of particles and gases.
Meteorology and Atomic Energy, 1968, TID-24190. Clearing-
house for Federal Scientific and Technical Information,
65-116.

Wilkins, E. M., 1971: Variational principle applied to numerical
objective analysis of urban air pollution distributions.
J. Appl. Meteor., 10, 974-981.

_____, 1972: Variationally optimized numerical analysis equa-
tions for urban air pollution monitoring networks. J. Appl.
Meteor., 11, 1334-1341.

Wyngaard, John C., 1973: On surface layer turbulence. Workshop
on Micrometeorology. American Meteorological Society,
Boston.

Yeh,Gour-Tsyh and Chin-Hua Huang, 1975: Three dimensional air
pollutant modeling in the lower atmosphere. Boundary-Layer
Meteorology, 9, 381-390.

APPENDIX A

DERIVATION OF THE EXPRESSION FOR DIFFUSIVITY

The derivation of the expression for diffusivity,

$$K_x = \frac{1}{2} \frac{d\sigma_x^2}{dt} ,$$

(A.1)

is shown in order to reveal the nature of the relevant character-
istic length and eddy velocity. Mixing length theory could be
used to define the diffusivity. However, as Pasquill (1974)
points out, there is a considerable element of vagueness in the
whole idea of a mixing length. Therefore, this approach is not
used since it does not contribute to a clear understanding of the
characteristic length and velocity.

It is well known (e.g., Pasquill, 1974) that, based on di-
mensional grounds, the diffusivity may be determined by the pro-
duct of a characteristic eddy velocity and a characteristic
length scale. Since, as shown in Section 3, the diffusivity is
proportional to the perturbation velocity variance at distances
far from the source, it is assumed that the characteristic ve-
locity is the standard deviation of the velocity perturbation.

Pasquill (1974) states that only those eddies of a size
similar to or less than that of the puff are effective in dif-
fusing it. It is therefore assumed that the characteristic
length in the downwind direction, l_c, is related to σ_x. Since
σ_x grows indefinitely, but l_c's growth may be limited by the size
of the largest eddies diffusing the puff, the relationship be-
tween l_c and σ_x is taken to be

$$l_c = C(t) \; \sigma_x .$$

(A.2)

At long travel times $C(t)$ must decrease so that l_c remains con-
stant.

Since the diffusivity may be determined by the product of
the characteristic length and velocity,

$$K_x = C_1 [\overline{u'^2} \; \sigma_x^2]^{\frac{1}{2}} ,$$

(A.3)

87

where C_1 is a time dependent proportionality parameter. The product may be replaced by the covariance of ℓ_x and u', $\overline{\ell_x u'}$, since the correlation between these quantities may be defined as

$$C_2 \equiv \frac{\overline{\ell_x u'}}{[\overline{u'^2} \; \overline{\ell_x^2}]^{\frac{1}{2}}} \; . \tag{A.4}$$

When tracer puffs are released many times under identical conditions, and ensemble average concentrations are obtained, the resulting distribution of particles must be identical to the concentration distribution. Therefore, the variance of ℓ_x is equivalent to the variance of the concentration as

$$\overline{\ell_x^2} = \sigma_x^2 \; . \tag{A.5}$$

Substitution of (A.4) and (A.5) into (A.3) yields

$$K_x = C_3 \; \overline{\ell_x u'} \; , \tag{A.6}$$

where $C_3 = C_1/C_2$.

The relationship between ℓ_x and u' must now be examined, in order to express the diffusivity in terms of measurable quantities. Using the fact that the usual laws of differentiation may be applied to the mean values of fluctuating variables and their products,

$$\frac{\overline{d(\ell_x^2)}}{dt} = 2\ell_x \frac{\overline{d\ell_x}}{dt} \; . \tag{A.7}$$

It may be seen from a comparison of Figs. 2 and 3 that $x'(t_f) \neq \ell_x$. However, the position of the puff centroid with respect to the abscissa, a, does not change as rapidly as the position of an individual particle does. Therefore, the time rate of change of a particle's position with respect to the puff centroid, C, is nearly equivalent to its rate of change with respect to the coordinate system, or

$$\frac{dx'}{dt} = \frac{d(\ell_x + a)}{dt} \approx \frac{d\ell_x}{dt} \; . \tag{A.8}$$

At short travel times the puff is small and the approximation is not a good one since the location of the puff centroid changes rapidly as large eddies transport the entire puff. However, as the puff becomes larger at longer travel times the eddies tend to diffuse rather than transport the puff and the approximation becomes better. Therefore, at longer travel times,

$$u' = d\ell_x/dt \ . \tag{A.9}$$

In those cases where (A.9) is valid (A.7) becomes

$$\overline{\ell_x u'} = \frac{1}{2} \frac{d\sigma_x^2}{dt} \ , \tag{A.10}$$

if (A.5) also is used.

The diffusivity may be related to the rate of spread of the puff by substituting (A.10) into (A.6), to obtain

$$K_x = \frac{C_3}{2} \frac{d\sigma_x^2}{dt} \ . \tag{A.11}$$

Using the definition $\sigma_x = a_1 t^{b_1}$ the diffusivity becomes

$$K_x = a_1^2 b_1 C_3 t^{2b_1 - 1} \ . \tag{A.12}$$

The constant C_3 may be evaluated by equating (A.12) with (12) when $b_1 = 1/2$, the condition under which (12) is valid, to obtain $C_3 = 1$. Therefore, (A.11) is equivalent to (A.1), so that, except close to the source, the diffusivity expressed by (A.1) is in fact proportional to the product of the assumed characteristic eddy velocity and characteristic length scale. When the assumption (A.8) is valid, the characteristic velocity is the standard deviation of the velocity perturbation, and the characteristic length scale is shown in (A.2). The product of the proportionality parameter and C(t), C1, is equivalent to the correlation coefficient, C2. Therefore, the diffusivity may be uniquely determined from $\sqrt{u'^2}$, σ_x and C_2.

APPENDIX B

CENTERED FINITE DIFFERENCE ALGORITHMS

The form of the finite-difference algorithm for non-equally spaced grid intervals may be obtained from a Taylor series expansion. Let P represent any dependent variable, while i, j, k and ℓ are the grid indicies along the x, y, z and t axes, respectively. For derivative evaluation at i, j, k or ℓ, only those subscripts different from i, j, k, or ℓ are identified.

Taylor series expansions to approximate P_{k-1} and P_{k+1} are

$$P_{k-1} = P - (z - z_{k-1}) \nabla_z P + \frac{(z - z_{k-1})^2}{2!} \nabla_{zz} P - \ldots \tag{B.1}$$

and

$$P_{k+1} = P + (z_{k+1} - z) \nabla_z P + \frac{(z_{k+1} - z)^2}{2!} \nabla_{zz} P + \ldots \tag{B.2}$$

Neglecting higher order terms (resulting in a truncation error), (B.1) and (B.2) may be solved for $\nabla_z P$. After some manipulation,

$$\nabla_z P = \frac{\dfrac{z_{k+1} - z}{z - z_{k-1}} (P - P_{k-1}) - \dfrac{z - z_{k-1}}{z_{k+1} - z} (P - P_{k+1})}{z_{k+1} - z_{k-1}}. \tag{B.3}$$

If

$$z_{k+1} - z = z - z_{k-1} = \Delta z, \tag{B.4}$$

$$\nabla_z P = \frac{P_{k+1} - P_{k-1}}{2\Delta z}. \tag{B.5}$$

Eqs. (B.1) and (B.2) may be solved for $\nabla_{zz} P$, again negleting the higher order terms, to obtain

$$\nabla_{zz} P = 2 \frac{\dfrac{P_{k+1} - P}{z_{k+1} - z} + \dfrac{P_{k-1} - P}{z - z_{k-1}}}{z_{k+1} - z_{k-1}}. \tag{B.6}$$

If (B.4) holds, this reduces to

$$\nabla_{zz}P = \frac{P_{k+1} + P_{k-1} - 2P}{(\Delta z)^2} \, .$$

(B.7)

Similar results may be obtained in the x, y and t axes. In Appendix C, algorithm (B.6) is used on the z axis, since the grid intervals here are non-equally spaced, and the equivalents of algorithm (B.7) are used for the other axes.

Significant errors can arise in numerical computations when a set of differential equations is written in an inconsistent finite-difference form (Sasaki et al., 1977). The inconsistent form, exemplified by using (B.5) and (B.7) together, results in a lack of satisfaction of the governing equations which may be equal to that obtained when the variational technique is not employed. A finite difference analog of the second derivative operator of the form

$$\nabla_z(\nabla_z P) = \nabla_{zz}P = \frac{P_{k+2} - 2P + P_{k-2}}{(2\Delta z)^2} \, ,$$

(B.8)

is consistent with (B.5). The use of a consistent finite-difference scheme is shown to force satisfaction of the governing equations. Therefore, (B.5) and (B.8) and their equivalent analogs for the other axes are employed in Appendix D. It is not necessary to use (B.8) in Appendix C since there are no inconsistencies there.

APPENDIX C

NUMERICAL SOLUTION OF THE ANALYSIS FUNCTIONAL

The variational functional in Section 5 may be written in finite-difference form as

$$J = \sum_{ijk\ell} \{\alpha_1(\bar{\chi} - \tilde{\chi})^2 + \alpha_2(\nabla_x\bar{\chi})^2 + \alpha_3(\nabla_y\bar{\chi})^2$$

$$+ \alpha_3(\nabla_z\bar{\chi})^2 + \alpha_4(\nabla_t\bar{\chi})^2\} \ . \tag{C.1}$$

The observational weight, α_1, is prespecified but not constant. A value of 1 is assigned when $\tilde{\chi}$ is obtained from the model, but $\alpha_1 = 20$ when an observation is available. The weights multiplying the filtering constraints are prespecified and constant in space and time.

The stationary value of the functional is found by equating its first variation to zero. The quadratic formulation of the functional insures that this value is a minimum (Sasaki, 1970a). The first variation of (C.1) is

$$\delta J = 0 = \sum_{ijk\ell} 2\{\alpha_1(\bar{\chi} - \tilde{\chi})\delta\bar{\chi} + \alpha_2\nabla_x\bar{\chi}\delta\nabla_x\bar{\chi} + \alpha_3\nabla_y\bar{\chi}\delta\nabla_y\bar{\chi}$$

$$+ \alpha_3\nabla_z\bar{\chi}\delta\nabla_z\bar{\chi} + \alpha_4\nabla_t\bar{\chi}\delta\nabla_t\bar{\chi}\} \ . \tag{C.2}$$

Repeated use of the commutation equations proven to be applicable for finite differencing (Sasaki, 1970a) yields

$$\sum_{ijk\ell} [\{\alpha_1(\bar{\chi} - \tilde{\chi}) - \alpha_2\nabla_{xx}\bar{\chi} - \alpha_3\nabla_{yy}\bar{\chi} - \alpha_3\nabla_{zz}\bar{\chi}$$

$$- \alpha_4\nabla_{tt}\bar{\chi}\}\delta\bar{\chi}] + [\text{Boundary Conditions}] = 0 \ . \tag{C.3}$$

The boundary conditions are satisfied by specifying $\bar{\chi}$ on the boundaries, so that $\delta\bar{\chi}$ is zero here. Therefore, in order to satisfy the extremum condition, $\delta J = 0$, for arbitrary and independent variations of $\delta\bar{\chi}$, its coefficient must vanish identically in the domain. This leads to the Euler-Lagrange equation,

$$\alpha_2\nabla_{xx}\bar{\chi} + \alpha_3(\nabla_{yy}\bar{\chi} + \nabla_{zz}\bar{\chi}) + \alpha_4\nabla_{tt}\bar{\chi} - \alpha_1(\bar{\chi} - \tilde{\chi}) = 0 \ . \tag{C.4}$$

Since the Euler equation is elliptic, it may be solved using a relaxation algorithm. Substituting the finite-difference analogs (B.6) and the equivalents of (B.7) into (C.4) and rearranging yields

$$F[-2\{\frac{\alpha_2}{(\Delta x)^2} + \frac{\alpha_3}{(\Delta y)^2} + \frac{\alpha_3}{z1} + \frac{\alpha_3}{z2} + \frac{\alpha_4}{(\Delta t)^2} + \frac{\alpha_1}{2}\} \, \bar{\chi}$$

$$+ \frac{\alpha_2}{(\Delta x)^2} (\bar{\chi}_{i+1} + \bar{\chi}_{i-1}) + \frac{\alpha_3}{(\Delta y)^2} (\bar{\chi}_{j+1} + \bar{\chi}_{j-1})$$

$$+ \frac{2\alpha_3}{z1} \bar{\chi}_{k+1} + \frac{2\alpha_3}{z2} \bar{\chi}_{k-1} + \frac{\alpha_4}{(\Delta t)^2} (\bar{\chi}_{\ell+1} + \bar{\chi}_{\ell-1})$$

$$+ \alpha_1 \bar{\chi}] = R^\nu , \qquad\qquad\qquad\qquad (C.5)$$

where $z1 \equiv (z_{k+1} - z)(z - z_{k-1}) + (z_{k+1} - z)^2$

and $\quad z2 \equiv (z - z_{k-1})^2 + (z_{k+1} - z)(z - z_{k-1})$.

The over-relaxation factor F is predetermined to speed the relaxation process. The residual R^ν at the ν-th iteration indicates that the $\bar{\chi}$'s do not satisfy (C.5) exactly on that iteration. On the succeeding iterations the residual may be reduced by choosing a more appropriate $\bar{\chi}$, such that

$$\bar{\chi}^{\nu+1} = \bar{\chi}^\nu + \frac{R^\nu}{2\{\frac{\alpha_2}{(\Delta x)^2} + \frac{\alpha_3}{(\Delta y)^2} + \frac{\alpha_3}{z1} + \frac{\alpha_3}{z2} \frac{\alpha_4}{(\Delta t)^2} + \frac{\alpha_1}{2}\}} . \qquad (C-6)$$

This recursion equation may be iterated until the residuals at all grid points are less than some arbitrary value. The root-mean-square (R.M.S.) of the residual is a measure of the relaxation procedure's success in obtaining a solution to the partial differential equation. For test P7 the R.M.S. was reduced from 79.94 to .01477 in 18 iterations, while in test P5 it was reduced from 1709 to .006688 in 24 iterations.

APPENDIX D

NUMERICAL SOLUTION OF THE FUNCTIONAL COMBINING

FLUX AND CONCENTRATION ESTIMATES

The finite-difference form of the variational functional in Section 6 is

$$J = \sum_{ijk\ell} \{ \gamma_1 (\chi - \langle \chi \rangle)^2 + \gamma_2 (F_x - \hat{F}_x)^2 +$$

$$\gamma_3 (F_y - \hat{F}_y)^2 + \gamma_4 (F_z - \hat{F}_z)^2 +$$

$$\lambda (\nabla_t \chi + \nabla_x F_x + \nabla_y F_y + \nabla_z F_z + \beta \chi) \} . \qquad (D.1)$$

The observational weights γ_1, γ_2, γ_3 and γ_4 are prespecified constants in this case. The Lagrange multiplier, λ, is one of the dependent variables.

As in Appendix C, the stationary value of the functional is found by equating the first variation to 0. Therefore,

$$\delta J = 0 = \sum_{ijk\ell} \{ 2\gamma_1 (\chi - \langle \chi \rangle) \delta \chi + 2\gamma_2 (F_x - \hat{F}_x) \delta F_x$$

$$+ 2\gamma_3 (F_y - \hat{F}_y) \delta F_y + 2\gamma_4 (F_z - \hat{F}_z) \delta F_z$$

$$+ \delta \lambda (\nabla_t \chi + \nabla_x F_x + \nabla_y F_y + \nabla_z F_z + \beta \chi)$$

$$+ \lambda \delta \nabla_t \chi + \lambda \delta \nabla_x F_x + \lambda \delta \nabla_y F_y + \lambda \delta \nabla_z F_z + \beta \lambda \delta \chi \} . \qquad (D.2)$$

Using the applicable commutation equations it may be shown that

$$\sum_{ijk\ell} \lambda \delta \nabla_t \chi = - \sum_{ijk\ell} \delta \chi \nabla_t \lambda + B1 , \qquad (D.3)$$

$$\sum_{ijk\ell} \lambda \delta \nabla_x F_x = - \sum_{ijk\ell} \delta F_x \nabla_x \lambda + B2 , \qquad (D.4)$$

$$\sum_{ijk\ell} \lambda \delta \nabla_y F_y = - \sum_{ijk\ell} \delta F_y \nabla_y \lambda + B3 \text{ , and} \tag{D.5}$$

$$\sum_{ijk\ell} \lambda \delta \nabla_z F_z = - \sum_{ijk\ell} \delta F_z \nabla_z \lambda + B4 \text{ ,} \tag{D.6}$$

where B1, B2, B3 and B4 represent the terms which are uncommutable. These terms may be made to vanish by choosing the Lagrange multiplier to be zero at the boundary grid points and also at the grid points next to the boundary. This is called a natural boundary condition. With B1 - B4 eliminated, (D.3)-(D.6) may be substituted into (D.2) and terms rearranged to obtain

$$[2\gamma_1(\chi - \langle\chi\rangle) - \nabla_t\lambda + \beta\lambda] \, \delta\chi + [2\gamma_2(F_x - \hat{F}_x)$$

$$- \nabla_x\lambda] \, \delta F_x + [2\gamma_3(F_y - \hat{F}_y) - \nabla_y\lambda] \, \delta F_y$$

$$+ [2\gamma_4(F_z - \hat{F}_z) - \nabla_z\lambda] \, \delta F_z + [\nabla_t\chi + \nabla_x F_x + \nabla_y F_y$$

$$+ \nabla_z F_z + \beta\chi] = 0 \ . \tag{D.7}$$

In order to satisfy the extremum condition, $\delta J = 0$, for arbitrary and independent variations of $\delta\chi$, δF_x, δF_y, δF_z and $\delta\lambda$, their coefficients must vanish identically in the domain. This leads to the appropriate Euler-Lagrange equations

$$2\gamma_1(\chi - \langle\chi\rangle) - \nabla_t\lambda + \beta\lambda = 0 \ , \tag{D.8}$$

$$2\gamma_2(F_x - \hat{F}_x) - \nabla_x\lambda = 0 \ , \tag{D.9}$$

$$2\gamma_3(F_y - \hat{F}_y) - \nabla_y\lambda = 0 \ , \tag{D.10}$$

$$2\gamma_4(F_z - \hat{F}_z) - \nabla_z\lambda = 0 \ , \text{ and} \tag{D.11}$$

$$\nabla_t\chi + \nabla_x F_x + \nabla_y F_y + \nabla_z F_z + \beta\chi = 0 \ . \tag{D.12}$$

Eqs. (D.8)-(D.11) may be substituted into (D.12) to obtain the finite-difference equivalent of an elliptic second order partial differential equation in λ,

$$\nabla_{tt}\lambda + \frac{\gamma_1}{\gamma_2} \nabla_{xx}\lambda + \frac{\gamma_1}{\gamma_3} \nabla_{yy}\lambda \, \frac{\gamma_1}{\gamma_4} \nabla_{zz}\lambda$$

$$-\lambda(\beta^2 + \nabla_t\beta) + 2\gamma_1(\nabla_t\langle\chi\rangle + \nabla_x F_x + \nabla_y F_y + \nabla_z F_z + \langle\chi\rangle) = 0 \ . \tag{D.13}$$

Using the finite-difference analogs of (13) and the definition of β, with the estimated ensemble averaged concentration,

$$\nabla_{tt}\lambda + \frac{\gamma_1}{\gamma_2} \nabla_{xx}\lambda + \frac{\gamma_1}{\gamma_3} \nabla_{yy}\lambda + \frac{\gamma_1}{\gamma_4} \nabla_{zz}\lambda$$

$$- \lambda[(\nabla_t \ln A)^2 - \nabla_{tt} \ln A] + 2\gamma_1(\nabla_t\langle\chi\rangle - K_x\nabla_{xx}\langle\chi\rangle$$

$$- K_y\nabla_{yy}\langle\chi\rangle - K_z\nabla_{zz}\langle\chi\rangle - \langle\chi\rangle\nabla_t \ln A) = 0 . \qquad (D.14)$$

This equation may be solved for λ using a relaxation scheme slightly different from that employed in Appendix C, because a consistent finite-difference scheme must be utilized. Convergence to a solution is rapid; the R.M.S. residual is reduced from 79.33 to .008791 in 19 iterations for test P5, and from 107.8 to .008475 in 20 iterations for test P7. Once λ is obtained, substitution back into (D.8) through (D.11) yields values for the dependent variables, χ, F_x, F_y and F_z, which satisfy the diffusion equation.

TECHNICAL REPORT DATA
(Please read Instructions on the reverse before completing)

1. REPORT NO. EPA-600/4-79-002	2.	3. RECIPIENT'S ACCESSION NO.

4. TITLE AND SUBTITLE ANALYSIS OF ENSEMBLE AVERAGED CONCENTRATIONS AND FLUXES IN A TRACER PUFF	5. REPORT DATE January 1979
	6. PERFORMING ORGANIZATION CODE

7. AUTHOR(S) Main R. Hutcheson	8. PERFORMING ORGANIZATION REPORT NO.

9. PERFORMING ORGANIZATION NAME AND ADDRESS School of Meteorology University of Oklahoma Norman, Oklahoma 73019	10. PROGRAM ELEMENT NO. IAA603 AB-13 (FY-78)
	11. CONTRACT/GRANT NO. Grant 804507

12. SPONSORING AGENCY NAME AND ADDRESS Environmental Sciences Research Laboratory - RTP, NC Office of Research and Development U.S. Environmental Protection Agency Research Triangle Park, NC 27711	13. TYPE OF REPORT AND PERIOD COVERED Final
	14. SPONSORING AGENCY CODE EPA/600/09

15. SUPPLEMENTARY NOTES

16. ABSTRACT

Ensemble averaged fluxes and concentrations in a tracer puff diffusing in the atmospheric surface layer were analyzed. The analysis used radiation data published by the Battelle Memorial Institute. Fluxes that satisfy the diffusion equation for a Gaussian puff with an arbitrary diffusion rate were obtained from the gradient transfer hypothesis, using the proper diffusivities. These fluxes were used as estimates of the ensemble averaged fluxes in the surface layer.

The radiation data, however, were too sparse to use alone in analyzing the tracer concentrations. Therefore, the data were combined with a modified Gaussian distribution in a variational technique to obtain concentration values. Since the ensemble averaged concentration distribution was more nearly normal than the distribution in an individual puff, the concentration estimates were obtained from a model using a Gaussian distribution in the horizontal, which constrained the estimates as close to the analyzed concentrations as possible.

The concentration and flux estimates were combined with the diffusion equation in a variational technique. The analyzed fluxes and concentrations obtained were close to the estimates and satisfied the diffusion equation. The values are assumed to be the true ensemble averaged concentrations and fluxes for the puffs examined.

17.	KEY WORDS AND DOCUMENT ANALYSIS	
a. DESCRIPTORS	b. IDENTIFIERS/OPEN ENDED TERMS	c. COSATI Field/Group
Air pollution Mathematical data *Atmospheric diffusion *Flux density Applications of mathematics		13B 04B 04A 12A

18. DISTRIBUTION STATEMENT RELEASE TO PUBLIC	19. SECURITY CLASS *(This Report)* UNCLASSIFIED	21. NO. OF PAGES 111
	20. SECURITY CLASS *(This page)* UNCLASSIFIED	22. PRICE

EPA Form 2220-1 (9-73)

If your address is incorrect, please change on the above label tear off; and return to the above address.
If you do not desire to continue receiving these technical reports, CHECK HERE ☐; tear off label, and return it to the above address.

EPA-600/4-79-002